1970

Transport Properties of Thallium and the Effects of Small Angle Scattering in Metals.

Robert Eugene Hamburg
Louisiana State University and Agricultural & Mechanical College

TRANSPORT PROPERTIES OF THALLIUM AND THE EFFECTS OF SMALL ANGLE SCATTERING IN METALS

A Dissertation

Submitted to the Graduate Faculty of the
Louisiana State University and
Agricultural and Mechanical College
in partial fulfillment of the
requirements for the degree of
Doctor of Philosophy

in

The Department of Physics and Astronomy

by
Robert Eugene Hamburg
B.S., John McNeese State College, 1961
M.S., Louisiana State University, 1964
January 1970

ACKNOWLEDGEMENTS

The author wishes to express his most sincere gratitude to Professor Claude G. Grenier for his guidance, assistance, and patience in the course of this experiment. Appreciation is extended to Pat Mills for her proofreading and typing of this manuscript, to both Vice President J. M. Reynolds and Dr. R. G. Goodrich for considerable assistance in the publication of this work, and to Dr. N. H. Zebouni for his guidance in earlier work.

Thanks are due to staff members Les Edelen, Fritz Overman, Phil Granata, and Heinz Eichenseer for their respective assistance. Members and former members of the low temperature group have given indispensable aid in the data taking. Among them, T. E. Bogle, J. B. Coon, and C. R. Crosby were instrumental in this work.

Financial assistance by the Atomic Energy Commission and the Charles E. Coates Memorial Fund of the L.S.U. Foundation donated by George H. Coates are gratefully acknowledged.

TABLE OF CONTENTS

LIST OF TABLES

LIST OF FIGURES

ABSTRACT

Electical and thermal transport coefficients were studied in a single crystal of thallium. A set of measurements were made at 4.1, 3.0, 2.0, and 1.6°K in magnetic fields ranging from 12.2 kG to 18.4 kG. Evidence was found supporting the hypothesis that open orbit electrons in thallium may be efficiently scattered into closed orbits by the mechanism of small-angle phonon scattering.

Formulas were derived which allowed the calculation of the average number of electron-phonon collisions necessary to remove an electron from an open orbit. Qualitative agreement was obtained between the experimental calculations and the expected theoretical predictions. Reasons for the lack of good quantitative agreement are discussed both from the point of view of experimental errors and in view of the over-simplifying assumptions and approximations of a problem of scattering which is basically complex.

The results indicate that the effect studied here, viz., the efficient small angle phonon scattering of open orbit electrons may be observable in other metals and is a useful method of studying the transport properties of metals.

I. INTRODUCTION

Since the primary topic of this work relates to the effect of small-angle scattering on open orbit conduction, one will firstly comment in some detail on the general problem of scattering of electrons in metals, its effect on both the electrical and thermal conduction, and secondly define and classify open orbits and some of their transport properties.

Electrons as charge carriers in the electrical conduction process respond differently to scattering than electrons as energy carriers in the thermal conduction process. There is a common behavior which is related to the process known as "horizontal" transition which occurs for elastic scattering, i.e., for scattering which does not change the energy of the carriers. In this case the efficiency of the scattering is dependent only on the degree of randomization of the carriers velocity achieved by the scattering. It is evident then that large angle elastic scattering, i.e., scattering which causes large changes in the direction of motion of the electrons, will be most efficient in both the electrical and thermal conduction processes.

Another type of scattering is the so called "vertical transition" in which the energy of the carrier is changed with a negligible change in the direction of motion. If the energy

change is of the order of kT then this is sufficient to make a "hot" electron "cold" and greatly affect its contribution to thermal conduction without affecting its contribution to electrical conduction. There are also scattering with large horizontal and vertical components and thus having both randomization and energy change. Therefore, since the horizontal transitions affect electrical and thermal conduction equally and vertical transitions affect only the thermal conduction then the different types of scattering may be classified accordingly.

Impurities, defects, and crystal boundaries scatter electrons elastically and contribute equally to electrical and thermal resistance. Phonons which scatter electrons according to the conservation laws, $k \pm q = k'$ and $\epsilon_k \pm \hbar\omega = \epsilon_{k'}$, cause both horizontal and vertical transitions.

On one hand, if the velocity V_k makes a large angle with $V_{k'}$, one has large angle scattering which when viewed as a horizontal transition is very efficient in causing both electrical and thermal resistance. This is the case for: a) high temperature phonons with q vectors of the same magnitude as the caliper size of the usually large pieces of Fermi surface (FS) in metals. b) Low temperature phonons where q is small but either the FS is small[1] or certain parts of the FS correspond to small calipers,[2] or the state k' belongs to another band,[3] another sheet of the same FS[4] or as in the umklapp process where the FS in the repeated zone scheme yields small caliper dimensions.

On the other hand, if the velocity V_k makes a small angle with $V_{k'}$, one has small angle scattering which in terms of horizontal transitions would be insufficient for both electrical and thermal resistance. The thermal scattering, however, will be made efficient through the vertical component of the transition if $|\epsilon_{k'} - \epsilon_k| = \hbar\omega$ is of the order of kT. This general behavior will be the case of low temperature phonons (with the exceptions of cases (b) listed above for which the electrical scattering is also efficient). To encompass those exceptions one may write the small angle scattering condition $\bar{q} \ll \Delta k_F$ where $\bar{q}$ is the average phonon wavelength for which $\hbar\omega \approx kT$ and Δk_F represents the smallest FS caliper as measured from k. To be more inclusive of any special topology, Δk_F could be the smallest distance for which $V_{(k + \Delta k_F)}$ differs markedly in direction relative to V_k.

When scattering yields the same efficiency in both the electrical and thermal cases, the Wiedemann-Franz (W-F) law is known to hold, i.e., it is expected that the Lorenz ratio will assume its theoretical value in the case of impurity scattering or for phonon scattering when $\bar{q} \approx \Delta k_F$. The W-F law is stated as: $\lambda_e/\sigma T = L_n$, where λ_e is the electron contribution to the thermal conductivity, σ is the electric conductivity, $\lambda_e/\sigma T$ is the Lorenz ratio and L_n is the Lorenz number.

When scattering does not yield the same efficiency in the electrical and thermal cases, the W-F law is not expected to hold. For example, in the case of low temperature phonon scattering,

with $\bar{q} \ll k_F$, in the absence of a magnetic field, one expects, because of the added vertical scattering contribution, a thermal conductivity smaller than indicated by the W-F law, i.e., a Lorenz ratio smaller than the Lorenz number, L_n.

One sees, therefore, the importance of the measurement of the Lorenz ratio whenever efficiency of small angle scattering is to be studied. This point will be emphasized later.

The usefulness of the general classification of scattering either in terms of horizontal and vertical transitions or in terms of large and small angle scattering depends on which physical quantity is affected by the scattering. The general rule outlined above holds well if the conductivities are measured in the absence of a magnetic field and also holds well in the presence of a magnetic field if the proper extension to include this parameter is made. But there will be cases where, because of the presence of the magnetic field, small angle scattering will yield an efficient randomization and therefore efficient scattering.

In the absence of a magnetic field, an electron in an initial state k remains in the same state with constant velocity V_k until scattered. In a magnetic field the electron continually changes its state and velocity and its average motion may be characterized by a drift velocity, V_D. There exist cases of neighboring states k and k' with a small angle difference in their velocities, V_k and $V_{k'}$, such that the motion in the field averages to drift velocities V_D and $V_{D'}$ which may be quite different, not only in direction but also in magnitude. Thus,

even though the scattering from state k to k' is a small angle scattering in terms of the final velocity V_k and the initial velocity $V_{k'}$, the effective scattering is a large angle scattering in terms of drift velocities V_D and $V_{D'}$ associated to the initial velocity V_k and $V_{k'}$, respectively.

The detailed mechanism of such an effect has been studied by Pippard. It pertains to multi-connected FS's which may present zones of hole-like carriers adjacent to zones of electron-like carriers, which under asymptotic conditions have drift velocities in opposite directions. Therefore, small-angle scattering from one zone to the adjacent one becomes equivalent to efficient scattering as the behavior in the longitudinal resistance of copper as studied by Powell[5] and analyzed by Pippard[6] seems to show.

A similar mechanism which is only mentioned in Pippard's work and which corresponds to the situation encountered in the present study pertains to multi-connected FS's which present zones of open orbit carriers adjacent to either or both zones of electron-like or hole-like carriers. In this case the drift velocity in the open orbit region may be several orders of magnitude larger than in the closed orbit regions. Thus any small angle scattering which shifts a carrier from an open orbit to a closed orbit is equivalent to an efficient scattering if the opposite scattering does not compensate for it. This is the situation found in thallium.

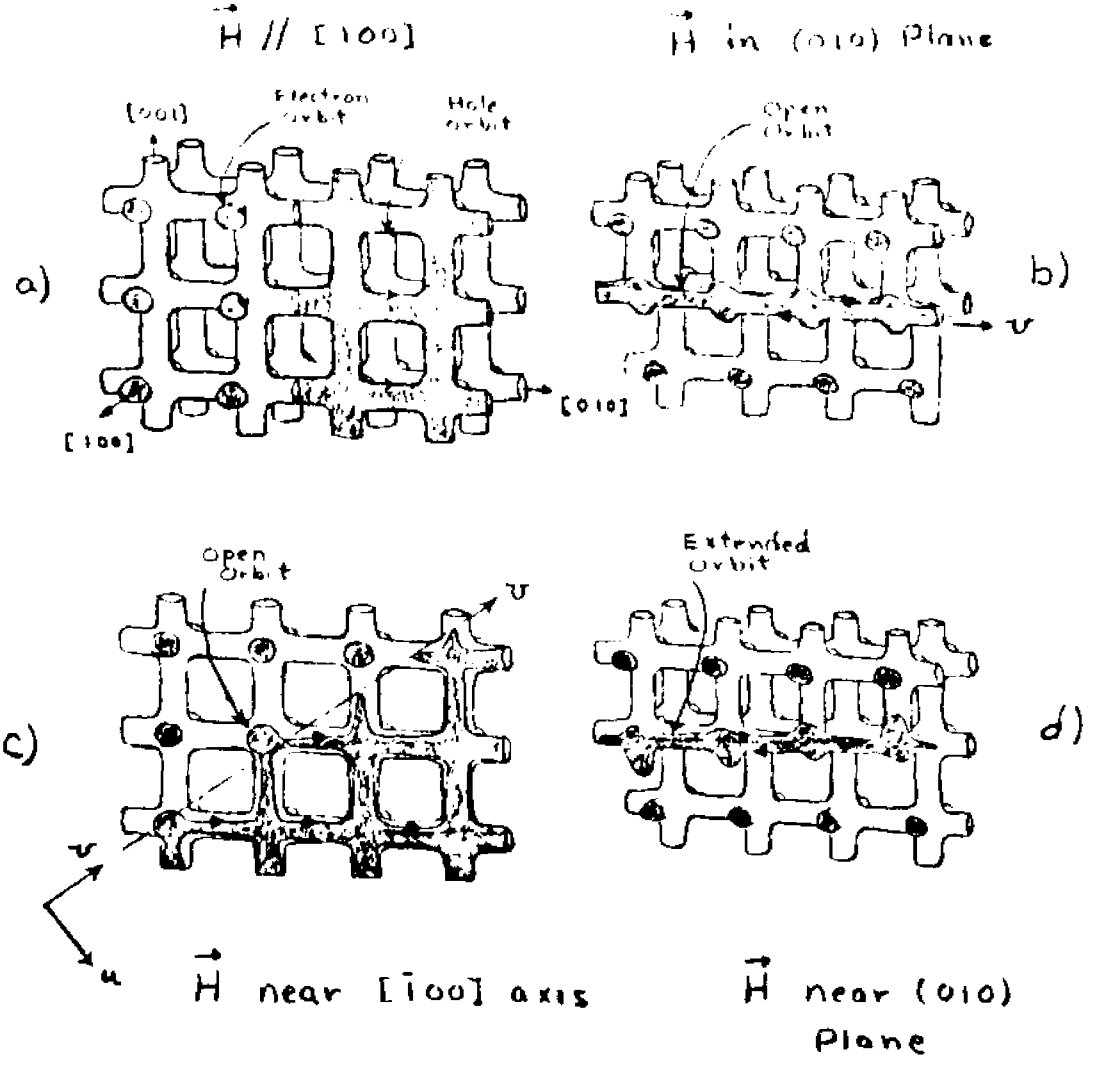
H // [100]
H in (010) Plane
[001]
Electron orbit
Hole orbit
a)
[100]
[010]
Open Orbit
b)
v
Open Orbit
v
c)
u
Extended Orbit
d)
H near [100] axis
H near (010) Plane

FIG. 1

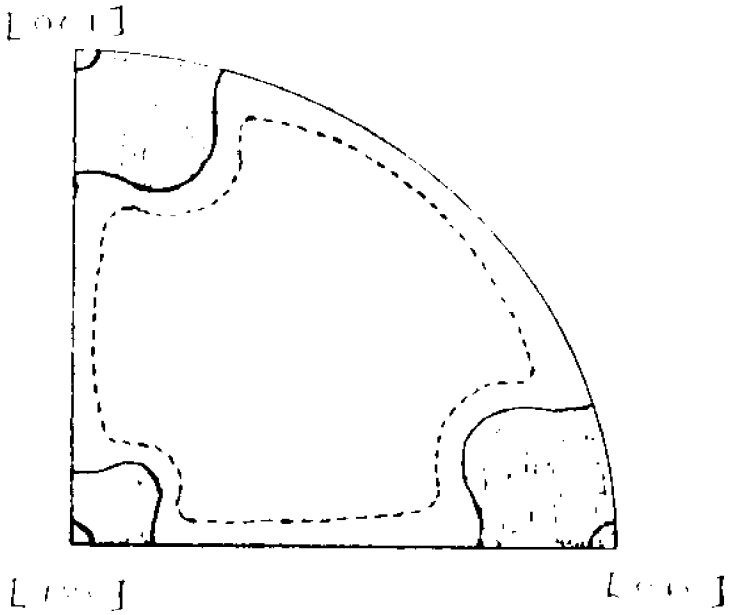

FIG. 2a

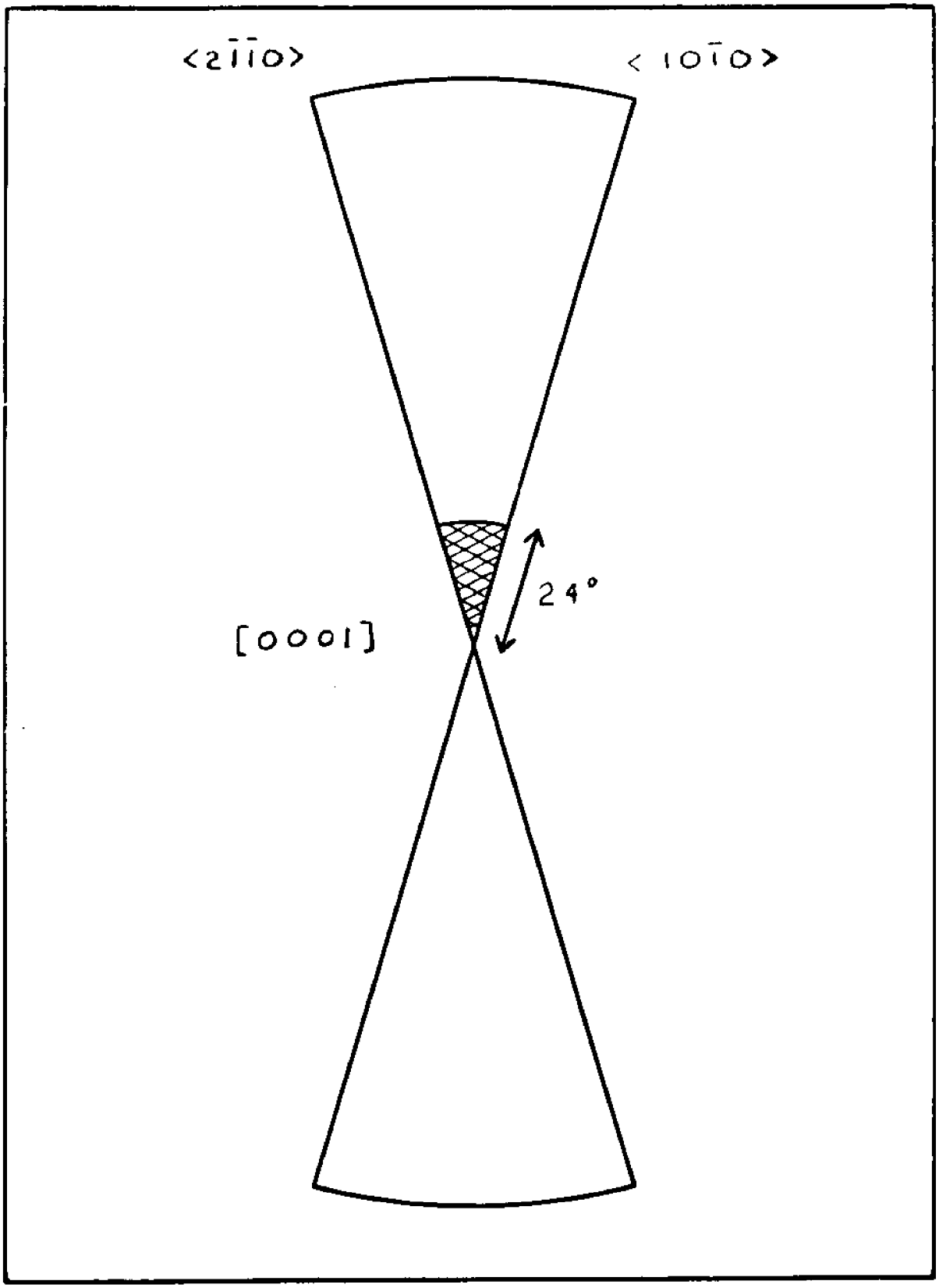

FIG. 2b

It seems appropriate to review briefly at this point a general concept of open orbits and to introduce some terminology which will be useful in describing the open orbit situation in thallium. As an illustration,[7] consider the case of a possible FS of a simple cubic metal as shown in Fig. 1. In this figure the periodically extended zone scheme is used to indicate some possible orbits for different magnetic field directions, $\vec{H}$. When $\vec{H}$ is parallel to the $[\bar{1}00]$ axis, as shown in Fig. 1(a) only closed orbits are possible.

If $\vec{H}$ is tilted from the $[\bar{1}00]$ axis but kept in the (010) plane, then a periodic open orbit is created in the direction labeled $\vec{v}$ in Fig. 1(b). This type of orbit is classified as a primary periodic open orbit since it always crosses the Brillouin zone boundary on the same [010] directed arm. Secondary periodic open orbits are formed when the orbit alternately crosses the zone boundary on one of two arms, e.g., if an orbit alternately followed the [010] and [001] arms then it would be classified as a secondary periodic open orbit and would have a general direction, $\vec{v}$, in the [011] direction. Higher order periodic orbits may be similarly defined.

If a stereogram, such as the one in Fig. 2(a) is used to indicate the field directions for which these periodic open orbits exist, then these directions are represented by lines. For this reason the primary, secondary, etc. periodic open orbits are sometimes referred to as one-dimensional or type I open orbits.

Figure 2(a) shows the primary open orbits as heavy lines. The high symmetry directions {100} must be excluded since only closed orbits exist for the field in these directions. Figure 2(b) is a stereogram for thallium and will be discussed in Chapter II.

Open orbits of the type shown in Fig. 1(c) result when the field is near the [100] axis but is directed in a non-symmetry plane. Here the open orbits are aperiodic and separate regions of hole-like closed orbits from regions of electron-like closed orbits. Since this type of open orbit exists for a solid angle of field directions represented on a stereogram as an area, then they are called two-dimensional or type II aperiodic open orbits. Type II orbits may be periodic if the direction of propagation corresponds to a rational direction in the plane perpendicular to the field. The type II orbits are illustrated in Fig. 2(a) as shaded areas.

As the angle between the field and the $[\bar{1}00]$ axis increases the open orbits collapse into extended orbits as shown in Fig. 1(d). An orbit is considered extended if it cannot be contained within one BZ. The stereogram shows the approximate boundary of the extended orbits as a dashed line.

A brief description of the FS of thallium will be given in Chapter II. In the same chapter some of the transport coefficients will be defined, the behavior of open and closed orbit scattering will be discussed, and the scattering parameters $\bar{r}'$ and $\bar{r}''$ will be derived from electrical and thermal conductivity equations.

Experimental details, including sample preparation and the apparatus, will be described in Chapter III. The experimental results and a discussion of these results are given in Chapters IV and V, respectively. Due to the exploratory nature of this work, much of the discussion in the body of this dissertation has been limited to general considerations. More specific phases of the work as well as some speculative considerations are discussed in the appendixes.

II. THEORY

A. The Fermi Surface of Thallium and the Occurrence of Open Orbits

The FS of thallium is relatively well known, having been established through a number of experimental and theoretical works. These include studies on the magnetoresistance of thallium by Alekseevskii and Gaidukov,[8] Mackintosh, Spanel, and Young,[9] Milliken and Young,[10] and by Young.[11] Ultrasonic attenuation data in thallium have been taken by Coon, Grenier, and Reynolds,[12] by Rayne[13] and by Eckstein, Ketterson, and Priestley.[14] Priestley[15] also made pulsed field de Haas-van Alphen measurements, finding good agreement with Soven's[16] relativistic O.P.W. model of the FS of thallium.

The fourth zone electron sheet of the FS of thallium of interest in our study consists of a honeycomb-like network as shown in Fig. 3. As Soven[16] has pointed out, open orbits as well as closed orbits may exist on the fourth zone surface when a magnetic field is tilted slightly from the hexagonal crystallographic direction. This is confirmed by the open orbit stereogram established experimentally by Milliken and Young[10] and shown in Fig. 2(b). The two-dimensional region surrounding the hexagonal direction indicates the existence of type II open orbits which are primary periodic if the tilt angle is in a

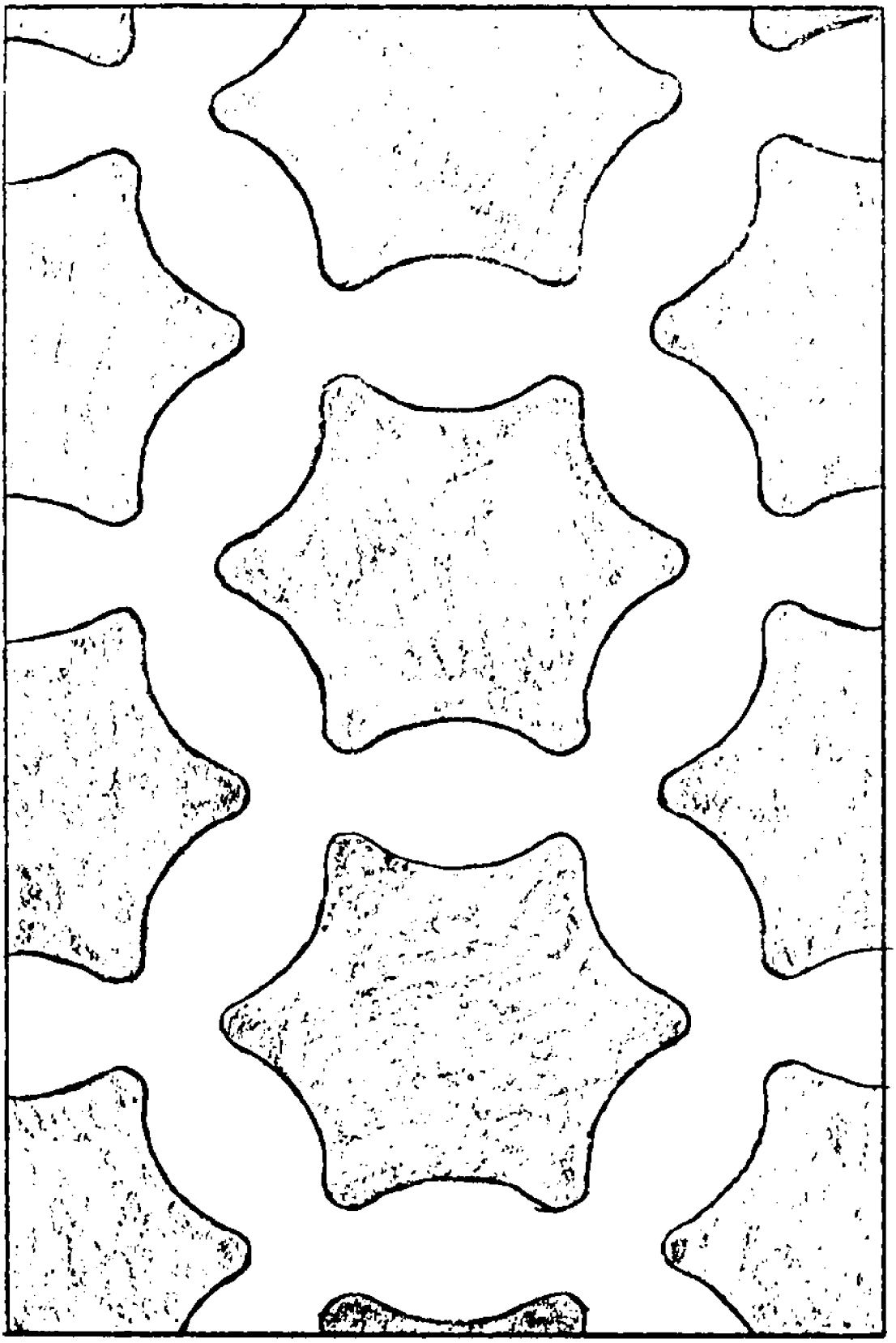

FIG. 3

$(10\bar{1}0)$ or $(11\bar{2}0)$ plane, and aperiodic or with higher order periodicity otherwise. The extent of the two-dimensional region is about 24^{o} from the c-axis. The open orbits are confined to the basal plane and extend, for the geometry used in this work, in the average direction of the $[10\bar{1}0]$ crystal axis. Figure 4 shows a schematic representation of the fourth zone surface with the magnetic field applied at an angle α' with the [0001] direction in the $(10\bar{1}0)$ plane. The shaded areas represent closed orbit regions and the open orbit regions are represented by the non-shaded areas. The narrow region of open orbits is sandwiched between electron-like and hole-like regions of closed orbits. The open orbits extend in the $[10\bar{1}0]$ direction with different orbit shapes occurring, depending on the position of the orbit within the slice of the FS. The width of the slice and thus the number of states in the open orbit region increases as the angle α' increases.

B. Definitions of the Resistivity Coefficients in Electrical and Thermal Conduction

The electrical and thermal magnetoresistances, the Hall effect and the Righi-Leduc effect were measured as functions of temperature and both magnitude and direction of the magnetic field. These four coefficients which are found to depend on small angle scattering in thallium need to be defined. To avoid ambiguity in their definitions, four sets of tri-rectangular coordinate systems will be defined. The coordinate systems will

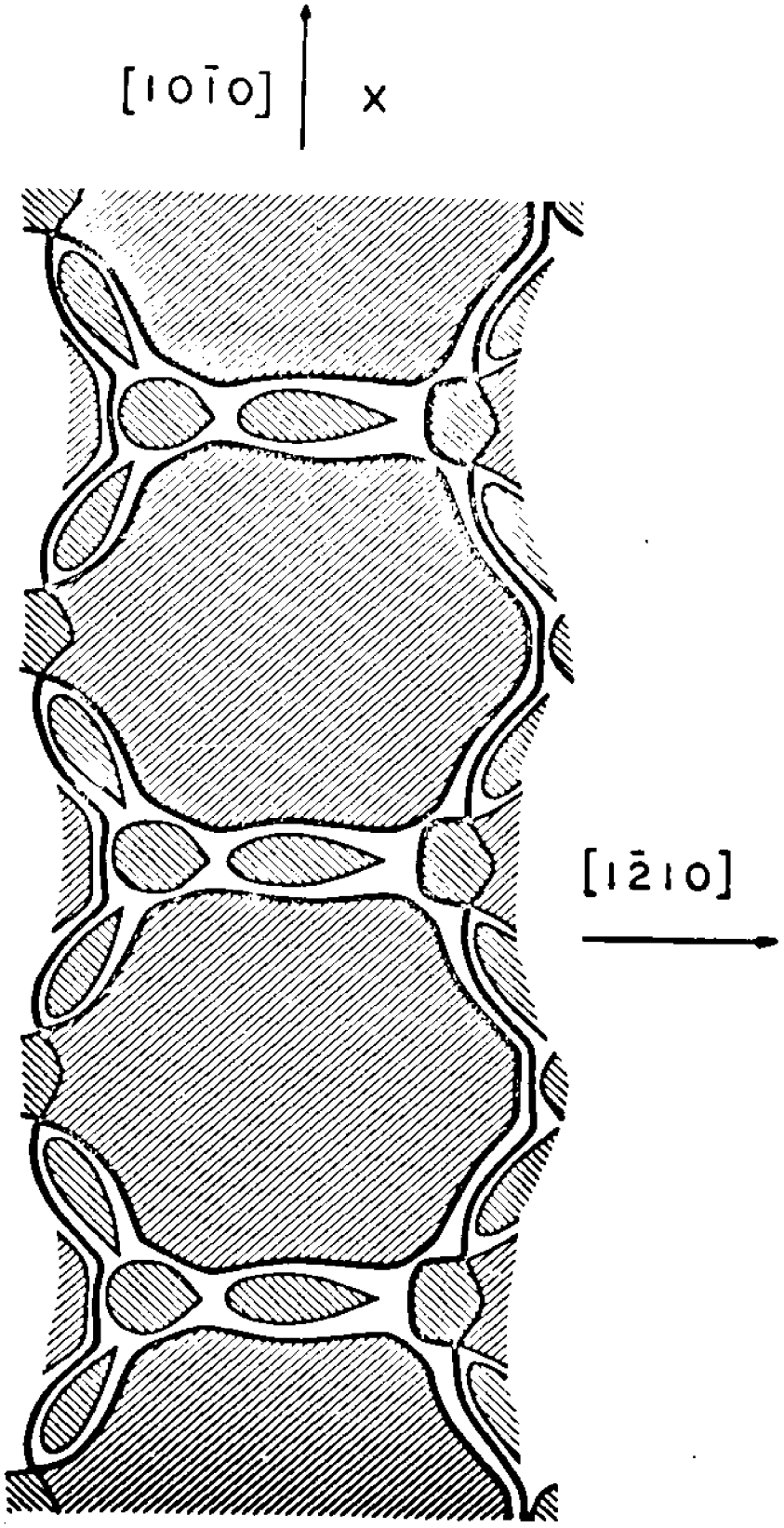

FIG. 4

be referred to as: 1,2,3; 1',2',3'; x,y,z; and u,v,z. In Fig. 5 the sample is shown cut as a parallelipiped slab with the directions 1,2,3 respectively for the length, width, and thickness directions. The slab was cut from a thallium monocrystal in such way that the 1,2,3 directions be coincident with the 1',2',3' axes where 1',2',3' corresponds to the crystallographic orientations, $[10\bar{1}0]$, $[\bar{1}2\bar{1}0]$, and [0001], respectively. The coincidence of the 1,2,3 and 1',2',3' axes will be assumed perfect except in specified cases in the appendixes. In Fig. 6(a) the "classic galvanomagnetic" set of coordinates x,y,z is oriented with respect to the magnetic field and current directions, with the current density in the x direction, the magnetic field in the z direction perpendicular to the current, and y perpendicular to both x and z. Experimentally the current flows along the length of the sample, so that if end effects are negligible, the x direction coincides with the 1 direction. Ambiguity exists if the magnetic field, which determines the direction of z, is not exactly perpendicular to the 1 direction since there will be then a small component of the current in the z direction. The main component of the current continues, of course, to be in the x direction. In the ideal case of the x and 1 directions parallel, the z axis is tilted relative to the 3 direction by a small angle α, as are the y and 2 directions. When the 3 and 3' directions coincide then $\alpha = \alpha'$.

The coordinates u,v,z which pertain to open orbit directions are defined in Appendix A.

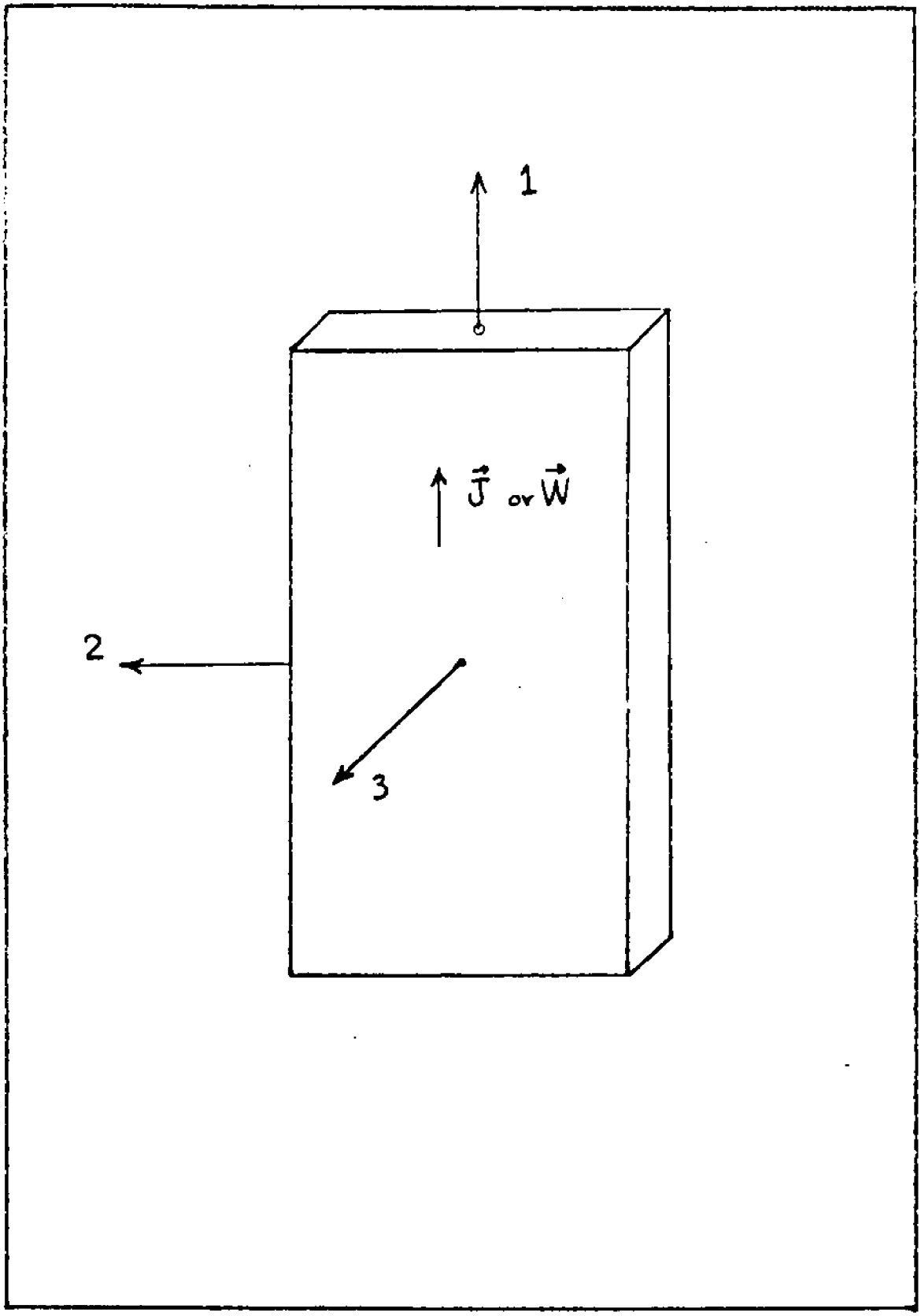

FIG. 5

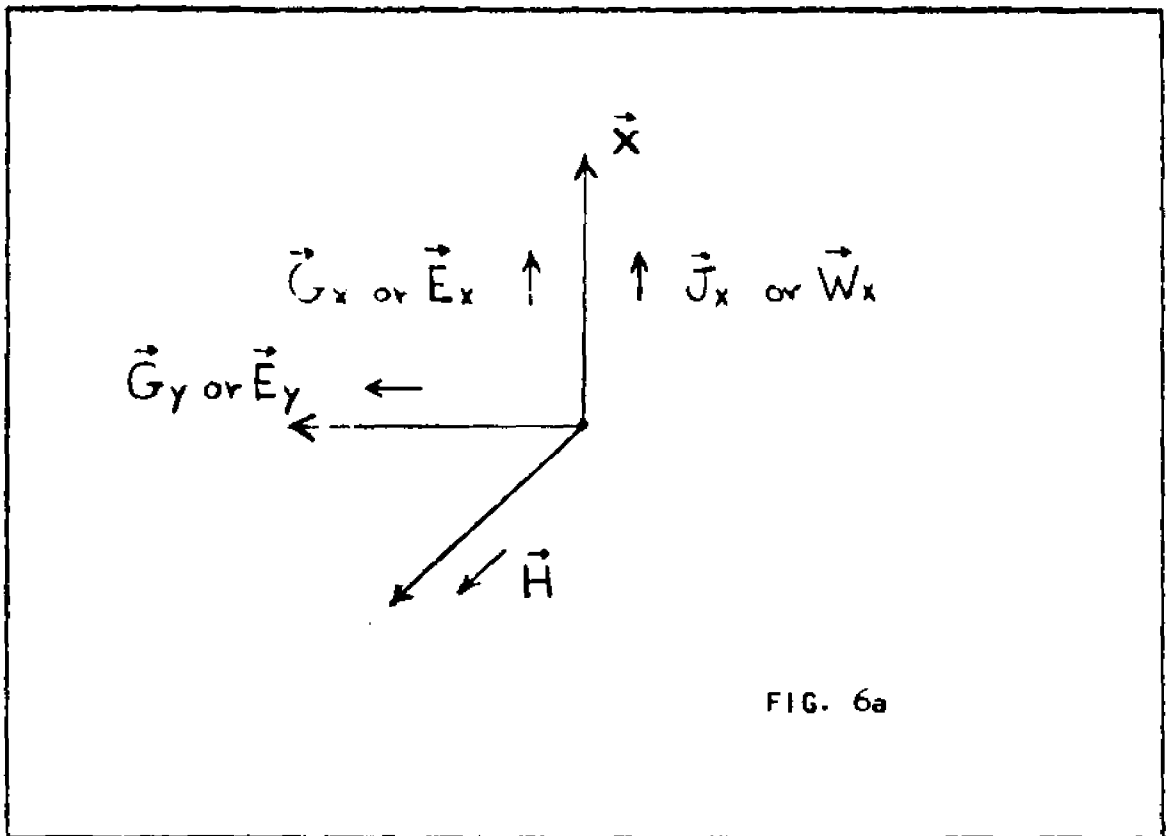
$\vec{x}$
$\vec{G}_x$ or $\vec{E}_x$
$\vec{J}_x$ or $\vec{W}_x$
$\vec{G}_y$ or $\vec{E}_y$
$\vec{H}$

FIG. 6a

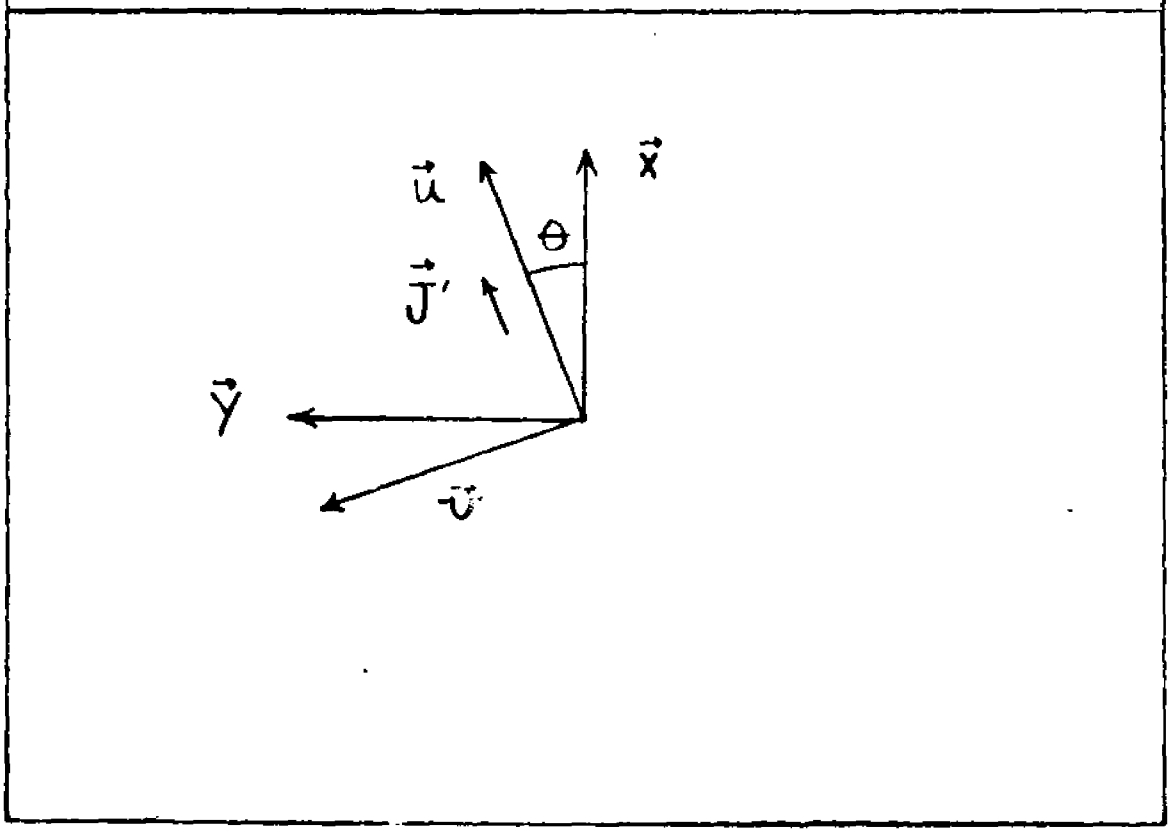
$\vec{u}$
$\vec{x}$
θ
$\vec{J}'$
$\vec{y}$
$\vec{v}$

FIG. 6b

When a magnetic field $\vec{H}$ (z-direction) is applied perpendicular to the flow (x-direction) of an electric current density $\vec{J}$ or a heat current density $\vec{W}$, then electric fields and/or thermal gradients appear. Under isothermal conditions, the electrical field components, E_x and E_y appear when an electrical current density J_x is applied. The isothermal galvanomagnetic coefficients are defined as $\rho_{xx} = E_x/J_x$, the magnetoresistivity, and $\rho_{yx} = E_y/J_x$, the Hall resistivity. Similarly, but under adiabatic conditions, when the heat current density W_x is applied gradients of temperature appear. The thermal resistivity coefficients are defined as $\gamma_{xx} = G_x/W_x$, the thermal magnetoresistivity, and $\gamma_{yx} = G_y/W_x$, the Righi-Leduc resistivity, where $G_x = -\Delta T/\Delta x$ and $G_y = -\Delta T/\Delta y$. The other coefficients which relate G to J and E to W have not been studied here and therefore will not be defined.

One may note that experimental conditions are such that the current flows in the 1-direction, and the electric fields and temperature gradients are measured in the 1 and 2 directions. Thus the measured coefficients should be labeled ρ_{11}, ρ_{21}, γ_{11}, and γ_{21}. The differences between these coefficients and the corresponding x,y coefficients are small and are generally compensated for by the measuring procedure. Thus, one still refers to the measured quantities as Hall, Righi-Leduc, etc. effects.

C. Effects of Open Orbit Conduction on the Resistivity Coefficients

There is a detailed calculation in Appendix A on the effects of open orbits on the electrical and thermal resistivity coefficients. Thus some details not brought out in the present section may be found in the appendix.

If both open and closed orbits exist simultaneously in a metal, the total conductivity tensor can be written as $\hat{\sigma}^T = \hat{\sigma}^c + \hat{\sigma}^o$, where $\hat{\sigma}^c$ is the contribution to the conductivity from the closed orbits and $\hat{\sigma}^o$ is the contribution due to the open orbits. When α', the angle between the magnetic field H and the [0001] crystal axis, is small, the closed orbit carriers still correspond to the case of a two-dimensional, isotropic metal with a conductivity

$$\hat{\sigma}^c = \begin{pmatrix} \sigma_{xx} & \sigma_{xy} \\ -\sigma_{xy} & \sigma_{xx} \end{pmatrix}$$

The open orbit conductivity tensor can be expressed in matrix form as:

$$\hat{\sigma}^o = \begin{pmatrix} \sigma^o \cos^2\theta & \sigma^o \cos\theta \sin\theta \\ \sigma^o \cos\theta \sin\theta & \sigma^o \sin^2\theta \end{pmatrix}$$

where θ is the angle between the real space open orbit direction and the current direction. The equation given above is Eq. A-2 in Appendix A.

The total resistivity is given by

$$\hat{\rho}^T = (\hat{\sigma}^T)^{-1}$$

so that by inverting the conductivity matrix and taking the known high field limits for the components of the closed orbit conductivity, viz., $\sigma_{xx} \to A/H^2$ and $\sigma_{xy} \to B/H$, then the high field transverse magnetoresistance is:

$$\rho_{xx} \approx \frac{A}{B^2} \frac{1 + \frac{H^2\sigma^\circ}{A}\sin^2\theta}{1 + \frac{\sigma^\circ A}{B^2}} \qquad (1)$$

and the Hall resistivity is:

$$\rho_{yx} \approx \frac{1}{B} \frac{H - \frac{H^2\sigma^\circ}{B}\sin\theta\cos\theta}{1 + \frac{A}{B^2}\sigma^\circ} \qquad (2)$$

which further simplifies if one takes

$$\rho_{yx}^{(-)} = \tfrac{1}{2}\left[\rho_{yx}(+H) - \rho_{yx}(-H)\right]$$

which becomes:

$$\rho_{yx}^{(-)} = B^{-1} \frac{H}{1 + \frac{A}{B^2}\sigma^\circ} \qquad (2')$$

These are the Eqs. A-11 obtained in Appendix A.

For a small tilt angle α' it is expected and a posteriori verified that $\sigma^\circ A/B^2 \ll 1$ so that Eq. 1 reduces to:

$$\rho_{xx} \approx A/B^2 + (\sigma^\circ \sin^2\theta)\, B^2 H^2 \qquad (3)$$

Therefore a plot of ρ_{xx} vs H^2 should yield a straight line whose slope $S' = (\sigma^{\circ} \sin^2\theta)/B^2$.

Another expression which is of interest is obtained by forming the ratio of $\rho_{xx}/\rho_{yx}^{(-)}$ which eliminates the common denominator, $1 + \frac{A}{B^2}\sigma^{\circ}$ and one obtains, even if $\frac{A}{B^2}\sigma^{\circ}$ is not negligible,

$$\frac{H\rho_{xx}}{\rho_{yx}^{(-)}} = \frac{A}{B} + \frac{\sigma^{\circ}\sin^2\theta}{B} H^2 \qquad (4)$$

Therefore to a better approximation than in the case of ρ_{xx}, the plot of $H\rho_{xx}/\rho_{yx}^{(-)}$ vs H^2 should yield a straight line. In this case the slope

$$S'' = \frac{\sigma^{\circ}\sin^2\theta}{B} \qquad (5)$$

If the experiment were performed under ideal conditions i.e., $\theta = \pm 90^{\circ}$ (for $\alpha \neq 0$) the slopes S' and S'' defined in Eqs. 3 and 4 would take the simple forms $\sigma^{\circ} B^{-2}$ and $\sigma^{\circ} B^{-1}$.

It is interesting to note that in either case the slopes are proportional to the open orbit conductivity, σ°, and that the quantity B is theoretically and experimentally simple and obtainable.

$B = ecn$ where $n = N_h - N_e$ is the excess of holes over electrons. When the approximation, $\frac{A}{B^2}\sigma^{\circ} \ll 1$, is valid, B is

simply the asymptotic value $H/\rho_{yx}^{(-)}$.

Many of the conclusions obtained here relative to the electrical resistivity components can be extended to the case of the thermal resistivity components. It should, nevertheless, be pointed out that the exact correspondence is possible only if the lattice conductivity, λ_g, can be neglected. Again, most of the detailed calculations are given in Appendix A with the main results expressed in Eq. A-15 as:

$$\gamma_{xx} = \frac{\lambda^{\circ}\sin^2\theta + \lambda_g + A'H^{-2}}{|\lambda|}$$

$$\gamma_{yx}^{(-)} = \frac{B'H^{-1}}{|\lambda|} \qquad (6)$$

$$\frac{H\gamma_{xx}}{\gamma_{yx}^{(-)}} = \frac{A'}{B'} + \frac{\lambda^{\circ}\sin^2\theta + \lambda_g}{B'} H^2$$

where $|\lambda| = A'^2 H^{-4} + B'^2 H^{-2} + A'(\lambda^{\circ} + 2\lambda_g)H^{-2} + \lambda_g(\lambda^{\circ} + \lambda_g)$. The second term of the sum is predominant in the field range studied, λ° is the thermal conductivity of the open orbit electrons, λ_g is the lattice conductivity, and A' and B' are determined by the high field approximation $\lambda_{xx} \approx A'H^{-2}$ and $\lambda_{xy} = B'H^{-1}$.

If all terms in the denominator can be neglected except for $B'^2 H^{-2}$, then the resistivity becomes:

$$\gamma_{xx} = \frac{A'}{B'^2} + \frac{\lambda^{\circ}\sin^2\theta + \lambda_g}{B'^2} H^2 \qquad (7)$$

Thus the slope of γ_{xx} vs H^2 is $(\lambda^{\circ}\sin^2\theta + \lambda_g)/B'^2$ and the slope of $H\gamma_{xx}/\gamma_{yx}^{(-)}$ vs H^2 is $(\lambda^{\circ}\sin^2\theta + \lambda_g)/B'$.

If the experiment could be performed under the ideal condition of $\sin^2\theta = 1$ then these slopes would simplify to

$$(\lambda^{\circ} + \lambda_g)\, B'^{-2} \qquad \text{and} \qquad (\lambda^{\circ} + \lambda_g)\, B'^{-1}$$

which would further simplify to $\lambda^{\circ}B'^{-2}$ and $\lambda^{\circ}B'^{-1}$ if λ_g is negligible. Again it is interesting to note that in either case the slopes are proportional to $\lambda^{\circ} + \lambda_g$ (or λ°) and furthermore that the term B' is simple to obtain. Indeed if one neglects phonon drag, $B' = BL_nT$ where L_n is the Lorenz number and B' is given as the value of $H/\gamma_{yx}^{(-)}$ in the range where the approximation $|\lambda| \approx B'H^{-2}$ can be made.

It is of interest, when one wants to compare thermal resistance with electrical resistance, to scale, for example, the thermal resistance with the Wiedemann-Franz ratio L_nT. Then if one studies the terms $\gamma_{xx}L_nT$ and $\gamma_{yx}L_nT$ one obtains with $B' = BL_nT$ the values for the slopes:

$$L' = \frac{\lambda^{\circ} + \lambda_g}{L_nT}\, B^{-2} \qquad L'' = \frac{\lambda^{\circ} + \lambda_g}{L_nT}\, B^{-1}$$

D. Definition and Determination of the Scattering Efficiency Relative to the Open Orbit Electrons

If r is the number of collisions necessary to scatter an

electron from a point in the open orbit region to a point in the adjacent closed orbit region, then r will depend on the initial position of the electron in the open orbit slice, the width of the slice, and the type of scattering involved. If the scattering is due only to small angle scattering by low energy phonons, the number of collisions, r_p depends on the phonon distribution as well. Therefore, averaging the initial states of the electrons over the width of the open orbit region, the average number of collisions $\bar{r}$ and $\bar{r}_p$ necessary for electron relaxation are expected to depend on the width of the slice and the phonon distribution, i.e., the tilt angle α and the temperature T. It may be noted that some electrons are being efficiently scattered without being brought out of the open orbit zone. Those cases are being included in the $\bar{r}$ average.

A good experimental determination of $\bar{r}$ can be obtained from the resistivity data in the following manner.

As pointed out in the introduction, when electrons are scattered by impurities, phonons, etc., i.e., when both randomization and vertical processes occur, the randomization process affects equally the electrical and thermal conduction. The vertical process acts solely on the thermal conduction. One may say then that the thermal conduction would be affected by most collisions, those being either randomizing or non-randomizing collisions. In the case of electrical conduction, on the other hand, only the randomizing collisions are effective, these being associated primarily with scattering from open to closed orbits.

In short, the thermal conductivity λ^{o} is limited by most collisions, and the electrical conductivity σ^{o} is limited mainly by those collisions which scatter an open orbit state into a closed orbit state. Thus comparison of λ^{o} and σ^{o} should indicate how many collisions, on the average, are necessary to efficiently scatter the electrons, i.e., remove them from the open orbit zone. As a matter of fact the Wiedemann-Franz law interprets just that. Writing $\lambda^{o} \sim \omega_c^{-1}$, i.e., the thermal conductivity inversely proportional to the collision frequency, and $\sigma^{o} \sim \omega_{eff}^{-1}$, i.e., the electrical conductivity inversely proportional to the frequency of effective collisions, it is found that $\sigma^{o}/\lambda^{o} \sim \omega_c/\omega_{eff}$. Thus the ratio of the conductivities is proportional to $\bar{r}$, the number of collisions necessary to produce efficient scattering. Since the Wiedemann-Franz law applies in the form $L_n T \sigma = \lambda$ when $\omega_{eff} = \omega_c$, and since λ^{o} and σ^{o} are proportional to ω_c^{-1} and ω_{eff}^{-1} then

$$\frac{L_n T \sigma^{o}}{\lambda^{o}} = \frac{\omega_c}{\omega_{eff}} = \bar{r}$$

Since the slopes of $H\gamma_{xx}/\gamma_{yx}^{(-)}$ and $H\rho_{xx}/\rho_{yx}^{(-)}$ are respectively $L' = (\lambda^{o} + \lambda_g)/L_n TB$ and $S' = \sigma^{o} B^{-1}$, then, when $\lambda_g = 0$, the ratio of the slopes

$$\frac{S'}{L'} = \frac{\sigma^{o} B^{-1}}{\lambda^{o} B^{-1}} L_n T$$

is just the quantity $\bar{r}$ defined above.

In the case where λ_g cannot be neglected, one should correct the $H\gamma_{xx}/\gamma_{yx}^{(-)}$ quantities for the λ_g term either by calculation of λ_g or by empirical corrections. Thus with B practically independent of α (i.e., λ°) the slope $L_0'' = (\lambda_g/L_nT)B^{-1}$ for $\alpha = 0$ should be subtracted from the experimental slope L'' at $\alpha \neq 0$ and one would expect that the quantity $S''/(L'' - L_0'')$ would give the quantity $\bar{r}$ more correctly. The slope ratio S''/L'' is referred to as $\bar{r}''$.

The same conclusions are reached when one considers the slopes determined in the $L_nT\gamma_{xx}$ and σ_{xx} equations. There one has

$$L' = \frac{\lambda^\circ + \lambda_g}{L_nT} B^{-2}$$

and $S' \approx \sigma^\circ B^{-2}$ and the quantity S'/L' is a good measure of $\bar{r}$ when λ_g is negligible. Otherwise, $S'/(L' - L_0')$ should be used with L_0' having a definition similar to the definition of L_0'. The value S'/L' will be referred to as $\bar{r}'$.

In short, $\bar{r}$, $\bar{r}'$, $\bar{r}''$ stand for the ratios: ω_c/ω_{eff}, S'/L', S''/L'', respectively. The corrected ratios $S'/(L' - L_0')$, $S''/(L'' - L_0'')$ are denoted as $\bar{r}_c'$ and $\bar{r}_c''$. One expects then $\bar{r} \approx \bar{r}_c' \approx \bar{r}_c'' \approx \bar{r}' \approx \bar{r}''$.

These results apply as well when the angle $\theta \neq 90^\circ$. Indeed,

$$\frac{S'}{L' - L_0'} \longrightarrow \frac{\sigma' \sin^2\theta \; B^{-1}}{\lambda^\circ \sin^2\theta \; B^{-1} L_nT}$$

i.e., $\bar{r}$, where it is understood that the experimental conditions (especially θ) are the same for both the electrical and thermal measurements.

III. EXPERIMENTAL DETAILS

A. Sample Preparation

The sample used in the experiment was prepared from a zone-refined bar of thallium metal obtained from Cominco Produces Inc.[17] (quoted purity: 99.9999%).

To obtain the sample the strain-anneal technique of crystal growth was adopted wherein a 2 in. length of the thallium bar was subjected to a longitudinal compression resulting in about a one percent deformation in length. The bar was then etched to remove the oxide coating and sealed in a Pyrex glass tube under vacuum. Next the bar was placed in an oven and annealed at 220°C for 10 days. The annealing temperature was chosen to be 10°C below the temperature of the transition from the body centered cubic to the hexagonal close-packed phase. As a result of the annealing, four or five large single crystals were produced in the bar and separated by spark cutting. One was chosen for use in this experiment. It was then cut and spark planed into a rectangular parallelepiped with dimensions 18.0 X 4.02 X 1.15 mm such that the length was parallel to a $[10\bar{1}0]$ crystal axis and the large face was perpendicular to the hexagonal direction [0001].

B. Thermometer Preparation and Thermometry

The determination of the thermal effects requires the measurement of temperature gradients in directions both parallel

and perpendicular to the direction of the heat current. This requires the use of four thermometers. Thus, in order to be adapted for use as low temperature thermometers, several carbon resistors (Allen Bradley, 47 Ω 1/10 watt) were stripped of their insulation. Formvar insulated copper wire was wound tightly around the exposed graphite of each resistor which was then coated with insulating varnish (G.E. 7031). The insulation was removed from the free end of the copper wire so it could be soldered to the sample. The thermometers thus prepared were matched in pairs by comparing the change in resistance of each thermometer as a function of temperature in the liquid helium range and as a function of magnetic field. Two pairs of thermometers, each pair having well matched characteristics, were soldered along and across the sample with 60/40 Bi-Cd eutectic. The same solder was used to attach the heater (30'' of Advance resistance wire wound on No. 22 insulated copper wire) to the lower end of the sample. The upper end of the sample was soldered to a copper piece which extended through the vacuum chamber containing the sample to the helium bath. The copper served as a good thermal conductor so that the upper end of the sample had close thermal contact with the helium bath. Thus, the heat generated by the heater flowed through the sample with only negligible losses through other parts.

Each thermometer resistance was determined by maintaining a constant current through the thermometers and measuring the voltage across it with a Leeds and Northrup type K-3 Universal

Potentiometer. The same instrument was used to measure the heater current and voltage values. Since the heater exhibited a significant magnetoresistance, it was necessary to determine the heater current and voltage each time the magnetic field was changed.

C. Apparatus for Electrical Measurements

To get the isothermal conditions necessary for the electrical measurements, the sample was immersed directly in the helium bath. The Hall and magnetoresistance probes (No. 30 Constantan wire) were attached to the corresponding thermal probes so that the measurements could be made at the same points. The lower crystal current copper lead was left in place only during electrical measurements since it would act as a heat leak for the thermal current.

The electrical measuring circuit consisted of a 6-dial Rubicon potentiometer, a d.c. amplifier (Keithly nanovolt detector) and a Brown strip chart recorder. At the highest sensitivity the peak to peak noise level for this system was approximately 5 nanovolts.

D. Temperature Regulators

Two different types of temperature regulators were used, one for temperatures above 2.4°K and one for 2.2°K and lower. These have been described by Long.[18] The vapor pressure of the helium bath was indicated by a Bourdon tube pressure gage (Texas Instruments, Inc.). The bath temperature could be maintained

constant within a millidegree of temperature by observing the pressure on the T.I. gage and manually correcting the temperature regulator.

E. Magnet

The iron core Weiss magnet used to produce the magnetic field had 8-inch diameter pole pieces with a 1 5/8" gap. A current of 80 amps produced a field of 18,410 G, which was the maximum field used. The magnet was mounted so that the field could be rotated 360° about a vertical axis.

F. Measurement Procedure

The sample was placed in the holder with the long dimension vertical. The currents $\vec{J}$ and $\vec{W}$ flowed vertically in the sample and were thus perpendicular to the field so as to fulfill the conditions for the definitions of the four desired effects, viz., ρ_{xx}, ρ_{yx}, γ_{xx}, and γ_{yx}. A rotation of the magnet by 180° provided the necessary reversal of field, + H to - H. With the field direction (z) near the [0001] crystallographic axis (3'), ρ_{xx} was first measured at four given values of the field, then ρ_{yx} was measured under the same circumstances. The field was then rotated by a small increment, $\Delta\alpha$, and the measurement of ρ_{xx} at the four field values was repeated and thereafter ρ_{yx} was measured. This procedure was repeated so as to have the ρ_{xx}, ρ_{yx} data corresponding to a span of $-10° < \alpha' < 10°$ around the 3' direction. Precise

determination of the 3' direction was pre-established by locating the sharp minimum in ρ_{xx} as a function of α' which occurs for this orientation.

The measurements of ρ_{yx} were repeated for every field orientation 180° from those used in the primary angular span so as to obtain $\rho_{yx}(-H)$. It was thought unnecessary to seek the $\rho_{xx}(-H)$ data.

The temperatures at which these sets of data were taken were 4.1, 3.0, 2.0, 1.6, and 1.25°K.

A similar procedure was followed in the determination of thermal resistivity coefficients except for a relatively lengthy determination at each range of temperatures of the calibration of the 4 thermometers at zero field and at the 4 field values used. In contrast to the ρ procedure, it was found necessary to determine $\gamma_{xx}(-H)$, whereas experimental difficulties made the measurements at 1.25°K unattainable. The lengthy procedure in the thermal case led to limiting the number of orientation points to about half those for the ρ data.

Beside these sets of data, some other exploratory or secondary experiments were made, such as tilting the crystal direction from the vertical position, studies with the field near the $[\bar{1}2\bar{1}0]$ direction and determination of thermoelectric and Nernst-Ettinghausen effects at the four temperatures. But most of those data are indirectly related to the effect under study and may only bring some justification to some of the approximations made in this work. These experiments are therefore not being analyzed here.

IV. EXPERIMENTAL RESULTS

The resistivity ratio ($\rho_{300^\circ K}/\rho_{4.2^\circ K}$) for the thallium sample was measured and found to be 10,400. This compares favorably with the ratio of 10,000 quoted by Alekeevskii and Gaidukov[19] and indicates that the sample was relatively pure and free of strain.

Electrical and thermal resistivity data were taken as a function of temperature as well as a function of the magnitude and direction of the magnetic field following the procedure outlined in the preceeding chapter.

Figure 7 is a composite of ρ_{xx} and γ_{xx} data corresponding to the first step in the experimental procedure, i.e., at a constant temperature. The values of ρ_{xx} at four different values of the magnetic field are determined as a function of the tilt angle α and are shown in the upper part of the figure. The curves in the lower part of this figure represent the corresponding results for γ_{xx} scaled with the Wiedemann-Franz law ratio, L_nT. Therefore, the scales for ρ_{xx} and $L_nT\ \gamma_{xx}$ are the same, viz., ohm-cm. The main feature of these curves is the existence of a minimum where $\alpha \rightarrow 0$. The rise of ρ_{xx} when $|\alpha|$ is increased is associated with the increased contribution of the open orbits through the term $\sigma^o \sin^2\theta\ H^2/B^2$. A similar term accounts for the same effect in the $L_nT\ \gamma_{xx}$ curve.

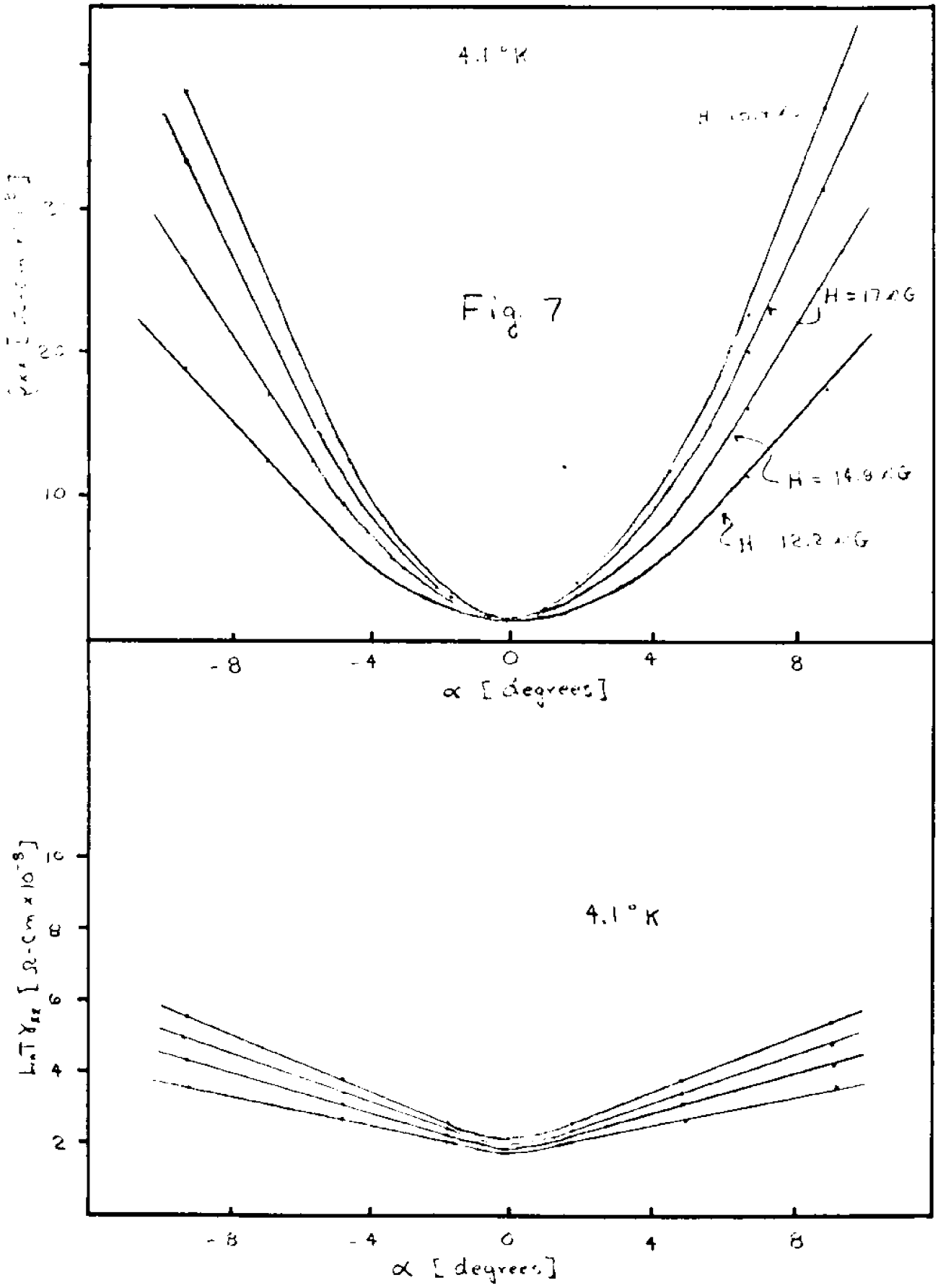
4.1 °K
H = 17.4 KG
H = 14.9 KG
H = 12.2 KG
20
10
-8
-4
0
4
8
α [degrees]
4.1 °K
10
8
6
4
2
-8
-4
0
4
8
α [degrees]

Fig. 7

The corresponding data at 3°K, 2°K and 1.6°K are shown in Figs. 8, 9, and 10, respectively.

The determination of the slopes $S' = \sigma^{\circ}\sin^2\theta/B^2$ were made graphically by the use of curves of the type shown in Fig. 11, where ρ_{xx} is plotted vs H^2. The data in Fig. 11 correspond to a temperature T = 2°K and are shown for different tilt angles α. The curves are approximated by straight lines to allow the determination of the slope coefficient S'. The curves cut the ordinate at the value A/B^2 independent of α for small values of that angle. As expected the slope increases as the angle α is increased.

The determination of the slopes

$$L' = \frac{\lambda^{\circ}\sin^2\theta + \lambda_2}{B'^2} L_nT$$

were similarly made through graphs of the type shown in Fig. 12 where $L_nT\,\gamma_{xx}$ at 2°K is plotted vs H^2 for different values of α.

Figure 13 shows the composite result of these determinations where the values of S' and L' at 2°K are represented vs the tilt angle, α. As expected, the values S' and L' almost vanish as α approaches zero.

Curves of the type 11, 12, and 13 corresponding to the determination of S' and L' at 1.6°K, 3°K, and 4.1°K are not shown, but the corresponding values of S' and L' are listed in Table I. It should be noted that the angle α listed in Table I is expressed in rather unorthodox units such that 10 of these units of angle are equivalent to 0.5675 degrees (i.e., 6400 units = 360°).

Fig. 8

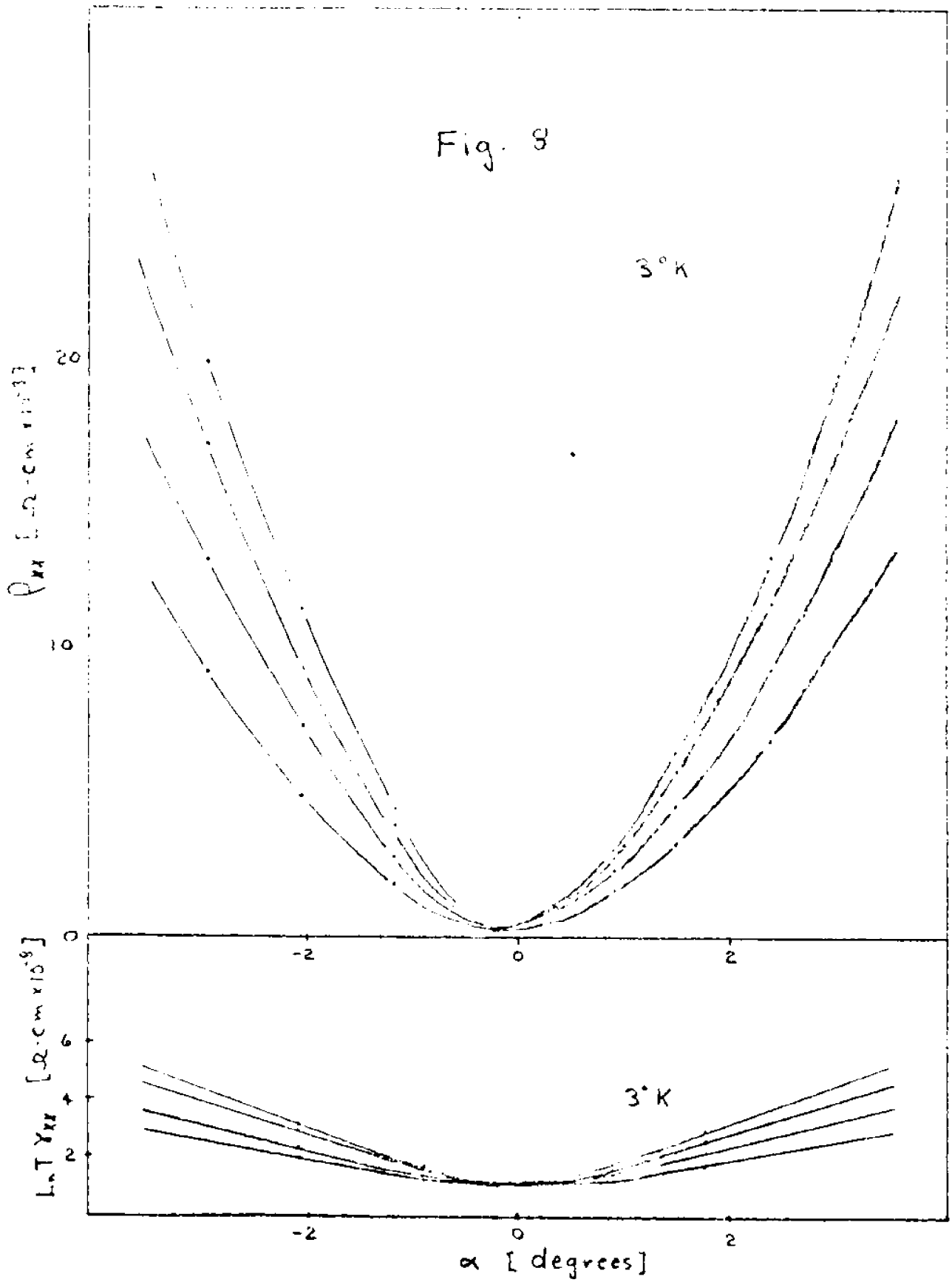

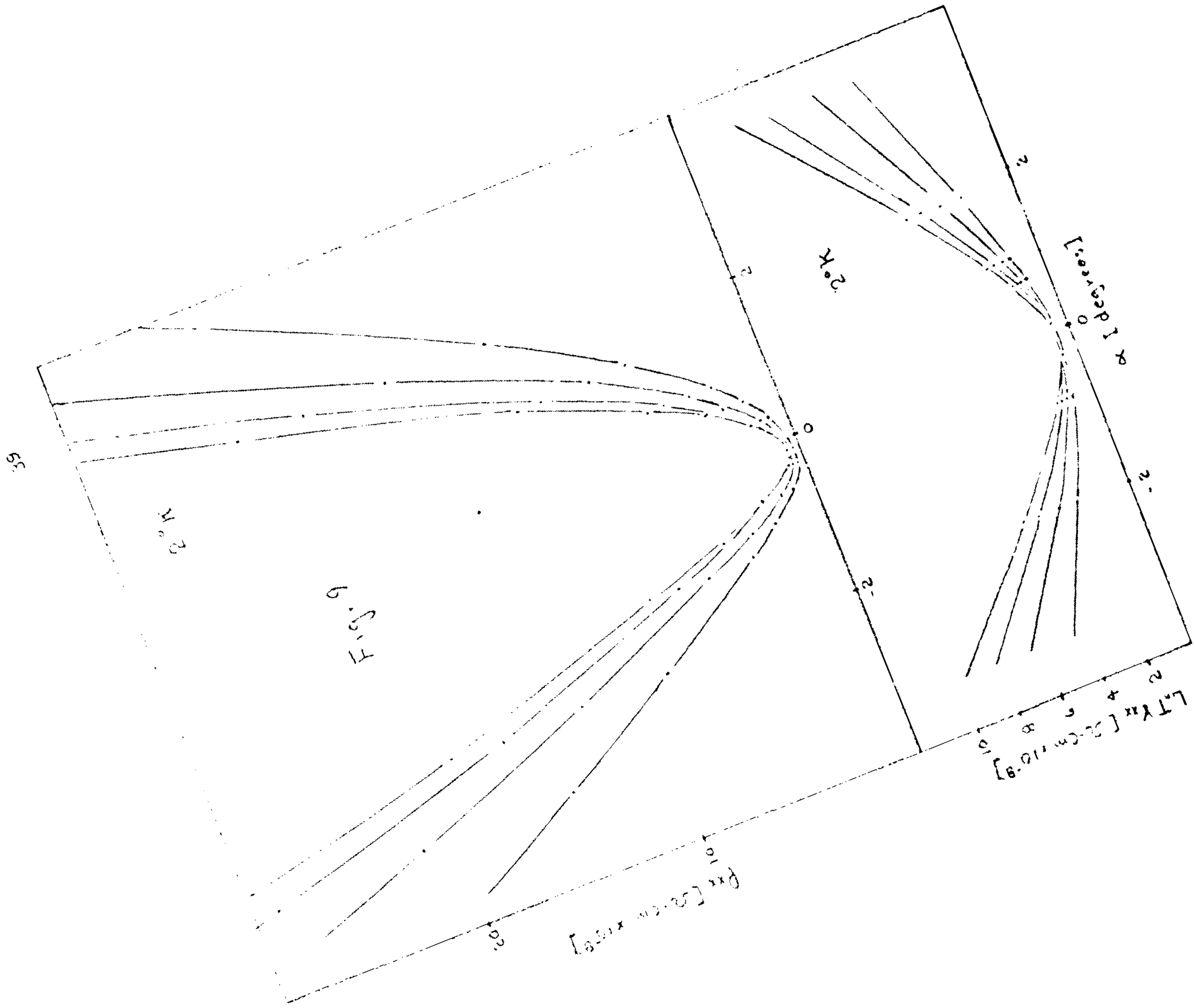
2.0
1.5
1.0
0.5
0
-0.5
-1.0
-1.5
-2.0
ρ_{xx} [Ω-cm x 10^{-5}]
ρ_{xy} [Ω-cm x 10^{-5}]
$L_T \chi_{xx}$ [Ω-cm x 10^{-9}]
$L_T \chi_{xy}$ [degrees]

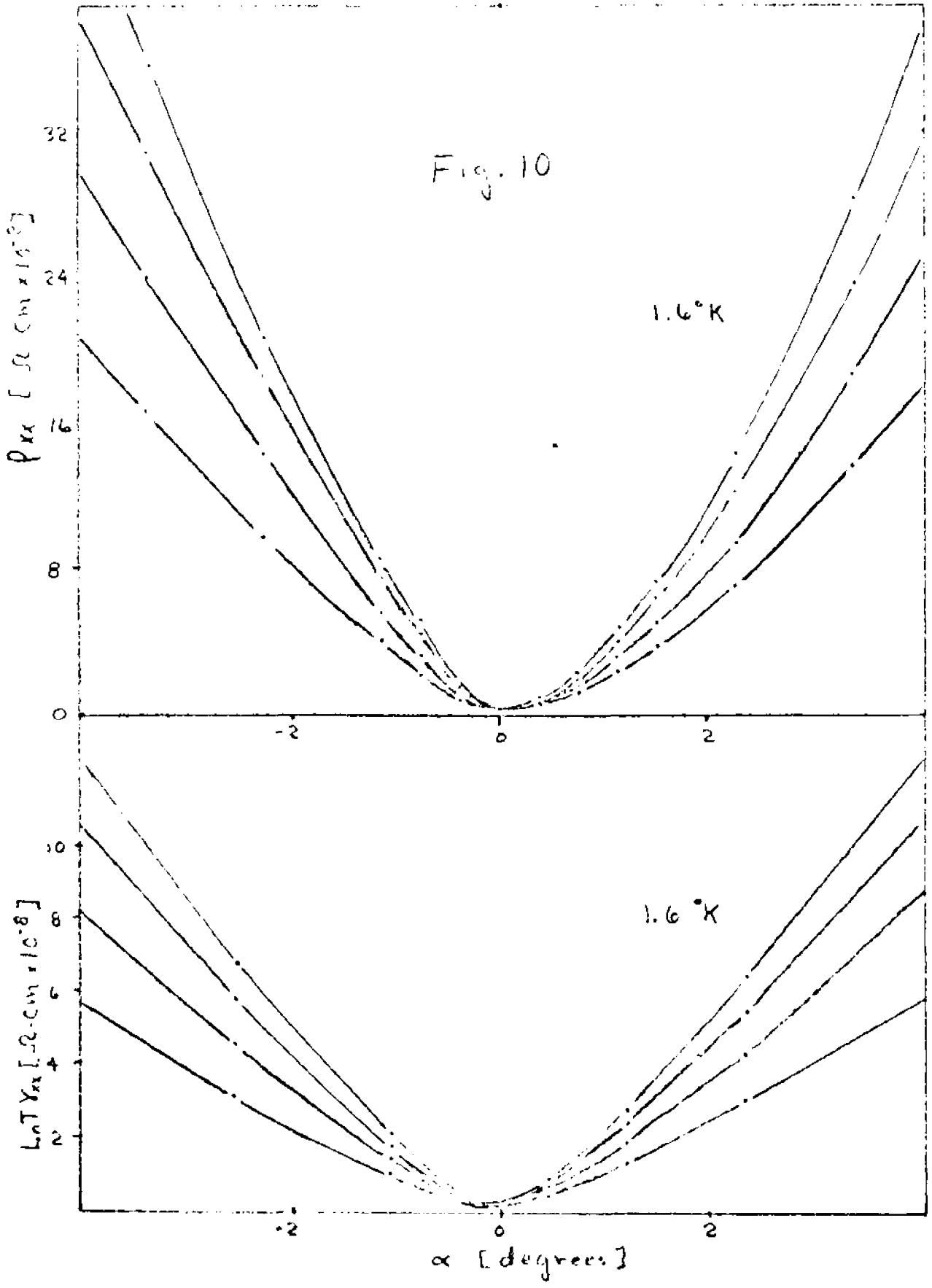

Fig. 10

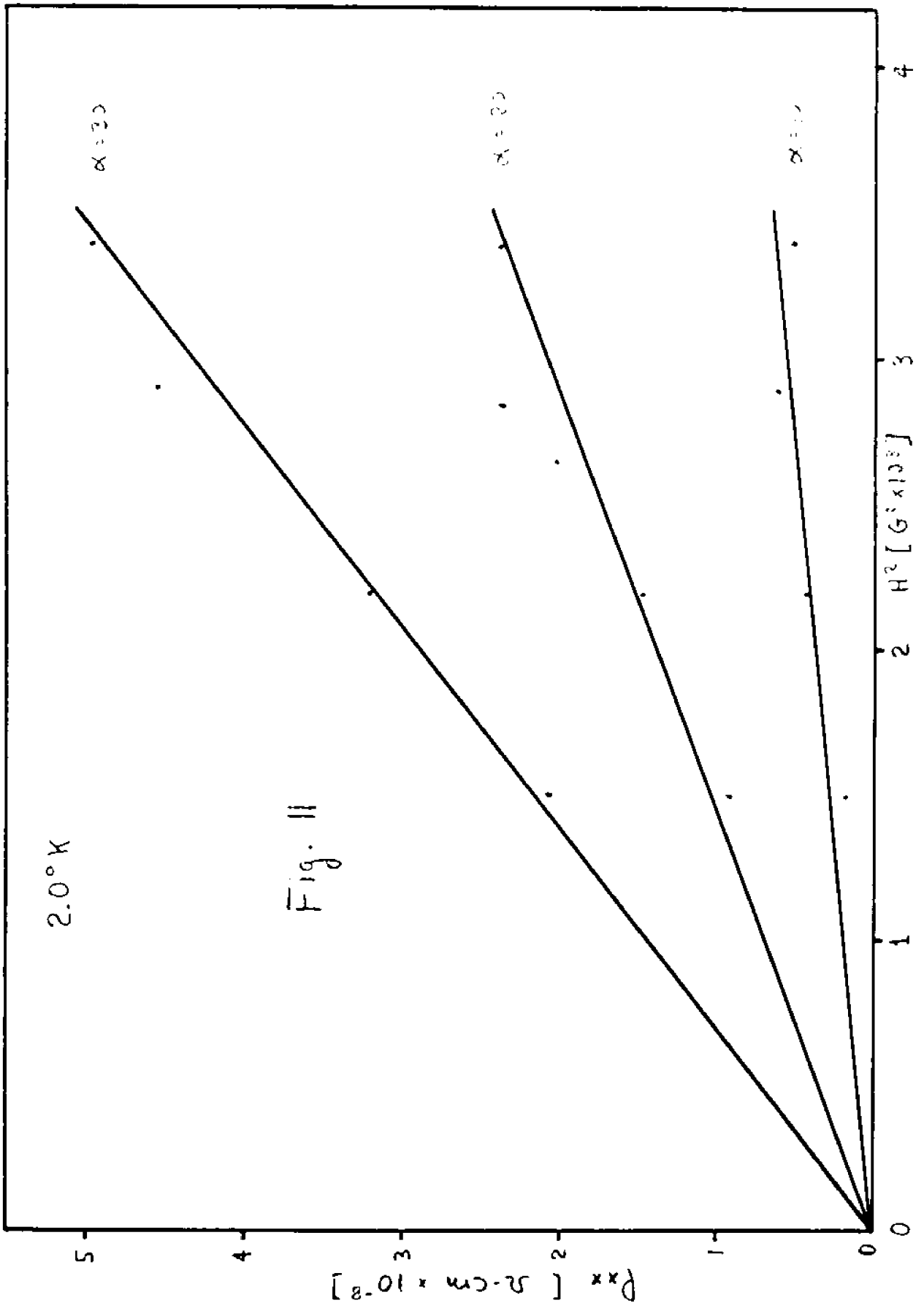
2.0°K
Fig. 11
ρ_{xx} [Ω-cm × 10^{-8}]
H^2 [$G^2 \times 10^{-8}$]
0
1
2
3
4
5

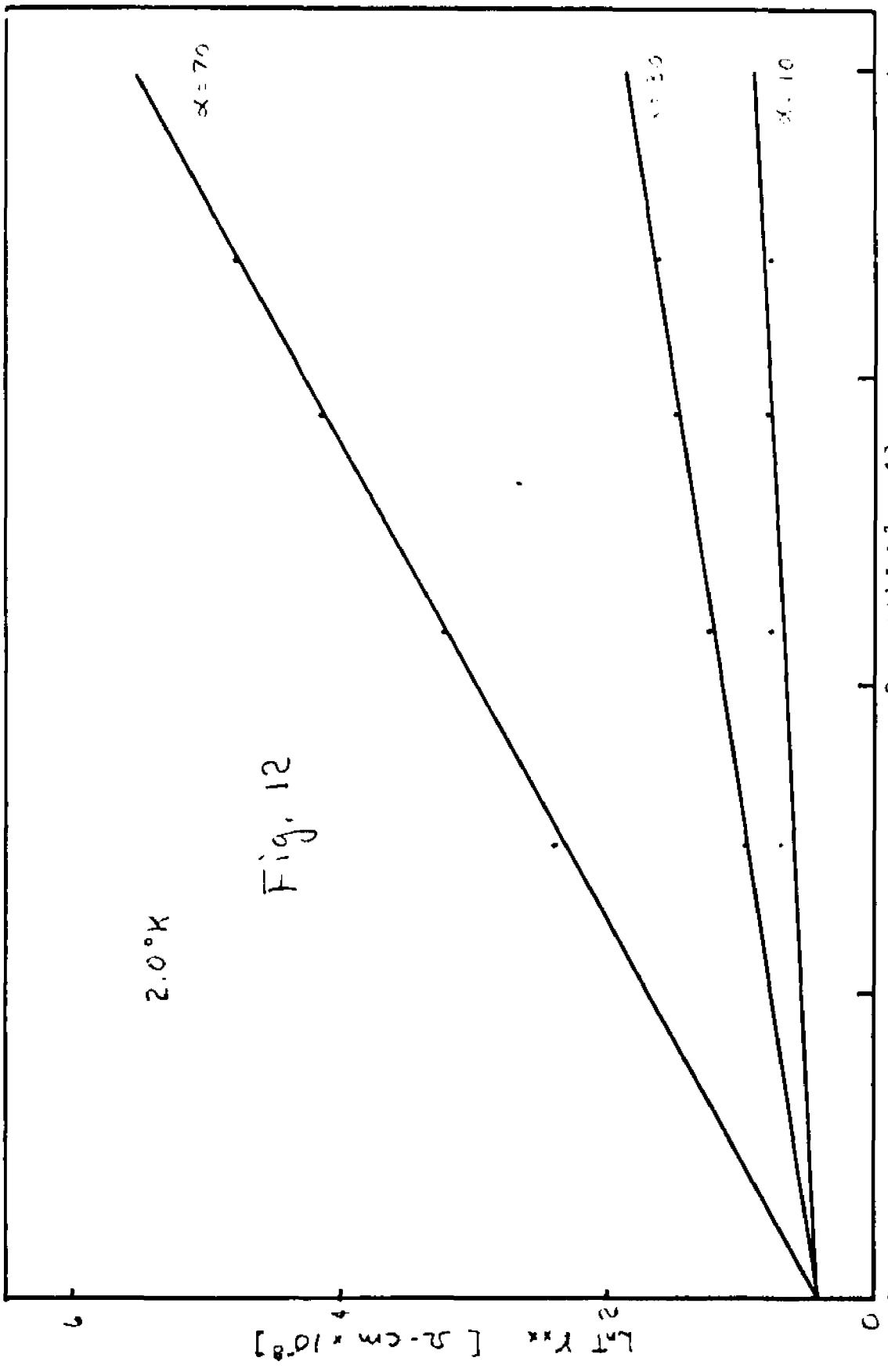

Fig. 12

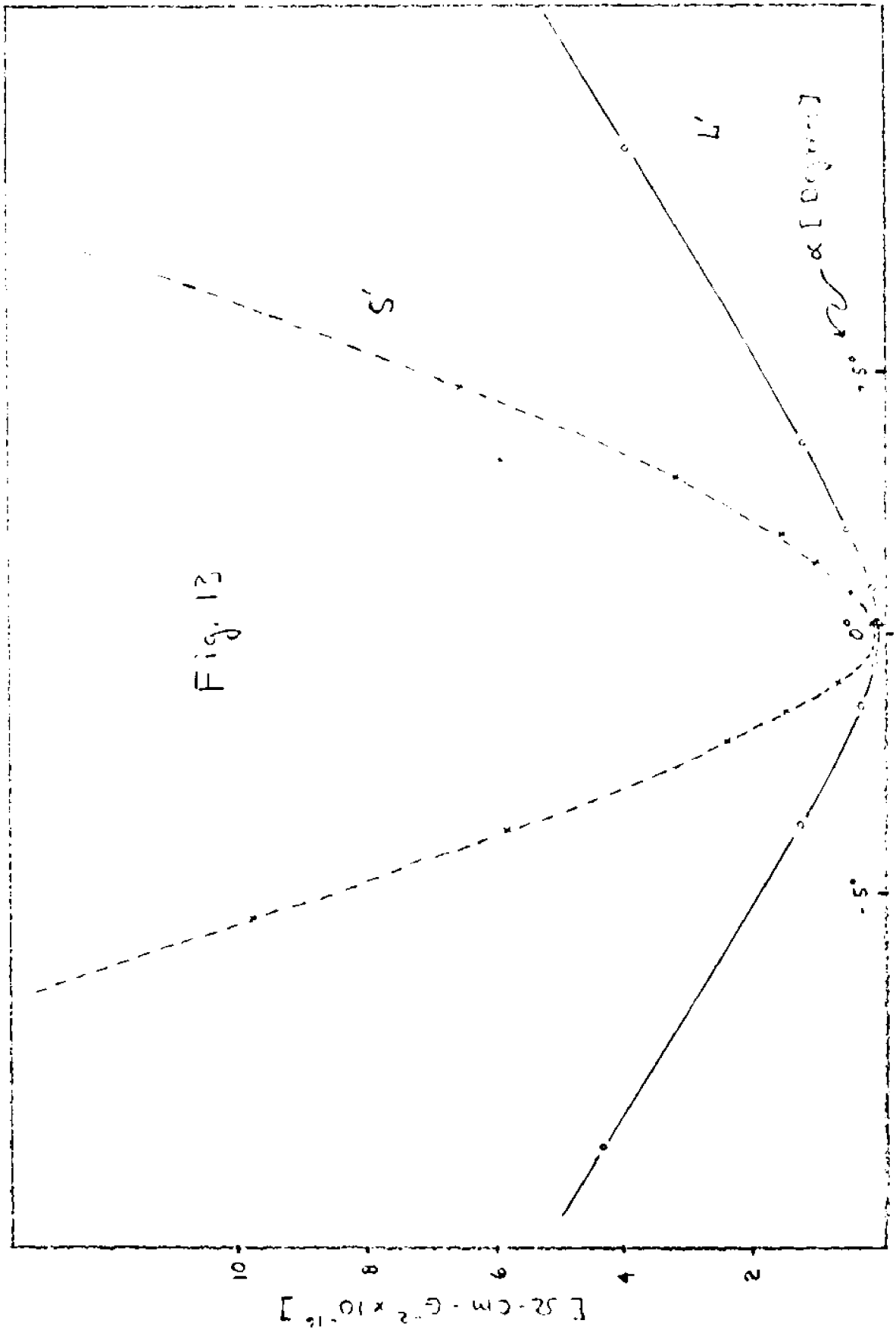

Fig. 12

TABLE I. S' and L' [Ω-cm-G^{-2} X 10^{-16}]

α	4.1°K S'	4.1°K L'	4.1°K $\bar{r}'$	3.0°K S'	3.0°K L'	3.0°K $\bar{r}'$	2.0°K S'	2.0°K L'	2.0°K $\bar{r}'$	1.6°K S'	1.6°K L'	1.6°K $\bar{r}'$
0	---	---	---	0.04	0.04	1.0	0.10	0.02	5.00	0.10	0.02	5.00
10	0.03	0.12	0.25	0.17	0.07	2.43	0.35	0.09	3.89	0.35	0.15	2.33
20	0.11	0.16	0.70	0.44	0.13	3.38	0.88	0.27	3.26	1.05	0.39	2.69
30	0.22	0.20	1.11	0.82	0.20	4.10	1.60	0.46	3.48	1.85	0.68	2.72
40	0.37	0.24	1.54	1.34	0.30	4.47	2.45	0.65	3.77	2.85	0.98	2.91
60	0.79	0.33	2.37	2.44	0.46	5.36	4.40	1.15	3.83	5.10	1.68	3.04
80	1.27	0.42	3.02	3.75	0.67	5.60	6.80	1.68	4.05	7.80	2.40	3.25
100	1.88	0.52	3.62	5.48	0.97	5.65	9.30	2.22	4.19	10.6	3.20	3.31
120	2.60	0.62	4.16	7.34	1.21	6.07	11.9	2.78	4.28	13.8	4.00	3.45
140	3.38	0.73	4.63	9.60	1.44	6.66	14.7	3.35	4.39	16.9	4.80	3.52
160	4.12	0.84	4.90	11.6	1.66	6.99	17.5	3.90	4.49	20.5	5.60	3.66
180	4.92	0.94	5.20	14.0	1.9	7.39	20.5	4.44	4.62	24.1	6.40	3.77

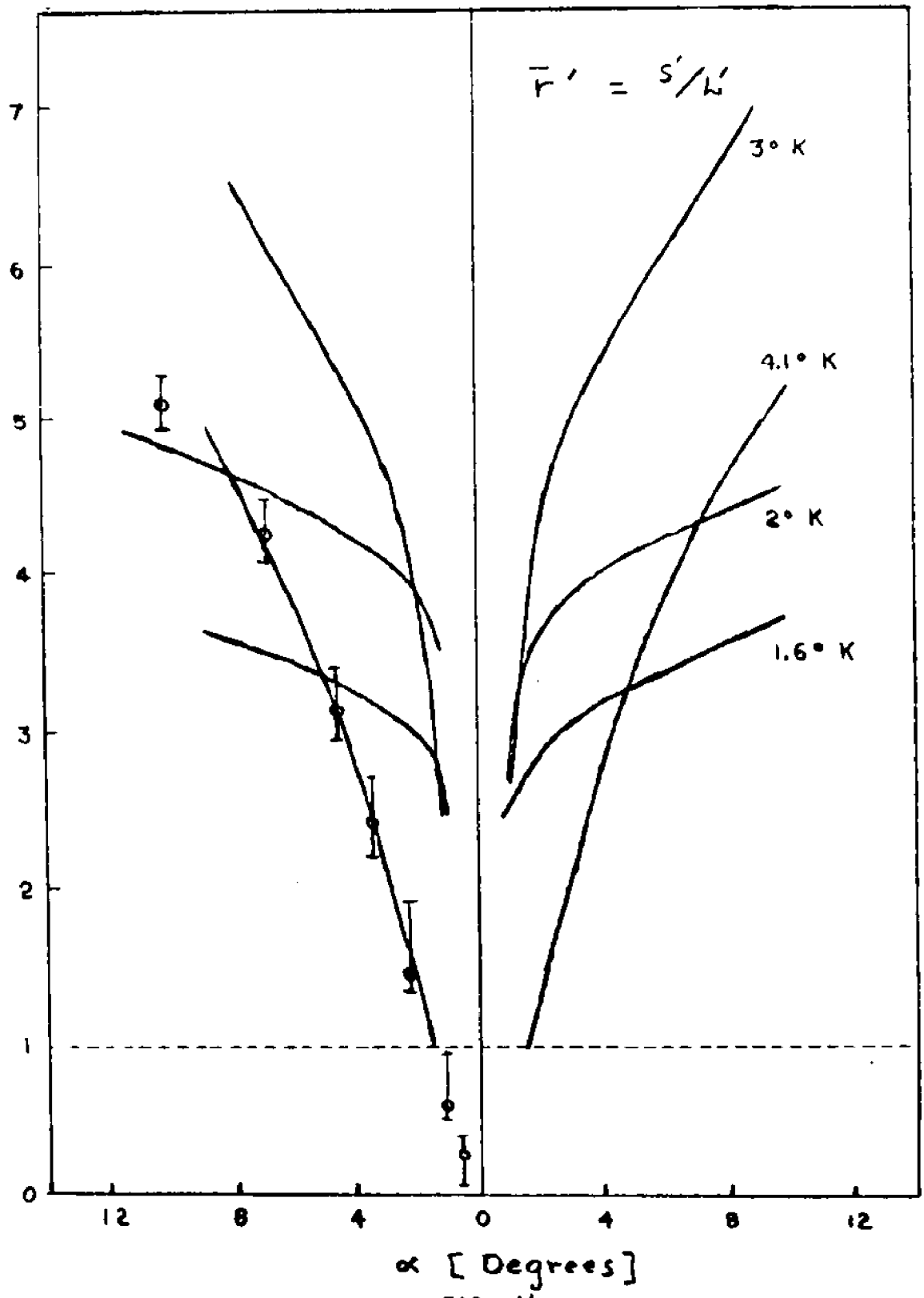

FIG. 14

The next step in the data analysis procedure is the determination of the ratio $\bar{r}'$ between the two slopes $S' = \sigma^{o} \sin^2\theta/\beta^2$ and

$$L' = \frac{\lambda^{o} \sin^2\theta + \lambda_g}{\beta'^2} \, L_n T$$

i.e., $\bar{r}' \approx (\sigma^{o}/\lambda^{o}) L_n T$. This ratio, in the case of negligible λ_g, leads to a reasonable determination of the average number of collisions necessary to have an efficient scattering. The values obtained for $\bar{r}'$ are listed in Table I and are also represented in Fig. 14. The estimated errors at $4.1^{o}K$ are indicated by error bars. The relative error increases as the angle α nears zero since the experimentally measured values near $\alpha = 0$ are small as are the slopes calculated from these values as may be seen in Fig. 13. Therefore, the ratio of the slopes carries a large absolute uncertainty near $\alpha = 0$ as compared to the data obtained at larger angles. The set of curves in Fig. 14 shows clearly that for all temperatures $\bar{r}'$ is of the order of a few unities for large α, indicating a poor efficiency of the scattering. The $\bar{r}'$ value falls to lower values as α nears zero, so as to form a dip in the representative curve. This implies that the scattering becomes more efficient over a small range of α around $\alpha = 0$.

It can also be seen that the width of the dip, i.e., the efficient scattering range increases with temperature. This

general behavior of the $\bar{r}'$ curves, i.e., the general behavior of the scattering efficiency is in agreement with the scattering mechanism outlined in the introduction and part D of the theory section, where it was seen that small angle phonon scattering becomes efficient when open orbit electrons are scattered into closed orbit states. The thinner the open orbit slice thickness Δk_z, the more probable it is for small q phonons to scatter electrons out of the slice. Indeed as Δk_z is decreased so as to be of the same order as or smaller than $\bar{q}$ (the mean phonon wave vector), the efficiency would approach unity. Since the open orbit slice thickness Δk_z is approximately proportional to the tilt angle α and since $\bar{q}$ is proportional to the temperature T, it can be understood that efficiency can be measured as α is varied as well as when T is varied. One may express this property by stating that the angular range of high efficiency will increase with the temperature so as to match the approximate euqation $\mu \cdot \Delta k_z \approx \bar{q}$. If one takes into account that the scattering displaces the electrons on the FS instead of in the k_z direction (except accidentally), one may use an averaged value for $\mu \approx 1.5$ to account for this topological feature. At $4.1^{\circ}K$ with $\bar{q} = 14 \times 10^6$ cm^{-1} the efficiency will be good, up to a value of $\Delta k_z \approx 10^7$ cm^{-1}, a slice thickness corresponding to a tilt angle of $\alpha \approx 2.5$ degrees.

The few degree range over which the dip of the $\bar{r}'$ curve extends, appears therefore quallitatively correct, even though

the proportionality of the dip's width with T does not materialize.

For large tilt angles where the scattering tends toward bulk scattering, the decrease in efficiency as T changes from 4.1°K to 3°K is characteristic of phonon scattering. As T decreases, an increasing fraction of the scattering is due to impurities and size. The better efficiency of these scattering processes is shown as a decrease in $\bar{r}'$ as T decreases to 2°K and 1.6°K.

As pointed out in the theory section, one might expect a better determination of the efficiency by studying the quantities, $H\rho_{xx}/\rho_{yx}^{(-)}$ and $H\gamma_{xx}/\gamma_{yx}^{(-)}$. This requires the determination of the corrected Hall effect,

$$\rho_{yx}^{(-)} = \frac{\rho_{yx}(+H) - \rho_{yx}(-H)}{2}$$

and the corrected Righi-Leduc effect,

$$\gamma_{yx}^{(-)} = \frac{\gamma_{yx}(+H) - \gamma_{yx}(-H)}{2}$$

It was found experimentally: 1) that these quantities were fairly linear in H as expected from Eq. 2' (see Fig. 15), 2) that $\rho_{yx}^{(-)}$ and $L_nT\,\gamma_{yx}^{(-)}$ were reasonably equal, and 3) that both were almost independent of the angle α and temperature T. This result is summarized in Fig. 16 where the average value of ρ_{yx}/H and $L_nT\,\gamma_{yx}/H$ are plotted vs the angle α for different

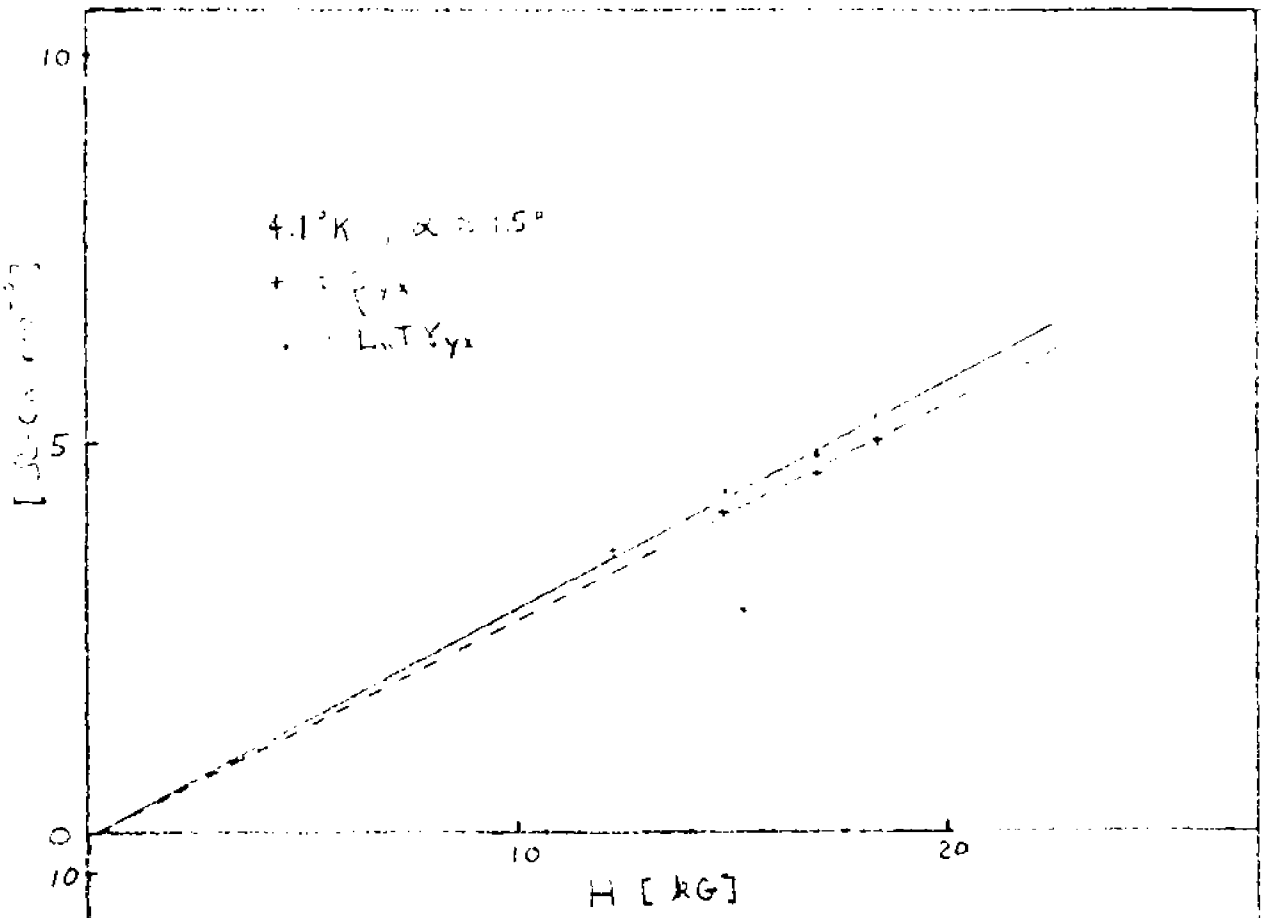

Fig. 15

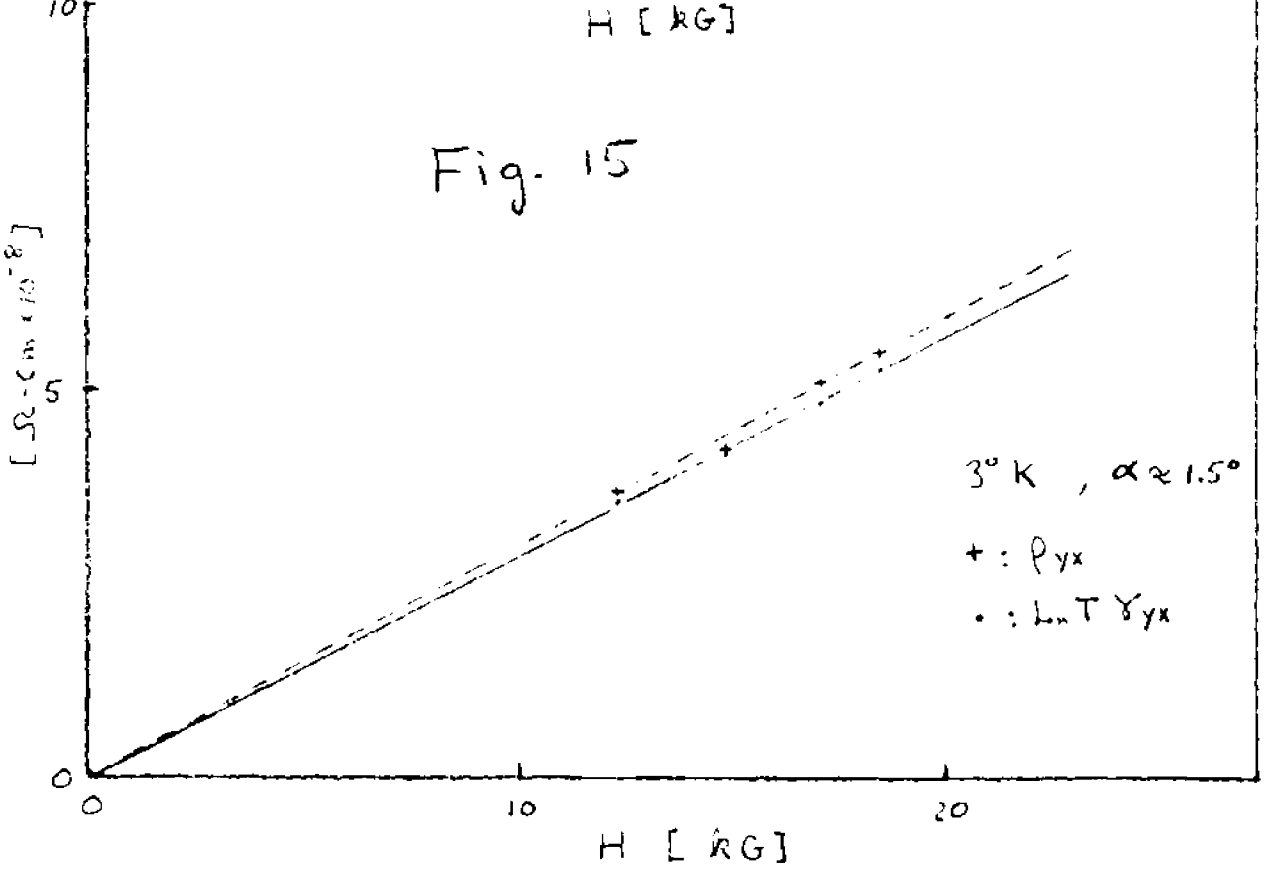

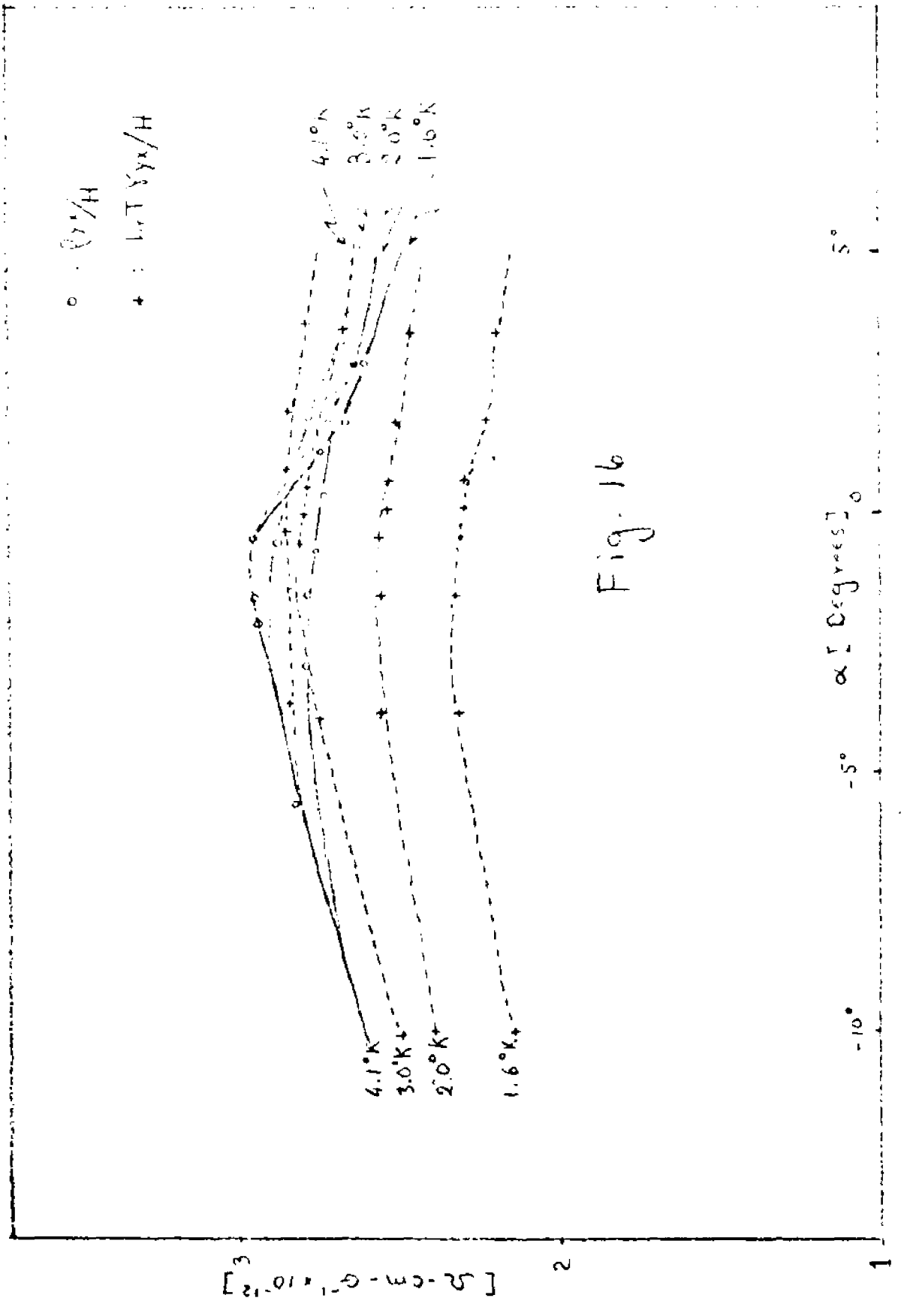
o : ρ_{yy}/H
+ : $1.T\ \rho_{yx}/H$
4.1°K
3.0°K
2.0°K
1.6°K
4.1°K
3.0°K
2.0°K
1.6°K
-10°
-5°
0
5°
α [degrees]
1
2
3
[Ω-cm - σ^{-1} x 10^{12}]

Fig. 16

temperatures. In Fig. 17 the same results are shown as a function of temperature for different tilt angles. One expects to obtain the value of $B = nec$ for $\alpha = 0$. Discounting the strange behavior of γ_{yx} at 2°K and 1.6°K, one gets $B^{-1} \approx 2.8 \times 10^{-12}$ ohm-cm/gauss or $n = 2.2 \times 10^{22}$. Some aspects of the Hall effect and Righi-Leduc effect will be reviewed in the discussion.

Using the experimentally determined $\rho_{yx}^{(-)}$ and $L_n T\, \gamma_{yx}^{(-)}$ quantities, the values of $H\rho_{xx}/\rho_{yx}^{(-)}$ and $H\gamma_{xx}/\gamma_{yx}^{(-)}$ were obtained and plotted vs H^2 to determine the slopes $S' = \sigma^{\circ}\sin^2\theta/B$ and $L'' = (\lambda^{\circ}\sin^2\theta + \lambda_g)/BL_nT$. In Fig. 18 the values of $H\rho_{xx}/\rho_{yx}^{(-)}$ as a function of H^2 at 2°K for three orientations are given. Similar curves corresponding to $H\gamma_{xx}/\gamma_{yx}^{(-)}$ are shown in Fig. 19. Table II lists the slope S'' and L'' as well as the ratio $\bar{r}''$ of these slopes. The representation of $\bar{r}''$ vs α for the different temperatures is seen in Fig. 20. No basic differences with Fig. 14 are found and the data analysis gave no real indication that the $\bar{r}''$ data were in any way superior to the $\bar{r}'$ data.

In the determination of $\bar{r}'$ or $\bar{r}''$ using the uncorrected slope (uncorrected for λ_g), the best that one may obtain is the quantity

$$\frac{\sigma^{\circ}\sin^2\theta}{\lambda^{\circ}\sin^2\theta + \lambda_g} L_nT$$

Since both $\sigma^{\circ}\sin^2\theta$ and $\lambda^{\circ}\sin^2\theta \to 0$ as $\alpha \to 0$, the value

$$\bar{r} = \left(\frac{\sigma^{\circ} L_nT}{\lambda^{\circ}}\right)\left(1 + \frac{\lambda_g}{\lambda^{\circ}\sin^2\theta}\right)^{-1} \simeq \frac{\omega_c}{\omega_{eff}}\left(1 + \frac{\lambda_g}{\lambda^{\circ}\sin^2\theta}\right)^{-1}$$

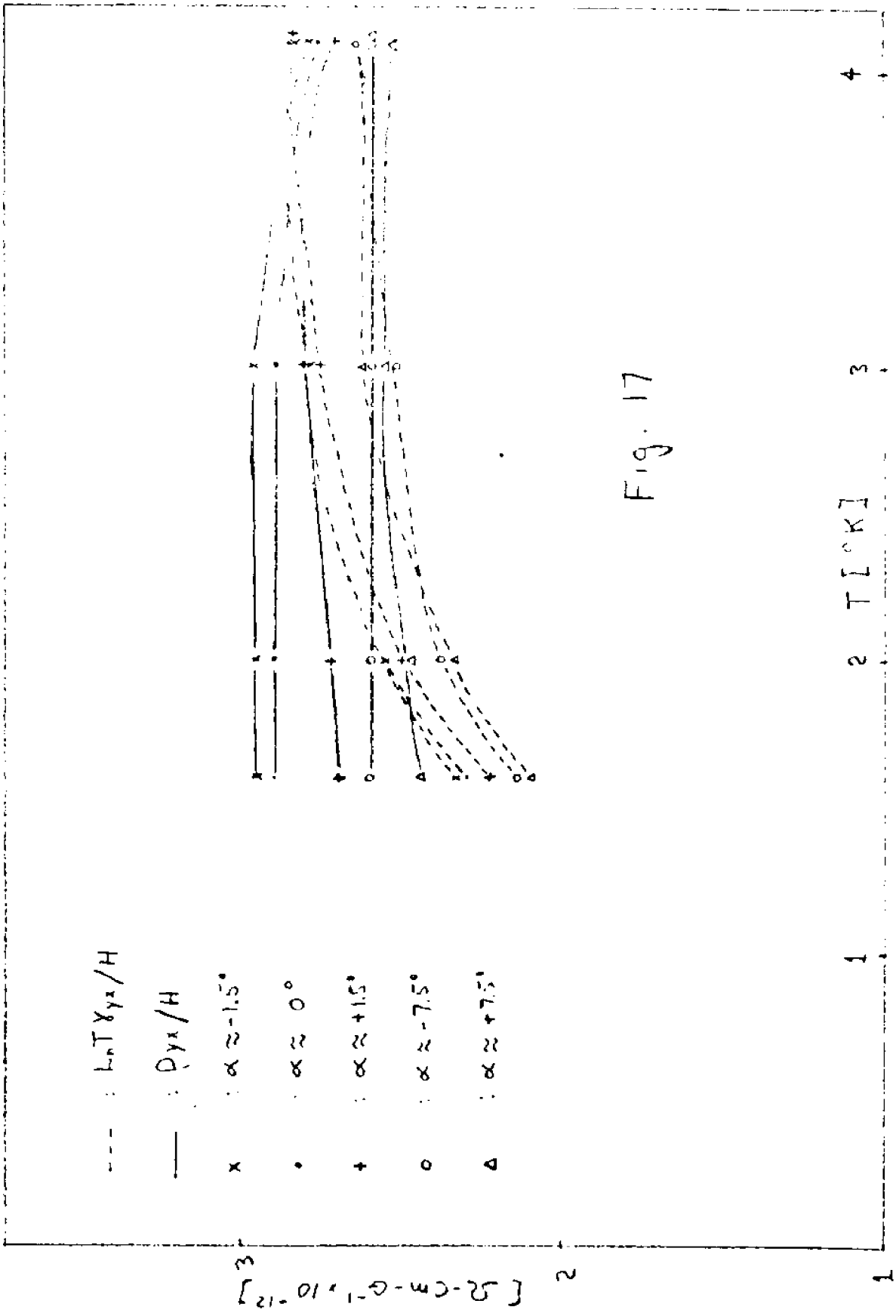
--- : $L_1 T \gamma_{yx}/H$
— : D_{yx}/H
x : $\alpha \approx -1.5°$
• : $\alpha \approx 0°$
+ : $\alpha \approx +1.5°$
o : $\alpha \approx -7.5°$
Δ : $\alpha \approx +7.5°$
$[\Omega\text{-cm}\cdot\text{G}^{-1}\cdot 10^{-12}]$
3
2
1
T [K]
1
2
3
4

Fig. 17

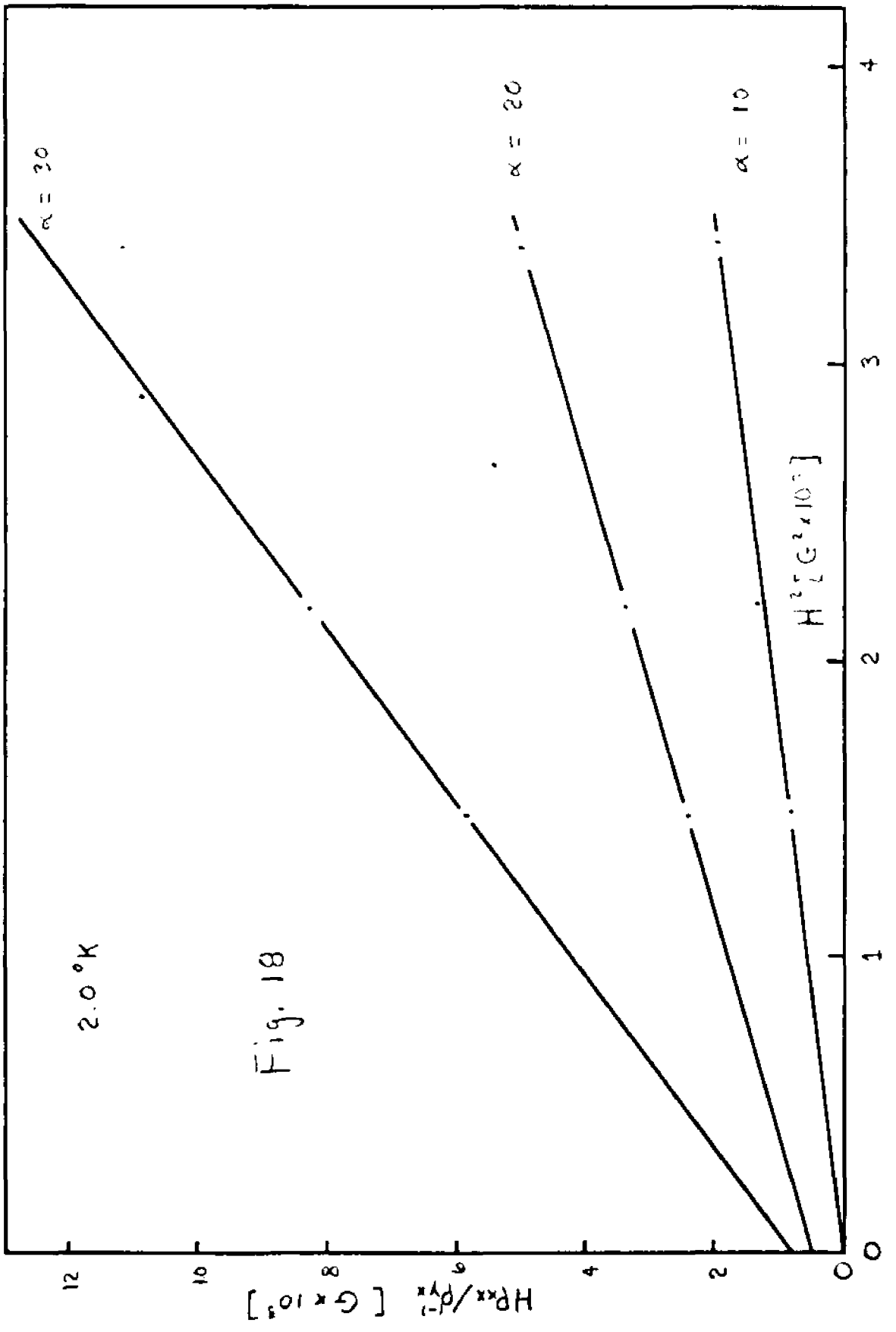

Fig. 18

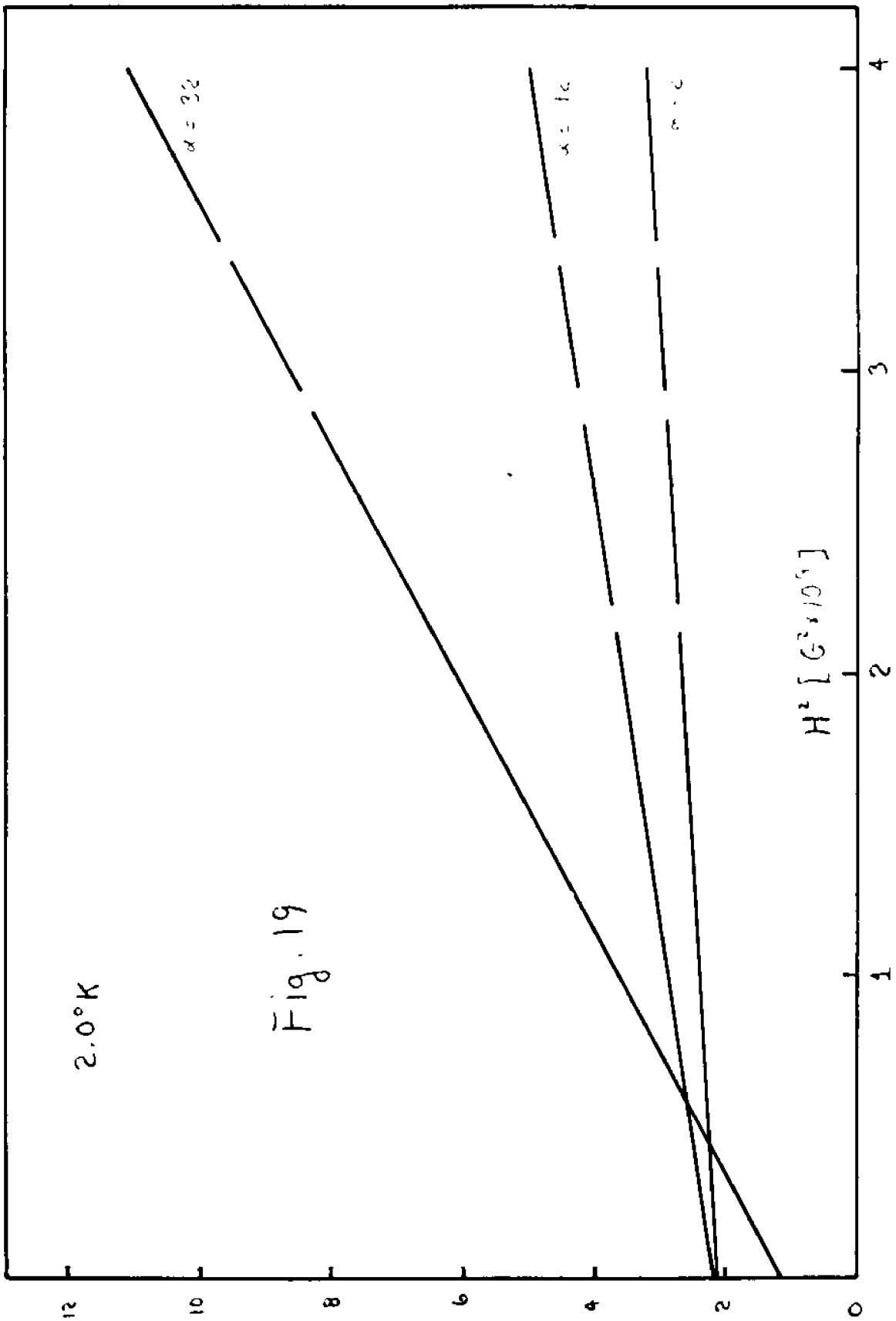

Fig. 19

TABLE II. S'' and L''[Ω-cm-G^{-2} X 10^{-16}]

α	4.1°K S''	4.1°K L''	4.1°K $\bar{r}$''	3.0°K S''	3.0°K L''	3.0°K $\bar{r}$''	2.0°K S''	2.0°K L''	2.0°K $\bar{r}$''	1.6°K S''	1.6°K L''	1.6°K $\bar{r}$''
0	---	0.44	---	0.05	0.25	0.20	0.20	0.07	2.86	0.25	0.20	1.25
10	0.09	0.47	0.19	0.45	0.37	1.22	1.10	0.4	2.75	1.40	0.60	2.33
20	0.41	0.56	0.73	1.50	0.62	2.42	2.70	1.12	2.41	3.60	1.50	2.40
30	0.90	0.70	1.29	3.00	0.93	3.22	5.30	1.95	2.72	6.60	2.80	2.36
40	1.43	0.90	1.59	4.90	1.30	3.77	8.30	2.84	2.92	10.2	4.40	2.32
50	2.15	1.10	1.95	6.80	1.65	4.12	11.8	3.75	3.15	14.2	6.10	2.33
60	3.00	1.30	2.31	9.00	2.00	4.50	15.8	4.80	3.29	18.7	7.90	2.37
70	3.95	1.50	2.63	11.3	2.42	4.67	20.0	5.90	3.45	23.7	9.70	2.44
80	4.85	1.71	2.84	14.0	2.75	5.09	24.8	7.00	3.54	29.5	11.6	2.54
90	6.05	1.92	3.15	17.1	3.15	5.43	29.-	8.12	3.66	35.7	13.5	2.64
100	7.25	2.14	3.39	20.4	3.52	5.80	35.0	9.35	3.74	41.7	15.5	2.69
110	8.65	2.36	3.66	24.0	3.92	6.12	40.7	10.6	3.84	48.0	17.5	2.74
120	10.3	2.59	3.98	27.8	4.30	6.46	46.7	11.8	3.96	55.2	19.5	2.83
130	11.9	2.82	4.22	31.4	4.70	6.68	53.2	12.9	4.22	62.0	21.4	2.90
140	13.4	3.02	4.44	35.4	5.10	6.94	59.5	14.2	4.19	69.5	23.4	2.97
150	15.1	3.22	4.69	39.2	5.50	7.13	65.7	15.4	4.27	76.5	25.3	3.02
160	16.8	3.43	4.90	43.3	---	---	72.0	16.6	4.34	83.5	27.2	3.07
170	18.5	3.65	5.07	47.8	---	---	78.5	---	---	91.0	---	---
180	20.4	---	---	---	---	---	---	---	---	97.5	---	---

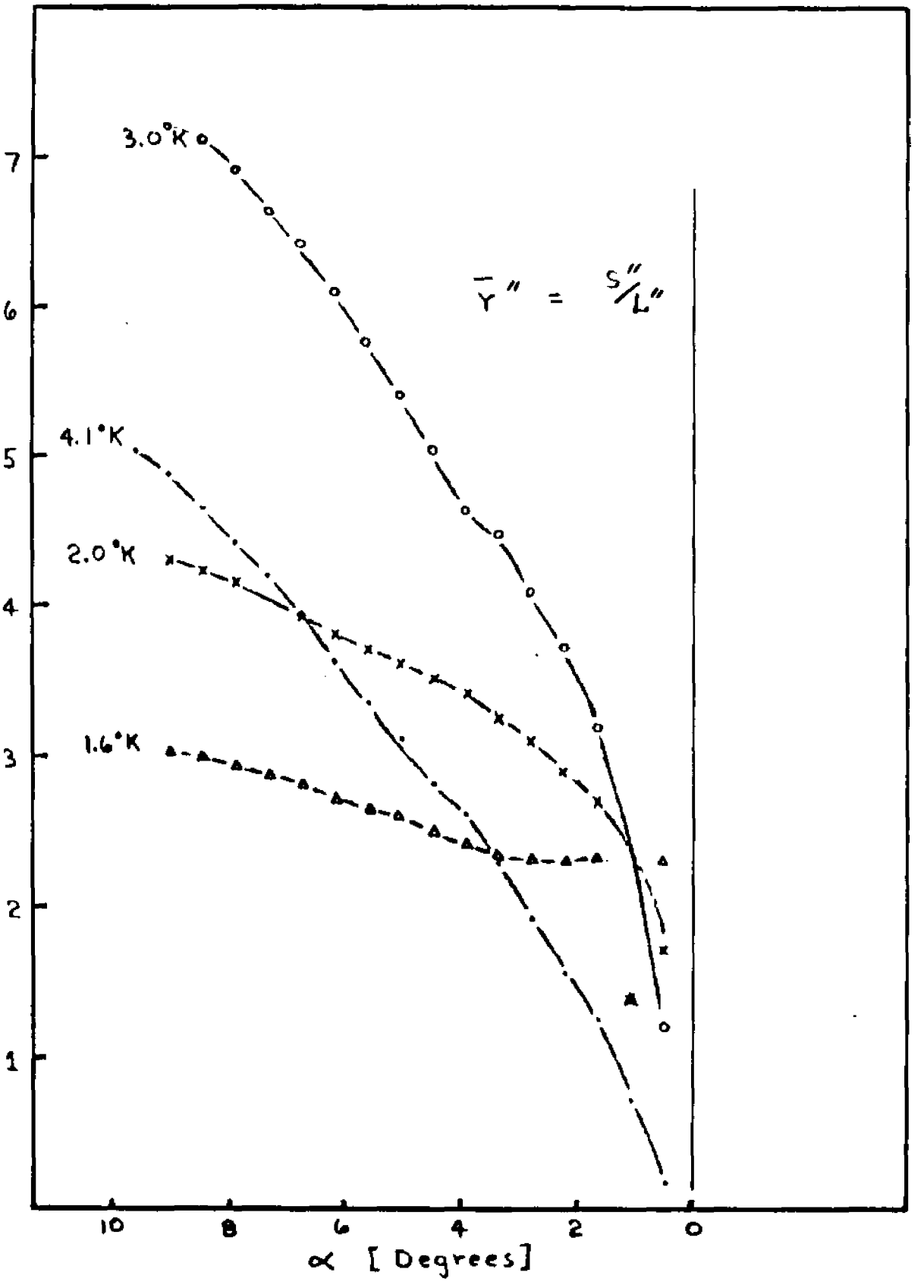

FIG. 20

does not give the expected value ω_c/ω_{eff}, but rather that value divided by the term $1 + \lambda_g/\lambda^o \sin^2\theta$ which increases to infinity as $\lambda^o \sin^2\theta \rightarrow 0$. Thus, the dip in the r curve could be due to the lattice conductivity. It is therefore essential that the value of λ_g be known or at least approximated so as to ascertain the otherwise precarious conclusion relative to the small angle scattering mechanism.

The first approximation of λ_g was made in the following way. The minimum value for the slope, L_0', should occur for $\alpha = 0$ and is in principle given by $L_0' = \lambda_g L_n T/B'^2$ from which one obtains $\lambda_g = L_0' B'^2/L_n T$. The precision of L_0' is very poor and an upper value for λ_g is given by $\lambda_g = 5.3 \times 10^{-3}\ T^2$ W-cm/°K, which is a rather large value for a phonon system scattered by metallic electrons.

The second approximation was attempted through the use of the formula,[20] $\lambda_g = 313(T/\theta)^4\ N_a^{-4/3}\ \lambda_i$ using the value for the phonon limited thermal conductivity of the electrons derived from Zavaritskii's[21] data and an approximated determination of N_a from the results of the work of Garfinkel and Lindenfeld.[22] This second approximation, which yields the set of values for λ_g of 5, 7, 15 and 22 $\times 10^{-3}$ W-cm/°K for 1.6, 2.0, 3.0, and 4.1°K, respectively, is nearer the expected order of magnitude. In view of the relatively good success of the formula as shown by Garfinkel, it is thought that the first approximation is too high. It is likely that the high L_0' value could be due to an effect similar to the effect which produces an unexpected non-zero value for S_0'. The

existence of the many saddle points[23] in the open orbit zone may be responsible for this behavior. It should also be pointed out that in the theory which led to the value $\lambda^{\circ}L_nT/B'^2$ for $L' - L'_o$ all second order effects were neglected, and it is likely that the term $\lambda^{\circ}L_nT/B'^2$ could be smaller or of the same order as those neglected second order terms.

Using the second approximation values for λ_g, the correction was introduced in the $\bar{r}'$ data and corrected values

$$\bar{r}' = S'\left(L' - \frac{\lambda_g L_n T}{B'^2}\right)^{-1}$$

were calculated. Figure 21 shows a plot of $\bar{r}_c'$ vs α. There appears to be no significant change in the $\bar{r}'$ values when the lattice thermal conductivity is taken into account. As should be expected, the $\bar{r}'$ value is increased at small tilt angles by taking into account λ_g, but the general shapes of the curves are unchanged. In contrast, the use of the first λ_g approximation yields $\bar{r}_c'$ values approaching infinity as $\alpha \to 0$ for $T < 3.0^{\circ}K$. This is an obvious overcorrection and results in an artificial suppression of the dip. In spite of this overcorrection however, the dip in the $\bar{r}_c'$ curve still remains at $4.1^{\circ}K$. In Table III the values for $\bar{r}_c'$ are given for the two cases. The adopted values are listed in the first column and the over-corrected values are listed in the second column.

TABLE III. $\bar{r}_c'$: ratio of slopes corrected for λ_g

Position	4.1°K		3.0°K		2.0°K		1.6°K	
	λ_g 2.1×10^{-2}	λ_g 9×10^{-2}	λ_g 1.4×10^{-2}	λ_g 4.7×10^{-2}	λ_g 0.72×10^{-2}	λ_g 2.1×10^{-2}	λ_g 0.46×10^{-2}	λ_g 1.3×10^{-2}
0	0	0	1.67	∞	12.5	∞	10.0	∞
10	0.294	0.60	3.15	8.55	4.49	6.14	2.50	2.85
20	0.786	1.25	3.86	5.55	3.41	3.71	2.76	2.88
30	1.22	1.72	4.46	5.47	3.57	3.75	2.76	2.83
40	1.67	2.18	4.72	5.36	3.84	3.97	2.94	2.99
60	2.51	3.00	5.56	6.02	3.87	3.94	3.05	3.08
80	3.16	3.63	5.73	6.05	4.08	4.13	3.26	3.29
100	3.75	4.18	5.74	5.96	4.21	4.25	3.32	3.34
120	4.28	4.68	6.15	6.33	4.30	4.33	3.46	3.47
140	4.75	5.12	6.74	6.91	4.40	4.43	3.53	3.54
160	5.01	5.35	7.06	7.20	4.50	4.52	3.67	3.68
180	5.31	5.62	7.46	7.59	4.63	4.65	3.77	3.78

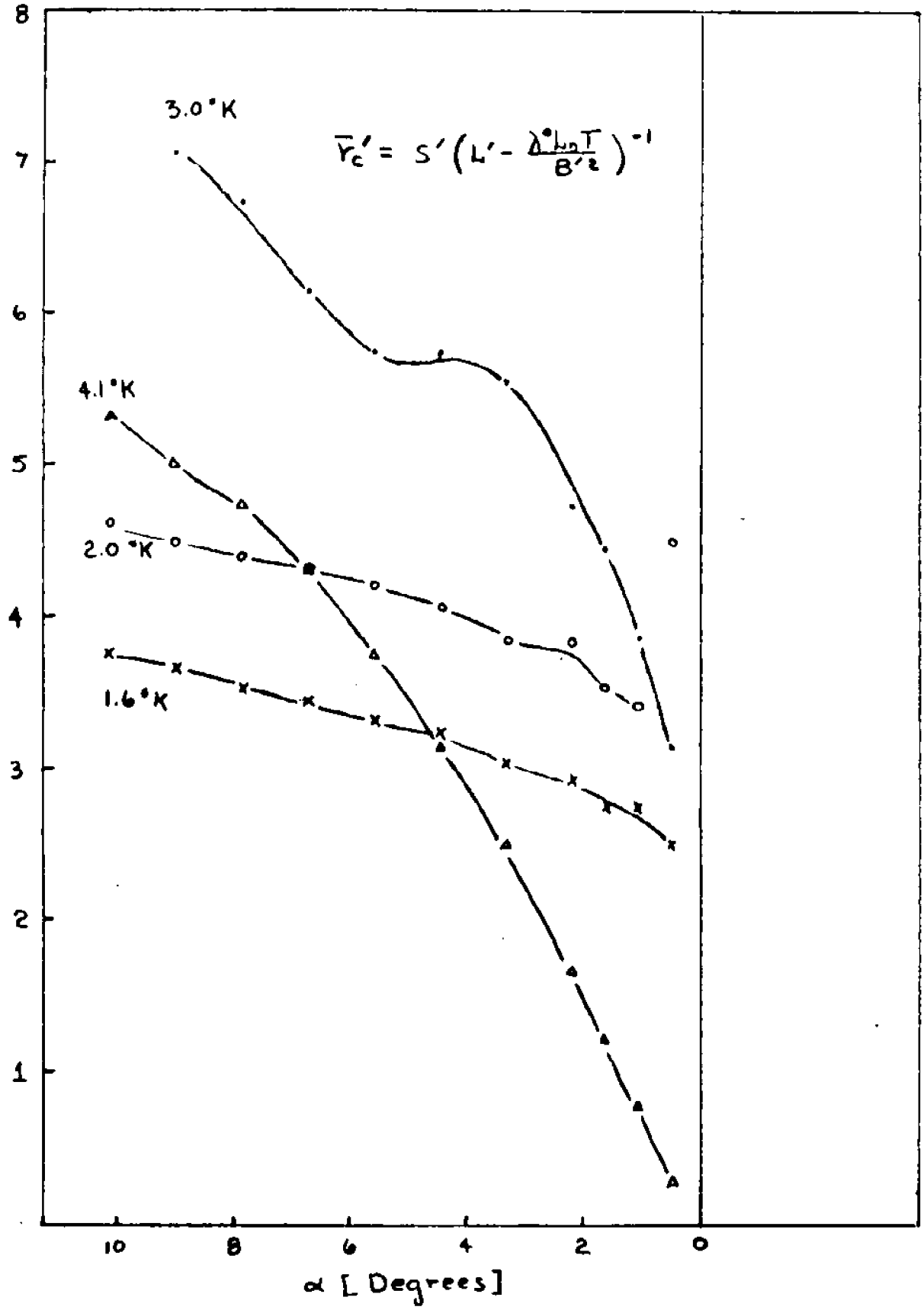
3.0°K
$\bar{r}_c' = s'\left(L' - \frac{\Delta^* \ln T}{B'^2}\right)^{-1}$
4.1°K
2.0°K
1.6°K
8
7
6
5
4
3
2
1
10
8
6
4
2
0
α [Degrees]

FIG. 21

V. DISCUSSION

The discussion of the results will be divided into two basic topics. Part A will include a discussion of the precision of the experimental measurements, the degree of error introduced by some of the approximations and an appraisal of the precision of the derived quantities. In Part B the validity of some of the hypotheses used in the theory will be discussed and an attempt is made to interpret the results in terms of electron phonon scattering. The meaningfulness of these interpretations are discussed in relation to the precision and to the complexity of the F.S. topology and the phonon distribution.

A brief discussion of the possibility of extending this study to other metals with open orbit electrons follows Part B.

A. Precision of the Measurement and of the Quantities Derived from those Measurements

1. Precision of the "raw" data. Readings of certain parameters necessary in the gathering or calculation of the experimental data were made with sufficient precision as to warrant no cause for concern. These are the magnitude of the magnetic field, H, the temperature of the crystal, T, the dimensions of the sample, the electric current through the sample, and the thermal current density. Other parameters may be subject to trivial errors, i.e.,

errors which do not limit the validity of the experiment. Such parameters are, for example, the distance between the electric contact points and/or the thermal contact points. Errors in the determination of these distances do not affect the comparative study of the different effects.

The main problem in the raw data precision is in the potentiometric voltage measurements and in the determination of the temperature gradients. The noise level limits the absolute precision of any voltage measurement to approximately 5×10^{-9} volts. This error is independent of α, T, and H. Therefore, in the determination of the slope, S', of ρ_{xx} vs H^2 one may expect, on the average, the same absolute error independent of α and T. The relative errors $\Delta S'/S'$ would therefore depend on the magnitude of S' and become very large as α approaches zero since S' approaches zero also. The same may be said of the determination of L and large relative errors $\Delta L/L$ appear near $\alpha = 0$.

The calculated ratio S'/L' will thus be known with very poor absolute precision as $\alpha \to 0$, i.e., for orientations where one would wish to have better precision.

2. Errors due to departure from ideal experimental conditions. These errors are due basically to misorientation and may be classified as follows:

a) The coordinate systems 1,2,3 and 1',2',3' are not identical.

b) The coordinate axes, 1, 1', x, and u are not identical

and the definitions of the currents J and W must be specified in each of the different systems.

c) The axes 3' and/or z are not horizontal, resulting in a non-vanishing slice thickness for $\alpha = 0$ and in a dependence of $\sin^2\theta$ on α rather than $\sin^2\theta = 1$.

d) The axes 3 and/or z are not horizontal, resulting in a current component J_z. This effect is fortunately not critical and is mentioned in Appendix A.

e) The rotation of the magnet does not yield identical directions for + H and - H, i.e., $z(\alpha + 180^\circ) \neq z(\alpha)$. The most important errors in this case are that $\sigma^o(\alpha + 180^\circ)$ does not correspond to $\sigma^o(\alpha)$ and that the angles $\theta(\alpha + 180^\circ)$ and $\theta(\alpha)$ also differ leading to unmatched values for $\sigma^o \sin^2\theta$.

f) The same predicament exists if the different sets of coordinates have shifted from one experiment to the next, i.e., for different temperatures or between corresponding γ and ρ measurements.

Most of the errors listed under part 2 affect the validity of the equations which give $\bar{r}'$ and $\bar{r}''$.

3. <u>Validity of the equation with regards to the approximations made</u>. The formula $\hat{\sigma}^T = \hat{\sigma}^c + \hat{\sigma}^o$ may be first considered valid with the following approximations made to obtain Eq. A-13.

a) If $\vec{u}$ is considered fixed relative to the asymptotic conditions (see Appendix A), then the value

$$\hat{\sigma}^e = \begin{pmatrix} \sigma^e & 0 \\ 0 & 0 \end{pmatrix}$$

in the fixed coordinate system, (u,v), is to be modified in the form

$$\hat{\sigma}^{o} = \begin{pmatrix} \sigma^{o} & -AH^{-1} \\ AH^{-1} & 0H^{2} \end{pmatrix}$$

Appendix B shows that this does not lead to a modification in the form of Eq. A-13. It does, however, lead to a re-evaluation of the coefficients A and B as shown in Appendix C and possibly to the accidental introduction of a small field dependent term in the σ^{o} coefficient.

b) The use of H^2 in the high field limit should, in the first approximation be replaced by $H^2 + H_s^2$ where $H_s = cm_s^*/e\tau_s$ does not change the expected slope but does affect the intercept.

c) The isotropic form of $\hat{\sigma}^{c}$ is valid for very small α but inexact for the larger angles. In the $(\vec{u},\vec{v})$ system $\hat{\sigma}^{c}$ may be reapproximated by

$$\hat{\sigma}^{c} = \begin{pmatrix} \sigma_{uu}^{c} & \sigma_{uv}^{c} \\ -\sigma_{uv}^{c} & \sigma_{vv}^{c} \end{pmatrix}$$

with $\sigma_{uu}^{c} \neq \sigma_{vv}^{c}$, i.e., by a new isotropic tensor plus the tensor

$$\begin{pmatrix} \sigma_{uu}^{c} - \sigma_{vv}^{c} & 0 \\ 0 & 0 \end{pmatrix}$$

of the same approximate form as $\hat{\sigma}^{o}$. One of the effects of this would be the apparent introduction in $\hat{\sigma}^{o}$ of small field dependent

(H^{-2}) terms (as in case 3-a). The extrapolation to $H^2 = 0$ of the ρ_{xx} vs H^2 curves depend on the tilt angle and may be in part caused by this effect.

d) The successive simplification of the denominator from Eq. A-10 to A-11 and primarily from Eq. A-11 to Eq. A-13 depends on the condition $A\sigma^{\circ} \ll B^2$. An a posteriori evaluation of this quantity justifies this approximation. The largest error should occur at 4.1°K for ρ_{xx} at the maximum tilt angle. An upper limit under these conditions for $A\sigma^{\circ}/B^2$ is $\approx .2$.

e) In the thermal case the same problems raised in 3-a,b,c and d will occur with an additional problem due to the lattice conduction. The incidence of λ_g is two-fold, coming first of all in the denominator of Eq. A-15, where instead of the condition (3-d) of $\sigma^{\circ}A \ll B^2$ one would like $(\lambda_0 + 2\lambda_g)A' + \lambda_g(\lambda_g + \lambda_0)H^2 \ll B'^2$. The relatively good linearity of γ_{xx} vs H^2 seems to indicate that at least the term $\lambda_g(\lambda_g + \lambda_0)H^2 \ll B'^2$. An upper limit under the worst conditions would be $\lambda_g(\lambda_g + \lambda_0)H^2B'^{-2} \approx 8\%$ for the largest tilt angle. The second incidence of λ_g is in the numerator of Eq A-15. The implications of this are discussed in the chapter on experimental results.

f) The determination of B and B' depend on the same approximations made to determine σ° and λ° in paragraphs 3-b,c, and d. For $\sin^2\theta = 1$, one has approximately

$$B^{-1}H = 1/\sigma_{12} \approx \rho_{yx}(1 + \sigma_{11}\rho_{xx})$$

and

$$1/\sigma^{o} \approx \left(\rho_{yx}^{2} / \rho_{xx}\right)\left(1 + \sigma_{11}\,\rho_{xx}\right)$$

i.e., $\sigma_{12}/\sigma^{o} = \rho_{yx}/\rho_{xx}$ which is similar to the last equation in A-12 with the A/B term neglected.

B. Validity of the Hypotheses

The approximations made on the form $\hat{\sigma}^{T} = \hat{\sigma}^{o} + \hat{\sigma}^{c}$ can always be considered exact when the proper assignment of $\hat{\sigma}^{o}$ and $\hat{\sigma}^{c}$ is made. This is not difficult when one considers that the conductivities are independent of each other. Complications arise when one considers the case of possible "band" to "band" interactions between open orbit "band" and closed orbit "bands." In the present situation one aspect of this problem was considered when the scattering of open orbit electrons to the closed orbit band was taken into account under the simplifying hypothesis that the scattered electrons were simply eliminated from any contribution to the conduction. This is, in a sense, an extension of the concept of independent contribution since the effect on $\hat{\sigma}^{c}$ of the scattered open orbit electrons was simply neglected. The reverse interaction was also simplified by the hypothesis that electrons were "created" uniformly from the scattering from the closed orbit band into the open orbit region which is, in a way, an extension of the independent contribution concept.

Another neglected problem relates to one aspect of phonon drag. Besides the fact that drag affects each electron band independently, to the first order, the mutual drag implies that the phonon system is dragged by the combined effect of both bands. Therefore, the effect of this compound phonon drag on either of the electron bands will be affected by the other. Qualitatively speaking, one open orbit electron would displace the phonon system by a larger amount than one closed orbit electron would. However, since there are a smaller number of open orbit electrons, the drag is heavily controlled by the closed orbit electrons. In other words, the phonons dragged by the open orbit electrons relax mainly on the other electrons so that the phonon system appears, to the open orbit electron, to be almost in the equilibrium state.

The qualitative argument given above seems to minimize this aspect of the drag on the open orbit. This is further justified by other arguments as noted in Appendix D.

A rigorous study of the scattering is out of the question in such a complex case, and the test of the different hypotheses and suggested mechanisms are made through the usual phenomenological time of relaxation simplifying concepts. Even in the use of such simplifying quantities, there is room to argue the way those quantities relate to the different scatterings and special mechanisms.

The most simplified forms of scattering, introduced in Part D of Chapter II, were sufficient to demonstrate the Pippard mechanism, but it remains to be seen to what extent further analysis could be

performed on the existing data. For example, one might attempt to separate the phonon and impurity scattering and see how well the temperature and angular dependence fits the expected results.

If one assumes additivity of the scattering frequency, then one has

$$\omega_{eff} = \omega_{imp} + \omega_{\rho}^{eff}$$

and (8)

$$\omega_c = \omega_{imp} + \omega_{\rho}^{c}$$

where ω_{ρ}^{eff} and ω_{ρ}^{c} are the scattering frequency by phonons in the electrical and thermal case, respectively, and ω_{imp} is the impurity scattering frequency. If one assumes the open orbit slice thickness to be large compared to the phonon momentum, i.e., $\Delta k_z > \bar{q}$, then the scattering displaces the electrons on the F.S. through small, random steps. Thus, diffusion theory may be applied which results in $\omega_{\rho}^{eff} \sim bT^5$ and $\omega_{\rho} \sim b'T^3$. Since ω_{imp} will be constant then one gets

$$\omega_{eff} \approx 1/\sigma_0 \approx 1/S' = a + bT^5$$
$$\omega \approx L_0 T/\lambda_0 \approx 1/(L'-L'_0) = a + b'T^3 \qquad (9)$$

The values of S'^{-1} and $(L' - L_0')^{-1}$ are shown in Figs. 22a and 22b in a log-log plot for different orientations. For low T each curve should saturate to a value a indicated by arrows on the left side of the S'^{-1} curves. As T increeases, the slope of the curves should tend toward 5 for the S'^{-1} and 3 for the $(L' - L_0')^{-1}$ curves when the scattering corresponds to the bulk case. Qualitative agreement is seen except for small angles in the $(L' - L_0')^{-1}$ curves. One might, at first thought, attribute this descrepancy to a poor correction of λ_g, but calculations indicate that no self-consistent adjustment in λ_g will correct for this. Some source of error other than λ_g must be the cause of it. Empirical correction can be made by extrapolation using other temperature data points and an adjusted temperature power law as schematized in Fig. 23b.

The phonon part of the scattering is shown in Figs. 23a and b where $S_p'^{-1} = (S'^{-1} - a)$ and $L_p'^{-1} = \{(L' - L_0')^{-1} - a\}$ are plotted versus T on a log-log scale. From Eq. 9, those quantities should be respectively proportional to ω_p^{eff} and ω_p, the relaxation frequency of electrons on the phonon system in the electrical and thermal case, respectively. For most of the orientations, the $L_p'^{-1}$ curves follow approximately a power law $b'(\alpha)T^{\beta(\alpha)}$ with $\beta(\alpha) \sim 2.45$ practically independent of α. This is smaller than the expected T^3 law but the independence with α agrees with the identification of ω with ω_c, the collision frequency in the thermal case.

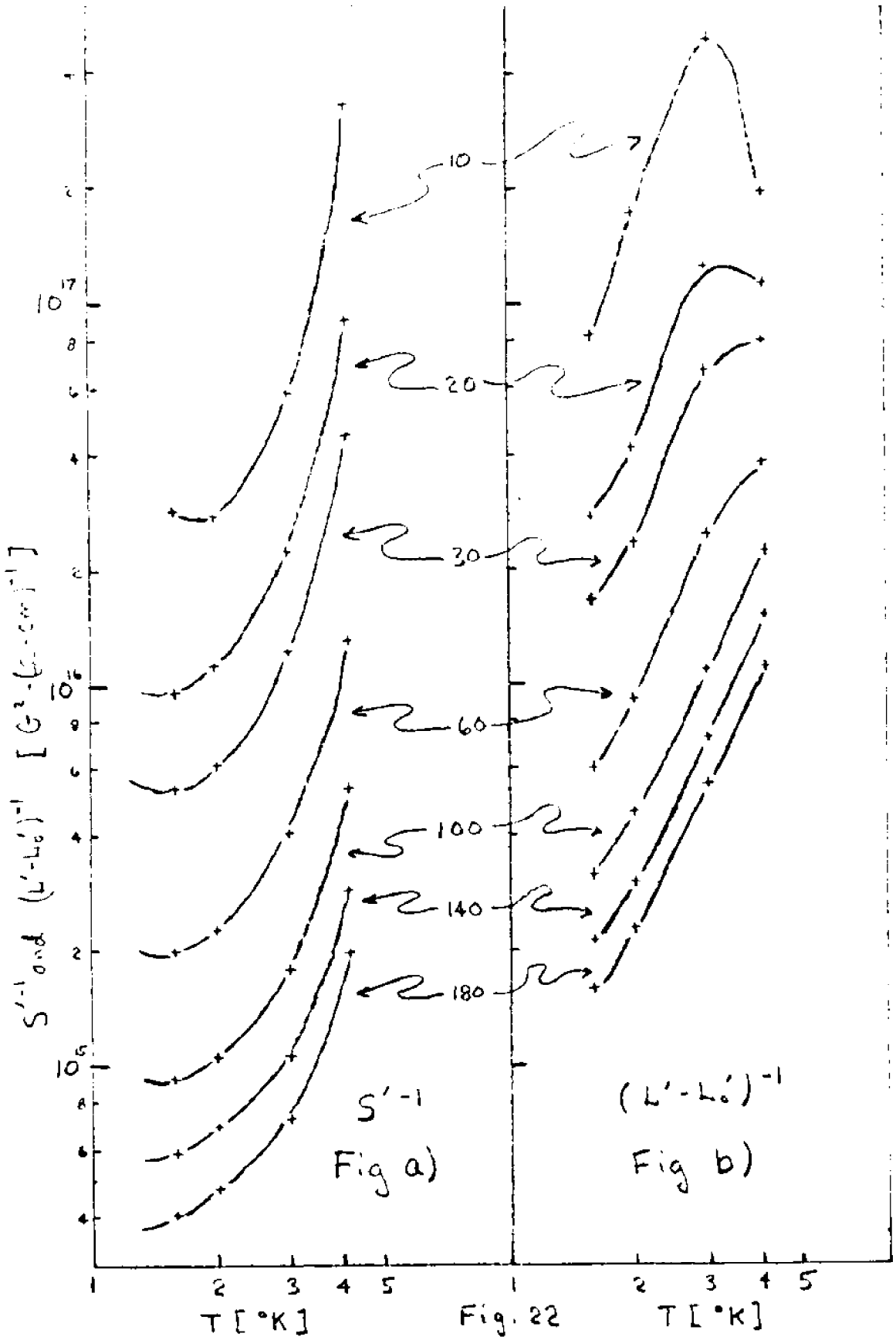

Fig. 22

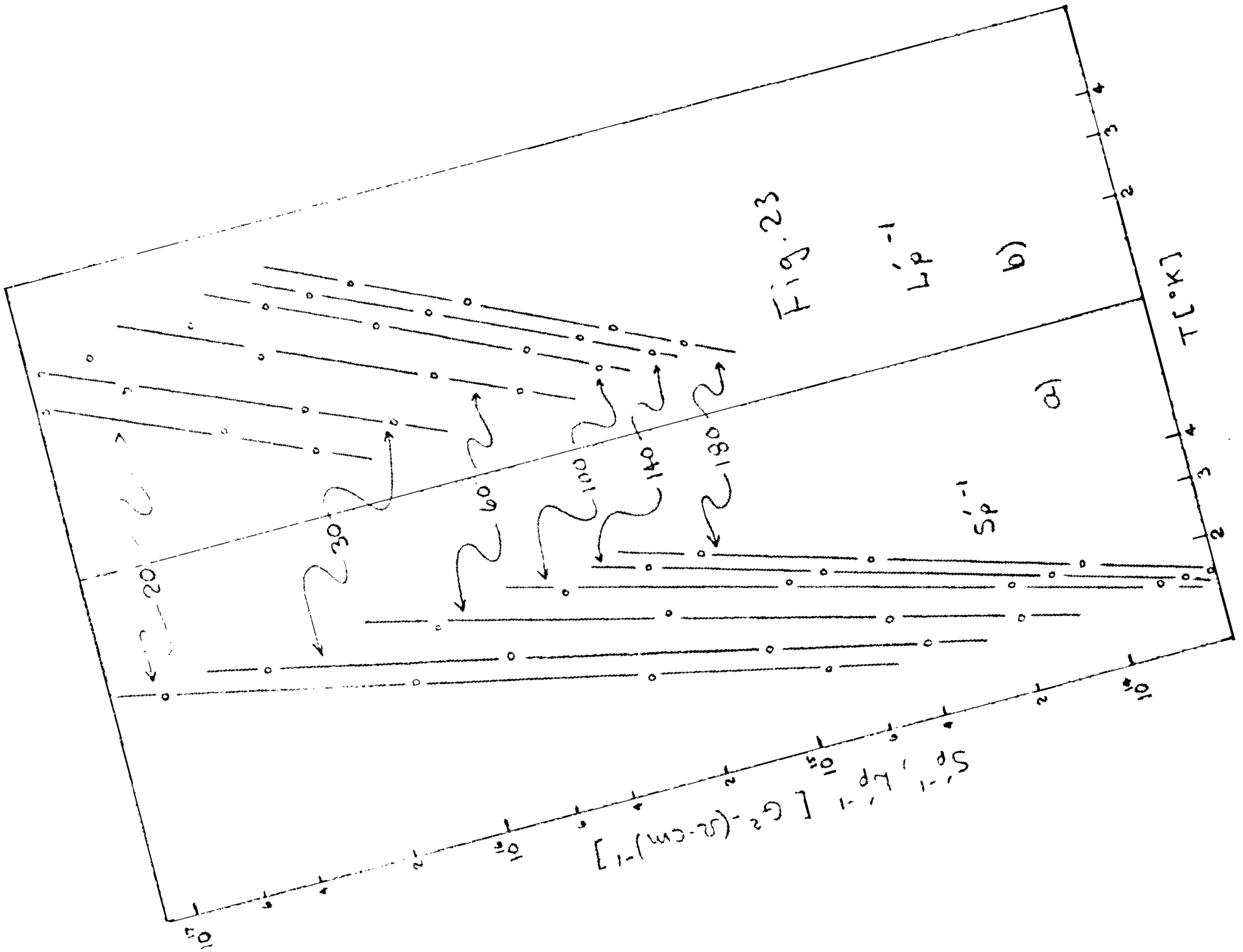
Fig. 23
a)
b)
$S_p'^{-1}$
$L_p'^{-1}$
T [°K]
20
30
60
100
140
180
$S_p'^{-1}$, $L_p'^{-1}$ [Ω^{-1}(Ω-cm)$^{-1}$]

The results for $(S'^{-1})_p$ follow almost the bulk T^5 law for the phonon scattering contribution to σ^o with a T exponent ≈ 4 for large α and ≈ 4.8 for small α. This result is in apparent contridiction with the idea of a more efficient scattering (T^3) for small α.

The impurity coefficient, a, depends on α. The inverse of this quantity, $a^{-1}(\alpha)$, referred to as S'_{imp} should give an indication of the variation of $\sigma^o(\alpha)$ if impurities were the only scatterers. As seen in Fig. 24, S'_{imp} does not decrease linearly with α, an indication that the impurity scattering may be more efficient for smaller α, or that due to misalignment one must consider the term $\sigma^o \sin^2\theta$ in which σ^o tends toward a finite value and $\sin^2\theta$ tends to zero as α^2.

Figures 25 and 26 illustrate the efficiency of the phonon scattering in the open orbit slice as a function of the angle α The data shown in Fig. 23 have been used and the ratio $\bar{r}_p = L_p'^{-1}/S_p'^{-1}$ represent, in principle, the number of collisions by phonons only, needed to scatter an open orbit electron into an adjacent band. Again $\bar{r}_p$ decreases as the open orbit slice thickness decreases, but does not tend toward unity as expected. This may be due to misallgnment which would prevent the slice thickness going to zero, but may also be due to the non-additivity of scattering frequencies ($\omega^{eff} \neq \omega_p^{eff} + \omega_{imp}$).

Any succession of collisions by phonons which terminate by an impurity scattering are classified as impurity scattering and do

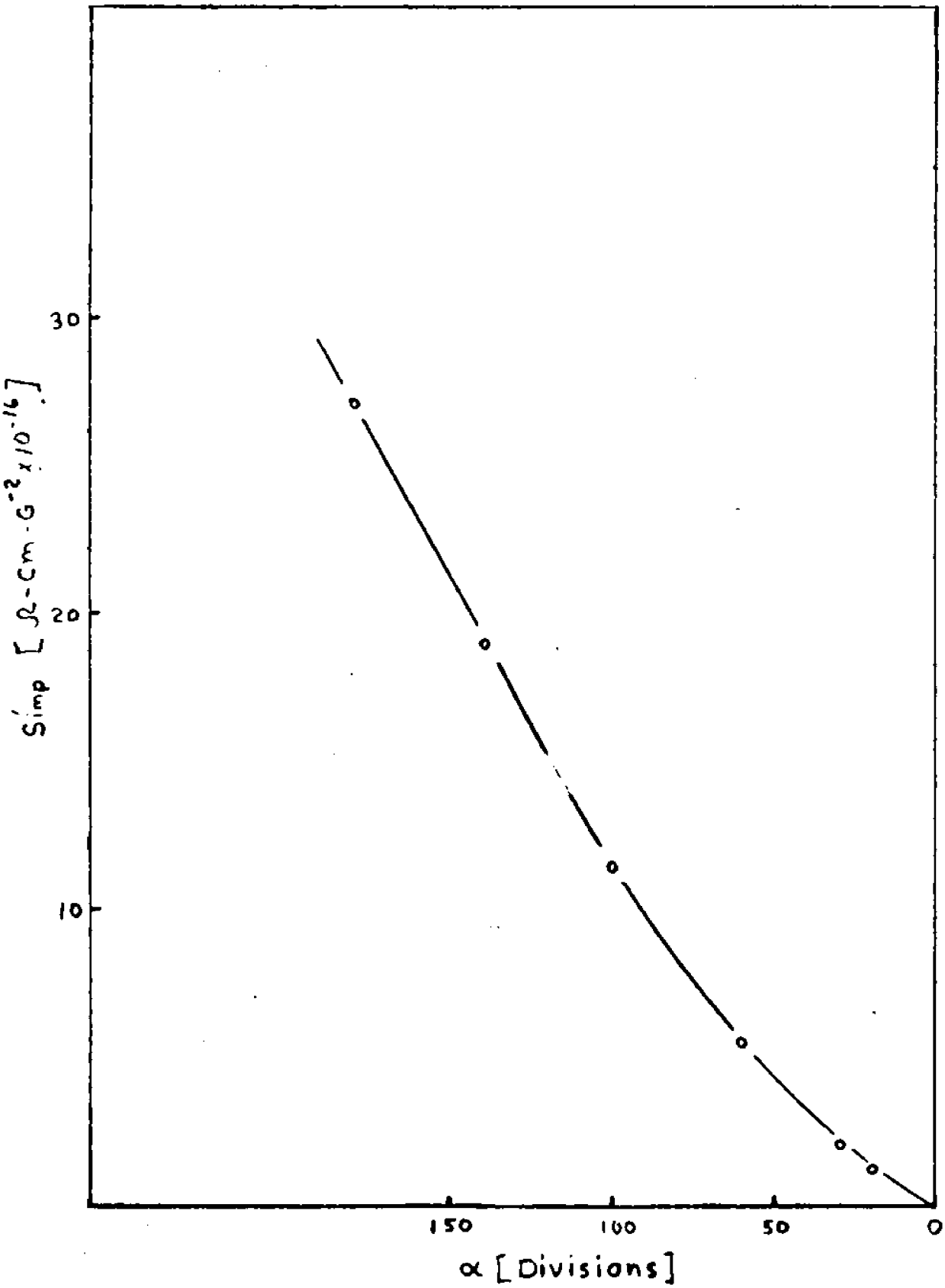

FIG. 24

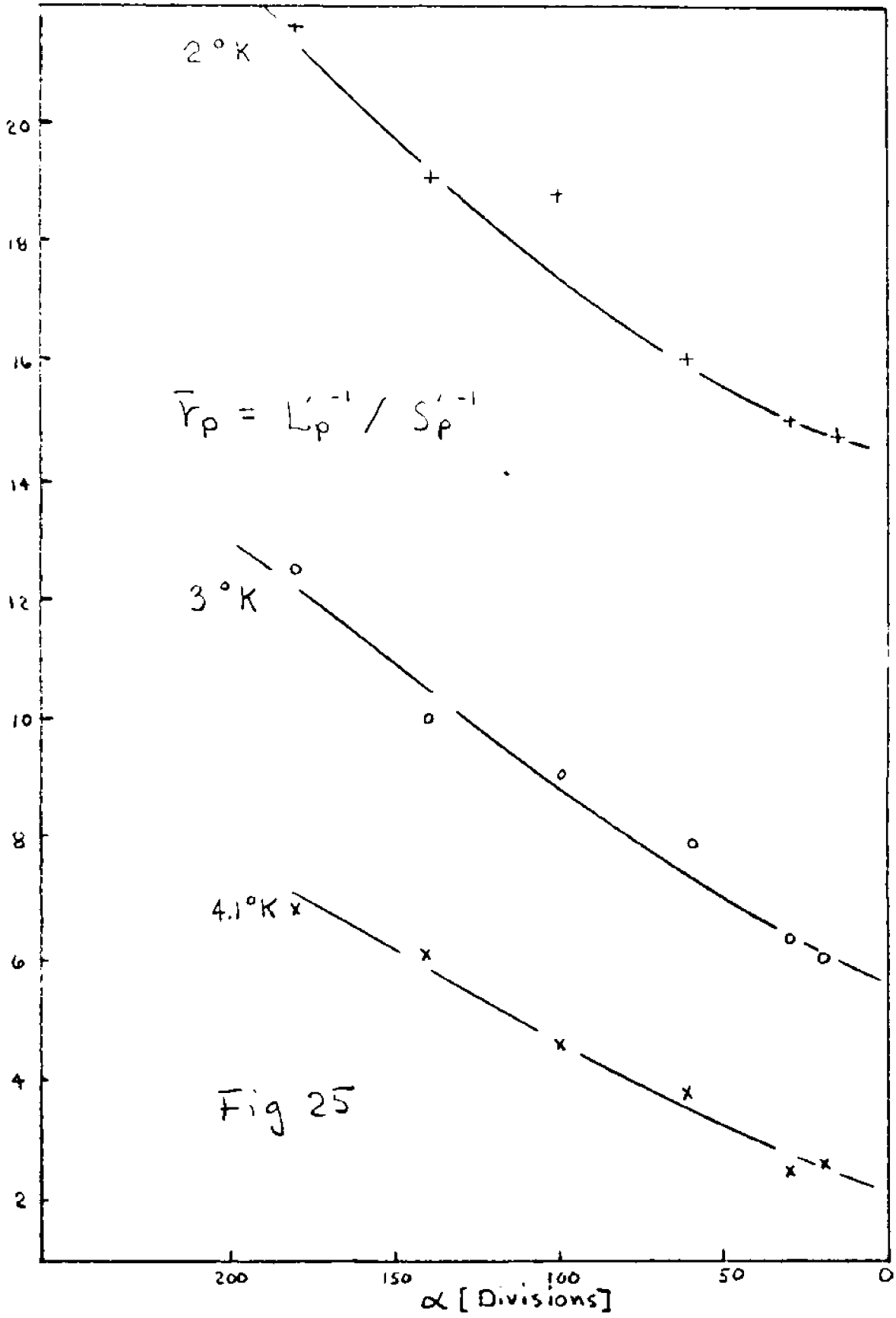
2°K
3°K
4.1°K
$\bar{r}_p = L'^{-1}_p / S'^{-1}_p$
20
18
16
14
12
10
8
6
4
2
200
150
100
50
0
α [Divisions]

Fig 25

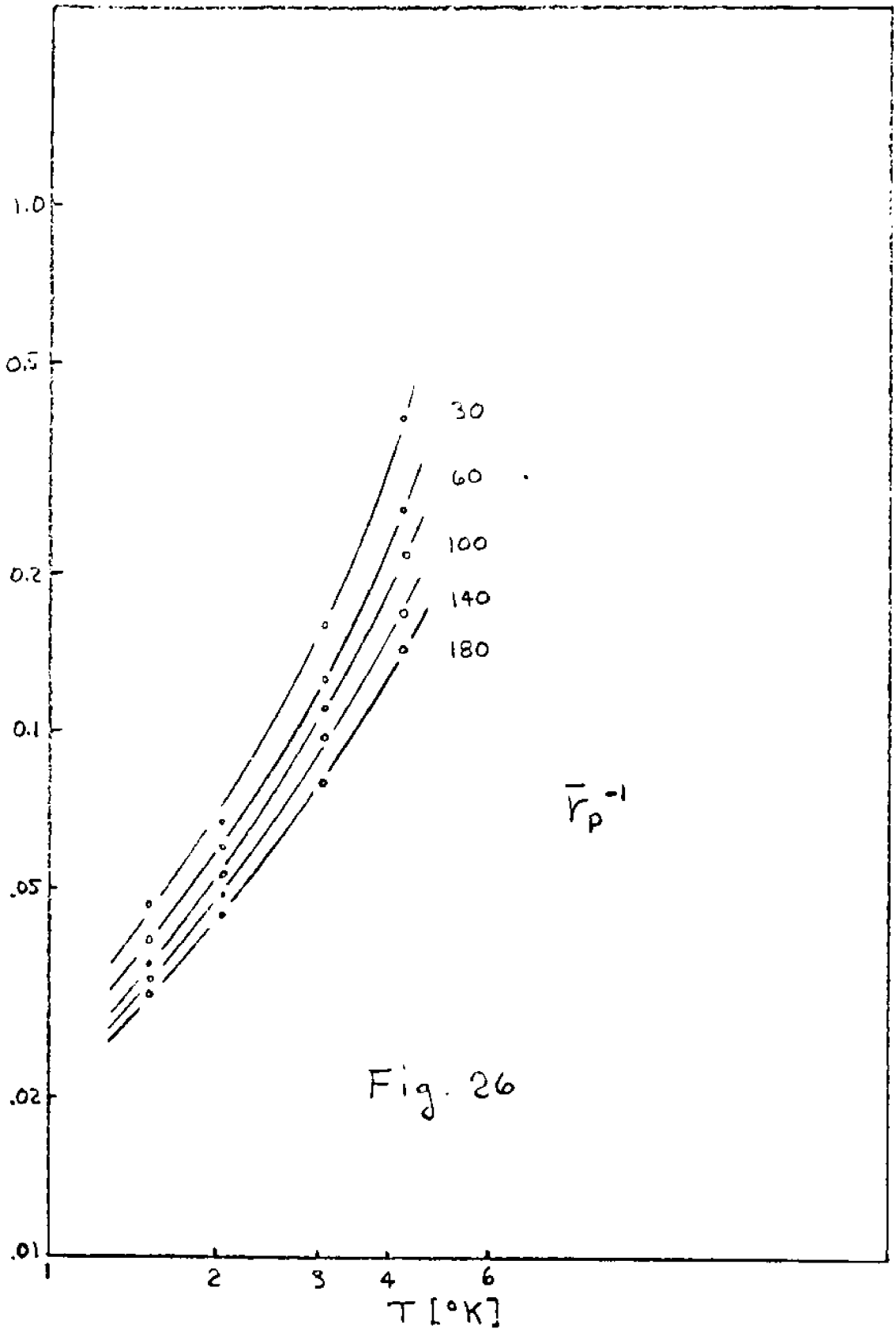

Fig. 26

not appear to contribute to the ω_p term. Therefore, these "hidden" phonon collisions when there are impurities would contribute to ω_p if the impurities were eliminated. In a pure sample, ω_p would be smaller than in an impure sample and curve 25 represents an upper limit of $\bar{r}_p$ without impurities. One has

$$\omega_{eff} = \omega_p^{eff} + \omega_{imp}$$

$$\omega_c = \omega_p^c + \Delta\omega_p^c + \omega_{imp}$$

where $\Delta\omega_p^c$ is the hidden collision frequency in the electric process. If the impurities were eliminated, then

$$\omega_{eff} \rightarrow \omega_p^{eff} + \Delta\omega_p^{eff}$$

$$\omega_c \rightarrow \omega_p^c + \Delta\omega_p^c$$

In the first case

$$\bar{r}_p \approx \frac{\omega_p^c + \Delta\omega_p^c}{\omega_p^{eff}}$$

and in the second case

$$\bar{r}_p \approx \frac{\omega_p^c + \Delta\omega_p^c}{\omega_p^{eff} + \Delta\omega_p^{eff}}$$

The data in Fig. 25 are also shown in Fig. 26, but the inverse of $\bar{r}_p$ is given as a function of T for different angles α. Significantly, $\bar{r}_p^{-1}$ is the apparent Lorenz ratio in the ideal phonon scattering, i.e., $\bar{r}_p^{-1} = L/L_n$. An approximate value for this ratio is given by $L/L_n \approx (\pi^2/3)(T/\theta^*)^2$ where θ^* is the effective Debye temperature for electron scattering which is dependent upon the size of the F.S., i.e., on the thickness of the slice. One may write $\theta^* \approx \hbar c_s(\mu \Delta k_z)$ where c_s is the velocity of sound. The values of $\theta^* = \pi T(\bar{r}_p/3)^{1/2}$ are shown in Fig. 27 as a function of α for different temperatures. Since θ^* is of the order of T, the formula for θ^* is only approximate and it is not surprising to find θ^* dependent on the temperature and not decreasing as fast with α as expected. Also, the same reasons which prevent the decrease of $\bar{r}_p$ as a function of α in Fig. 25 would prevent the decrease of θ^*.

Another point in the discussion relates to the complexity of the open orbit slice itself. The projection sketch in Fig. 4 shows that the contact between open orbit bands and closed orbit bands is not along a single line but along several, and the shapes of those lines are not simple. Thus, generalities involving simplified open orbits as shown in Fig. 28 in Appendix B may not hold.

The z component of the electron velocity, V_z, was neglected altogether as was the relative values between $V_{x,y}$ and V_z. Along a single link of the repeating open orbit pattern there as many

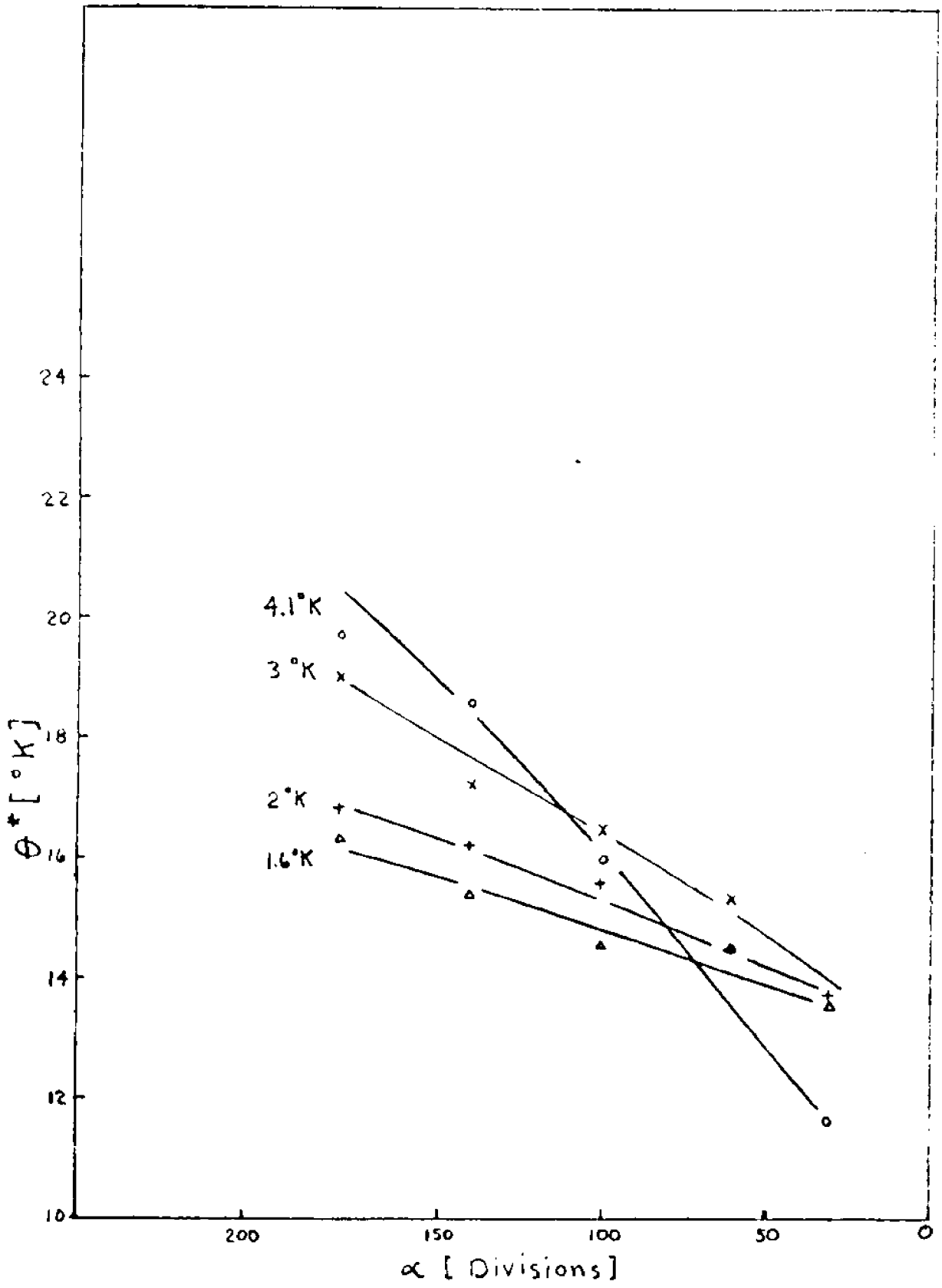
24
22
20
18
16
14
12
10
Φ* [°K]
4.1°K
3 °K
2°K
1.6°K
200
150
100
50
0
α [Divisions]

FIG. 27

as 8 saddle points. An electron arriving at a saddle point reaches a zero velocity in the x-y plane, which terminates the path of the electron and acts as would a scattering into a closed orbit region. The fact that those saddle points are adjacent to the closed orbit region may make their effect inseparable from the mechanism studied. Localization of the scattering has, nevertheless, a large importance on the position of the orbit terminal point and the open orbit contribution to the Hall effect.

C. Applications to Other Metals

In spite of all the difficulties encountered in this study, this method of observing small angle scattering should be, in principle, applicable to several metals. The primary requirements for a metal to be suitable for this technique are first, that open orbits exist on the F.S. of the metal, and second, that the width of the open orbit slice be dependent on the tilt angle of the magnetic field. These criteria are met in most metals. Open orbits are usually indicated by an H^2 dependence of the magneto-resistance. The stereographic projections of many metals, including thallium, Cu, Sn, Nb, Ag, and Au show two dimensional regions surrounding axes of 3, 4, or 6-fold symmetry such that when the magnetic field direction lies within one of these regions, then open orbits exist. Since these are two dimensional regions the problem of aligning the magnetic field so as to observe the small angle scattering effect is not so very difficult. Since the

tilt angles are small and because of the high symmetry (≥ 3-fold) the conductivity tensor σ^c can still be written as a 2 X 2 matrix and the technique described earlier can be applied. If the regions surround a point of low symmetry (2-fold), e.g., Pb and Hg then the analysis must be modified.

The stereograms of many metals show that the high symmetry directions are not surrounded by regions of open orbit field directions, but are however, located at the intersections of lines which indicate field directions for which open orbits exist. In these cases, the method described earlier should hold, but the experimental requirements are more stringent. Here the field must be rotated so that its direction corresponds to a line on the stereogram. This may be rather difficult to achieve experimentally.

The temperature range in which the effect is observable should vary, depending on the Debye temperature of the metal. For example, in Cu, Sn, Nb, and Au the useful temperature range is between 4 and 12°K. In this temperature range the lattice conductivity will be significant and must be accounted for.

The preliminary results obtained on Sn in the range 1.3 to 4.2°K show that the scattering is dominated already by impurities and, as suggested above, that higher temperatures should be used should the small angle scattering mechanism be demonstrated in this metal.

APPENDIX A

Consider a two dimensional coordinate system whose basis vectors, $\vec{u}$ and $\vec{v}$, are chosen such that $\vec{u}$ is coincident with the vector $\vec{J}$ which represents the magnitude and direction of the open orbit electrical current in real space. Then one may write the tensor equation, $\vec{J}_{u,v} = \hat{\sigma}^{o}_{u,v}\ \vec{E}_{u,v}$, where $\hat{\sigma}^{o}$ is the open orbit conductivity tensor, $\vec{E}$ is the vector representing the applied electric field and the subscripts identify the coordinate system. In the high field limit the conductivity tensor may be written in matrix form as $\hat{\sigma}^{o}_{u,v}$ $\begin{pmatrix} \sigma^{o} & 0 \\ 0 & 0 \end{pmatrix}$ so that the tensor equation becomes: $\begin{pmatrix} J_u \\ J_v \end{pmatrix} = \begin{pmatrix} \sigma^{o} & 0 \\ 0 & 0 \end{pmatrix} \begin{pmatrix} E_u \\ E_v \end{pmatrix}$.

If $\vec{J}$ and $\vec{E}$ are to be expressed in a basis $\vec{x}$ and $\vec{y}$ as shown in Fig. 6b, then one writes $\vec{J}_{u,v} = \hat{\theta}\ \vec{J}_{xy}$ and $\vec{E}_{u,v} = \hat{\theta}\ \vec{E}_{x,y}$ where $\hat{\theta} = \begin{pmatrix} \cos\theta & \sin\theta \\ -\sin\theta & \cos\theta \end{pmatrix}$ with θ the angle between the x axis and the real space open orbit direction. Since $\vec{J}_{uv} = \hat{\sigma}^{o}_{uv}\ \vec{E}_{uv}$, then

$$\hat{\theta}\ \vec{J}_{x,y} = \hat{\sigma}^{o}_{u,v}\ \hat{\theta}\ \vec{E}_{x,y}$$

or

$$\vec{J}_{x,y} = \hat{\theta}^{-1}\ \hat{\sigma}^{o}_{uv}\ \hat{\theta}\ \vec{E}_{x,y}$$

In matrix form this becomes:

$$\begin{pmatrix} J_x \\ J_y \end{pmatrix} = \begin{pmatrix} \cos\theta & -\sin\theta \\ \sin\theta & \cos\theta \end{pmatrix} \begin{pmatrix} \sigma^\circ & 0 \\ 0 & 0 \end{pmatrix} \begin{pmatrix} \cos\theta & \sin\theta \\ -\sin\theta & \cos\theta \end{pmatrix} \begin{pmatrix} E_x \\ E_y \end{pmatrix}$$

or

$$\begin{pmatrix} J_x \\ J_y \end{pmatrix} = \begin{pmatrix} \sigma^\circ \cos^2\theta & \sigma^\circ \sin\theta\cos\theta \\ \sigma^\circ \sin\theta\cos\theta & \sigma^\circ \sin^2\theta \end{pmatrix} \begin{pmatrix} E_x \\ E_y \end{pmatrix} \qquad (A\text{-}1)$$

Dropping the subscripts, with the understanding that the quantities are measured in the x-y coordinate system, the electrical open orbit current in the high field limit may be expressed as:

$$\vec{J} = \hat{\sigma}^\circ \vec{E}$$

with

$$\hat{\sigma}^\circ = \begin{pmatrix} \sigma^\circ \cos^2\theta & \sigma^\circ \sin\theta\cos\theta \\ \sigma^\circ \sin\theta\cos\theta & \sigma^\circ \sin^2\theta \end{pmatrix} \qquad (A\text{-}2)$$

It may be noted that the direction $\vec{u}$ as initially defined would depend on the magnitude of the field H, and therefore with x,y fixed would make the angle θ field dependent. Later on, by specifying the high field tensor limit, we tacitly adapted the coordinate system $\vec{u}$, $\vec{v}$ fixed relative to the high field limit

open orbit direction. Neglecting any possible freak scattering, this will make the $\vec{v}$ direction the intersection of the basal plane (1',2') with the plane perpendicular to the magnetic field direction (z).

It is of some interest to consider the consequences which would result if the conductivity tensor as expressed in the u-v basis had contained more than one non-zero matrix element.

A conductivity matrix of the form $\begin{pmatrix} \sigma^{\circ} & 0 \\ 0 & \sigma^{\circ}{}' \end{pmatrix}$ implies the existence of open orbits in two mutually perpendicular directions, viz., parallel to the u and v axes, respectively. Thus

$$\begin{pmatrix} J_x \\ J_y \end{pmatrix} = \begin{pmatrix} \cos\theta & -\sin\theta \\ \sin\theta & \cos\theta \end{pmatrix} \begin{pmatrix} \sigma^{\circ} & 0 \\ 0 & \sigma^{\circ\prime} \end{pmatrix} \begin{pmatrix} \cos\theta & \sin\theta \\ -\sin\theta & \cos\theta \end{pmatrix} \begin{pmatrix} E_x \\ E_y \end{pmatrix} \qquad (A\text{-}3)$$

so that

$$\begin{pmatrix} J_x \\ J_y \end{pmatrix} = \begin{pmatrix} \sigma^{\circ}\cos^2\theta + \sigma^{\circ\prime}\sin^2\theta & (\sigma^{\circ} - \sigma^{\circ\prime})\sin\theta\cos\theta \\ (\sigma^{\circ} - \sigma^{\circ\prime})\sin\theta\cos\theta & \sigma^{\circ}\sin^2\theta + \sigma^{\circ\prime}\cos^2\theta \end{pmatrix} \begin{pmatrix} E_x \\ E_y \end{pmatrix} \qquad (A\text{-}4)$$

This equation reduces to Eq. A-1 if $\sigma^{\circ} \gg \sigma^{\circ}{}'$. The resistivity becomes

$$\hat{\rho} = \hat{\sigma}^{-1} = \frac{\hat{\sigma}}{|\hat{\sigma}|}$$

where $|\sigma|$ is invariant under a similarity transformation so that $\left|\begin{smallmatrix} \sigma^{\circ} & 0 \\ 0 & \sigma^{\circ}{}' \end{smallmatrix}\right| = \sigma^{\circ}\sigma^{\circ}{}'$. Therefore,

$$\hat{\rho} = \frac{1}{\sigma^{\circ}\sigma^{\circ\prime}} \begin{pmatrix} \sigma^{\circ}\sin^2\theta + \sigma^{\circ\prime}\cos^2\theta & (\sigma^{\circ\prime} - \sigma^{\circ})\sin\theta\cos\theta \\ (\sigma^{\circ\prime} - \sigma^{\circ})\sin\theta\cos\theta & \sigma^{\circ}\cos^2\theta + \sigma^{\circ\prime}\sin^2\theta \end{pmatrix}$$

Thus the open orbit contribution to the ρ_{xx} component of the magnetoresistance is:

$$\rho_{xx} = \frac{1}{\sigma^{\circ\prime}}\sin^2\theta + \frac{1}{\sigma^{\circ}}\cos^2\theta \qquad (A\text{-}6)$$

This equation shows that $\rho_{xx} \to \infty$ for all angles except $\theta = 0$ if $\sigma^{\circ\prime} = 0$.

In the thermal conductivity process, the contribution due to the open orbit electrons is $\begin{pmatrix} \lambda^{\circ} & 0 \\ 0 & 0 \end{pmatrix}$ in the u-v basis. If the lattice conductivity $\begin{pmatrix} \lambda_g & 0 \\ 0 & \lambda_g \end{pmatrix}$ is included, then

$$\begin{pmatrix} W_u \\ W_v \end{pmatrix} = \begin{pmatrix} \lambda^{\circ} + \lambda_g & 0 \\ 0 & \lambda_g \end{pmatrix} \begin{pmatrix} G_u \\ G_v \end{pmatrix}$$

This is a case similar to the preceeding one where $\lambda^{\circ} + \lambda_g$ and λ_g replace σ° and $\sigma^{\circ\prime}$, respectively. The result is

$$\begin{pmatrix} W_x \\ W_y \end{pmatrix} = \begin{pmatrix} \lambda^{\circ}\cos^2\theta + \lambda_g & \lambda^{\circ}\sin\theta\cos\theta \\ \lambda^{\circ}\sin\theta\cos\theta & \lambda^{\circ}\sin^2\theta + \lambda_g \end{pmatrix} \begin{pmatrix} G_x \\ G_y \end{pmatrix}$$

where the 2 X 2 matrix is the contribution to the thermal conductivity by the open orbit electrons and the lattice. The inverse of this matrix gives their contribution to the thermal

magnetoresistance. The γ_{xx} component is

$$\frac{1}{\lambda_g} \sin^2\theta + \frac{1}{\lambda_g + \lambda^o} \cos^2\theta$$

This equation and Eq. A-6 are of limited value because even though the contribution of the closed orbit carriers to the electrical conduction is small, they will strongly influence the way ρ_{xx} in Eq. A-6 tends toward infinity when $\sigma^{o}{}'$ is zero. Good isotropic conditions for the closed orbit carriers exist when H is near a 3, 4, or 6-fold crystal axis. The resulting isotropic tensor,

$$\hat{\sigma}_c = \begin{pmatrix} \sigma_{1'1'} & \sigma_{1'2'} \\ -\sigma_{1'2'} & \sigma_{1'1'} \end{pmatrix}_c = \begin{pmatrix} \sigma_{xx} & \sigma_{xy} \\ -\sigma_{xy} & \sigma_{xx} \end{pmatrix}_c = \begin{pmatrix} \sigma_{uu} & \sigma_{uv} \\ -\sigma_{uv} & \sigma_{uu} \end{pmatrix}_c$$

is invariant with respect to a change of coordinates as long as 1',2'; x,y; u,v define the same plane or nearly so. In the u-v coordinate system:

$$\hat{\sigma}_{u,v} = \begin{pmatrix} \sigma^{o} & 0 \\ 0 & 0 \end{pmatrix} + \begin{pmatrix} \sigma_{11} & \sigma_{12} \\ -\sigma_{12} & \sigma_{11} \end{pmatrix}_c \qquad (A\text{-}7)$$

From here on the indices 1,2 are to be used instead of xy or uv to represent the isotropic contribution of the closed orbits and to simplify the notation the index c is to be dropped. Thus, $\sigma_{11} \equiv \sigma_{1'1'c} = \sigma_{xxc} = \sigma_{uuc}$.

The Eq. A-7 expresses the electrical conductivity in terms of unidirectional open orbit carriers and closed orbit carriers.

Transformation to the x-y coordinate system yields

$$\hat{\sigma}_{x,y} = \begin{pmatrix} \sigma^\circ \cos^2\theta + \sigma_{11} & \sigma^\circ \sin\theta \cos\theta + \sigma_{12} \\ \sigma^\circ \sin\theta \cos\theta - \sigma_{12} & \sigma^\circ \sin^2\theta + \sigma_{11} \end{pmatrix}$$

The thermal conductivity, expressed in terms of the u-v coordinate system, is given by

$$\hat{\lambda}_{u,v} = \begin{pmatrix} \lambda^\circ & 0 \\ 0 & 0 \end{pmatrix} + \begin{pmatrix} \lambda_g & 0 \\ 0 & \lambda_g \end{pmatrix} + \begin{pmatrix} \lambda_{11} & \lambda_{12} \\ -\lambda_{12} & \lambda_{11} \end{pmatrix}$$

and when transformed to the x-y system $\hat{\lambda}$ becomes

$$\hat{\lambda}_{x,y} = \begin{pmatrix} \lambda^\circ \cos^2\theta + \lambda_{11} + \lambda_g & \lambda^\circ \sin\theta \cos\theta + \lambda_{12} \\ \lambda^\circ \sin\theta \cos\theta - \lambda_{12} & \lambda^\circ \sin^2\theta + \lambda_{11} + \lambda_g \end{pmatrix}$$

To get the $\hat{\rho}$ and $\hat{\gamma}$ matrices, the inverses of the $\hat{\sigma}$ and $\hat{\lambda}$ matrices must be taken. The result for $\hat{\rho}$ is

$$\hat{\rho} = \frac{1}{|\hat{\sigma}|} \begin{pmatrix} \sigma^\circ \sin^2\theta + \sigma_{11} & -\sigma^\circ \sin\theta \cos\theta - \sigma_{12} \\ -\sigma^\circ \sin\theta \cos\theta + \sigma_{12} & \sigma^\circ \cos^2\theta + \sigma_{11} \end{pmatrix} \qquad (A\text{-}8)$$

The γ matrix has the same form with λ_g's added to the diagonal terms. The denominators are

$$|\hat{\sigma}| = (\sigma_{11}^2 + \sigma_{12}^2) + \sigma^\circ \sigma_{11}$$

$$|\hat{\lambda}| = (\lambda_{11}^2 + \lambda_{12}^2) + (\lambda^\circ + \lambda_g)(\lambda_{11} + \lambda_g) + \lambda_{11}\lambda_g$$

Expressions for the magneto-, Hall, magnetothermal, and Righi-Leduc resistivity coefficients are given, in that order, as follows:

$$\rho_{xx} = (\sigma^{\circ}\sin^2\theta + \sigma_{11})(\sigma_{11}^2 + \sigma_{12}^2 + \sigma^{\circ}\sigma_{11})^{-1}$$

$$\rho_{yx} = (-\sigma^{\circ}\sin\theta\cos\theta + \sigma_{12})(\sigma_{11}^2 + \sigma_{12}^2 + \sigma^{\circ}\sigma_{11})^{-1} \qquad (A\text{-}9)$$

$$\gamma_{xx} = (\lambda^{\circ}\sin^2\theta + \lambda_{11} + \lambda_g)[\lambda_{11}^2 + \lambda_{12}^2 + (\lambda^{\circ} + \lambda_g)(\lambda_{11} + \lambda_g) + \lambda_{11}\lambda_g]^{-1}$$

$$\gamma_{yx} = (-\lambda_{\circ}\sin\theta\cos\theta + \lambda_{12})[\lambda_{11}^2 + \lambda_{12}^2 + (\lambda^{\circ} + \lambda_g)(\lambda_{11} + \lambda_g) + \lambda_{11}\lambda_g]^{-1}$$

Most of the first order approximations at high fields can be discussed when the asymptotic limit of the different terms are introduced. These limits are: $\sigma_{11} \simeq AH^{-2}$, $\lambda_{11} \simeq A'H^{-2}$, $\sigma_{12} \simeq BH^{-1}$, and $\lambda_{12} \simeq B'H^{-1}$. It should be noted that the σ_{12} and λ_{12} expressions are odd functions of the field while σ_{11} and λ_{11} are even functions of H as are the field independent quantities, σ°, λ°, and λ_g.

The asymptotic forms of Eqs. A-9 become

$$\rho_{xx}(H) = \frac{\sigma^{\circ}\sin^2\theta + AH^{-2}}{A^2H^{-4} + B^2H^{-2} + \sigma^{\circ}AH^{-2}} = \frac{\sigma^{\circ}\sin^2\theta}{|\sigma|} + \frac{AH^{-2}}{|\sigma|}$$

$$\rho_{yx}(H) = \frac{-\sigma^{\circ}\sin\theta\cos\theta + BH^{-1}}{A^2H^{-4} + B^2H^{-2} + \sigma^{\circ}AH^{-2}} \qquad (A\text{-}10)$$

$$\rho_{yx}^{(-)}(H) = \frac{\rho_{yx}(+H) - \rho_{yx}(-H)}{2} = \frac{BH^{-1}}{|\sigma|}$$

$$\rho_{yx}^{(+)}(H) = \frac{\rho_{yx}(+H) + \rho_{yx}(-H)}{2} = \frac{-\sigma^{\circ}\sin\theta\cos\theta}{|\sigma|}$$

The term A^2H^{-4} in $|\sigma|$ is negligible so that

$$\rho_{xx} \rightarrow \frac{\sigma^{\circ}\sin^2\theta}{B^2 + \sigma^{\circ}A} H^2 + \frac{A}{B^2 + \sigma^{\circ}A}$$

$$\rho_{yx}^{(-)} \rightarrow \frac{B}{B^2 + \sigma^{\circ}A} H \qquad (A\text{-}11)$$

$$\rho_{yx}^{(+)} \rightarrow \frac{-\sigma^{\circ}\sin\theta\cos\theta}{B^2 + \sigma^{\circ}A} H^2$$

The equation

$$\frac{H\rho_{xx}}{\rho_{yx}^{(-)}} = \frac{\sigma^{\circ}\sin^2\theta}{B} H^2 + \frac{A}{B} \qquad (A\text{-}12)$$

is a relation generally more valid than Eqs. A-11

If the term $\sigma^{\circ}A \ll B^2$, the Eqs. A-11 simplify to

$$\rho_{xx} = \frac{\sigma^{\circ}\sin^2\theta}{B^2} H^2 + \frac{A}{B^2}$$

$$\rho_{yx}^{(-)} = B^{-1} H \qquad (A\text{-}13)$$

$$\rho_{yx}^{(+)} = \frac{\sigma^{\circ}\sin\theta\cos\theta}{B^2} H^2$$

In the experimental situation where $\theta = 90^{\circ}$ the equations reduce further to

$$\rho_{xx} = \frac{\sigma^{\circ} H^2}{B^2} + \frac{A}{B^2}$$

$$\rho_{yx}^{(-1)} = B^{-1} H \qquad (A\text{-}14)$$

$$\rho_{yx}^{(+1)} = 0$$

$$\frac{H \rho_{xx}}{\rho_{yx}^{(-1)}} = \frac{\sigma^{\circ}}{B} H^2 + \frac{A}{B}$$

Separation of the two terms in the ρ_{xx} equation is easily obtained experimentally from a plot of ρ_{xx} vs H^2 which gives the slope

$$S' = \frac{\sigma^{\circ} \sin^2 \theta}{B^2 + \sigma^{\circ} A}$$

and the intercept

$$\frac{A}{B^2 + \sigma^{\circ} A}$$

It should be noted that

$$\frac{H^2 S'}{\rho_{yx}^{(+1)}} = \tan \theta$$

could be of interest in the determination of the direction of the

open orbits, but, unfortunately, $\rho_{yx}^{(+)}$ is subject to probe misalignment errors.

The thermal case, following from Eqs. A-9 and corresponding to the Eqs. A-10 are

$$\gamma_{xx} = \frac{\lambda^\circ \sin^2\theta + \lambda_g + A' H^{-2}}{|\lambda|}$$

$$\gamma_{yx} = \frac{-\lambda^\circ \sin\theta\cos\theta + B' H^{-1}}{|\lambda|}$$

$$\gamma_{yx}^{(-)} = \frac{B' H^{-1}}{|\lambda|} \qquad (A-15)$$

$$\gamma_{yx}^{(+)} = \frac{-\lambda^\circ \sin\theta\cos\theta}{|\lambda|}$$

$$\frac{H\gamma_{xx}}{\gamma_{yx}^{(-)}} = \frac{\lambda^\circ \sin^2\theta + \lambda_g}{B'} H^2 + \frac{A'}{B'}$$

where

$$|\lambda| = A'^2 H^{-4} + B'^2 H^{-2} + (\lambda^\circ + 2\lambda_g) A' H^{-2} + \lambda_g (\lambda^\circ + \lambda_g)$$

Each of these equations except $H\gamma_{xx}/\gamma_{yx}^{(-)}$ depends on the importance of the different terms in the denominator, $|\lambda|$. Evidently, if λ_g is negligible relative to the other terms in $|\lambda|$, the γ equations are identical to the Eqs. A-10, A-11, A-12, A-13, and A-14 for ρ, and the slope L' of γ_{xx} vs H^2 is given by

$$L' = \frac{\lambda^\circ \sin^2\theta}{B'^2 + \lambda^\circ A'} \simeq \frac{\lambda^\circ \sin^2\theta}{B'^2} \qquad (A-16)$$

The intercept is $A'/(B'^2 + \lambda^\circ A')$. In the case where λ_g is not negligible, it may be noted that the slope L'' of $H\gamma_{xx}/\gamma_{yx}^{(-)}$ vs H^2 is given by

$$\frac{\lambda^\circ \sin^2\theta + \lambda_g}{B'}$$

and the intercept by A'/B'. When $\lambda^\circ = 0$ or $\theta = 0$, this slope would determine λ_g/B', i.e., the lattice conductivity which may then be substituted as a known parameter, allowing the determination of $\lambda^\circ \sin^2\theta/B'$. The direct analysis of γ_{xx} and γ_{yx} may be rather complex since, as H increases, the term, $(B'^2 + \lambda^\circ + 2\lambda_g)H^{-2}$ in $|\lambda|$ is first preponderant over the term $\lambda_g(\lambda^\circ + \lambda_g)$. At much higher field the opposite occurs. Consequently,

$$\gamma_{yx}^{(-)} \approx \frac{B'H}{B' + (\lambda^\circ + 2\lambda_g)A'} \qquad (A\text{-}18)$$

at intermediate field and

$$\gamma_{yx}^{(-)} \rightarrow \frac{B'H^{-1}}{\lambda_g(\lambda^\circ + \lambda_g)} \qquad (A\text{-}18)$$

at very high field. The departure of the proportionality of $\gamma_{yx}^{(-)}$ with H is, therefore, a good way to check the importance of λ_g in the transport effect.

At intermediate fields γ_{xx} is given by

$$\gamma_{xx} \approx \frac{\lambda^\circ \sin^2\theta + \lambda_g}{B'^2 + (\lambda^\circ + 2\lambda_g)A'} H^2 + \frac{A'}{B'^2 + (\lambda^\circ + 2\lambda_g)A'} \qquad (A\text{-}19)$$

and saturates to

$$\gamma_{xx} \rightarrow \frac{\lambda^0 \sin^2\theta + \lambda_g}{\lambda_g(\lambda^0 + \lambda_g)}$$

Effect of Misalignment

When the hexagonal axis of the crystal makes a small angle β with the plane of rotation of the magnetic field, the ρ_{xx} minimum does not correspond to a perfect alignment of the field with the hexagonal direction and a finite slice of open orbits remains. The angle β will be referred to as the misalignment angle which, together with α, determines the open orbit direction θ. When both α and β are small, some approximations can be made in the u,v,z coordinate system. Since z is near the hexagonal axis, nearly isotropic conditions exist in the u-v plane and the conductivity matrix σ may be written as

$$\sigma_{u,v,z} \approx \begin{pmatrix} \sigma^0 & 0 & \sigma_2 \\ 0 & 0 & 0 \\ \sigma_2 & 0 & \sigma_3 \end{pmatrix} + \begin{pmatrix} AH^{-2} & BH^{-1} & \delta C H^{-1} \\ -BH^{-1} & AH^{-2} & \delta E H^{-1} \\ -\delta C H^{-1} & -\delta E H^{-1} & \sigma_{33} \end{pmatrix}$$

with the two matrices coming, respectively, from the open and closed orbits. The terms containing δ's are small and vanish for alignment of the field with the hexagonal direction, as do the σ's in the

first matrix. The $(\sigma)_{xyz}$ matrix takes the form

$$\sigma_{xyz} = \begin{pmatrix} \sigma^{\circ}\cos^2\theta + AH^{-2} & \sigma^{\circ}\sin\theta\cos\theta + BH^{-1} & \delta CH^{-1} + \sigma_2 \\ \sigma^{\circ}\sin\theta\cos\theta - BH^{-1} & \sigma^{\circ}\sin^2\theta + AH^{-2} & \delta EH^{-1} \\ -\delta CH^{-1} + \sigma_2 & -\delta EH^{-1} & \sigma_{33} + \sigma_3 \end{pmatrix}$$

Thus,

$$\rho_{xx} = \frac{(\sigma_{33} + \sigma_3)(\sigma^{\circ}\sin^2\theta + AH^{-2}) + (\delta E)^2 H^{-2}}{|\sigma|}$$

and

$$\rho_{yx} = \frac{-(\delta CH^{-1} + \sigma_2)\delta EH^{-1} - (\sigma_{33} + \sigma_3)(\sigma^{\circ}\sin\theta\cos\theta + BH^{-1})}{|\sigma|}$$

Since σ_{33} is large compared to the other σ terms and δ terms, then

$$|\sigma| \approx (\sigma_{33} + \sigma_3)|\sigma|_{uv}$$

and to the same approximations as A-11,

$$\rho_{xx} = \frac{\sigma^{\circ}\sin^2\theta\, H^2 + \left(A + \frac{\delta^2 E^2}{\sigma_3}\right)}{(B^2 + \sigma^{\circ}A)}$$

and

$$\rho_{yx} = \frac{-\left(B + \frac{\sigma_2 \delta E}{\sigma_{33}}\right) H}{(B^2 + \sigma^{\circ}A)}$$

Except for negligible terms, these are the same results as A-11. Therefore, the main effect of the misalignment will be, as mentioned earlier, the direct influence of β on the angle θ with $\tan\theta \simeq \alpha/\beta$ and the non-vanishing of the open orbit slice for $\alpha \neq 0$. The functional dependence of the slice thickness, i.e., of σ^{o} and λ^{o} with α should be replaced by a dependence with $\sqrt{\alpha^2 + \beta^2}$.

APPENDIX B

Another pertinent point in the discussion of the conduction of a single open orbit is that beside the asymptotic behavior,

$$\hat{\sigma}' = \begin{pmatrix} \sigma' & 0 \\ 0 & 0 \end{pmatrix}$$

one should consider the way the other terms of the tensor tend to zero with the field. If the open orbits are perfectly straight in the $\vec{u}$ direction, the elements of the tensor are zero except for the $\sigma_{11} = \sigma'$ term. For an undulating orbit one expects that for H=0, a component $\sigma_{22}(0)$ should exist whose importance relative to $\sigma_{11}(0) \simeq \sigma'$ depends on how pronounced the undulations are. For example, if the undulations consist of semi-circles connected by short straight links then $\sigma_{22}(0) \simeq \sigma_{11}(0) \simeq \sigma'$. One also expects $\sigma_{22}(H) \rightarrow CH^{-2}$, just as a circular closed orbit. The question of the σ_{12} and σ_{21} terms is more delicate and the effective path method developed by Pippard[24] to solve some other transport problems may be applied here. With H kept constant one may imagine a short impulse of field E during a time dt. The current response J(t) may be used to deduce the effect of a steady E field by forming $\int_0^\infty J(t)dt$. Under the field impulse the Fermi surface is displaced by $\hbar^{-1}eEdt$ and the number of electrons generated from an element of surface dS by this displacement is

$eE \cdot dS\ dt/4\pi^3\hbar$ i.e., at a rate $eE \cdot dS/4\pi^3\hbar$. Each of these particles travels under the influence of the Lorentz force until destroyed by efficient scattering. The average distance traveled between creation and randomization is $\Lambda = \langle \int_0^\infty v dt \rangle$, so that the contribution by dS to the current is

$$dJ = \frac{e^2 E \cdot dS}{4\pi^3 \hbar} \Lambda \qquad (A\text{-}20)$$

The total current may be obtained by integrating over the F.S. Omitting the component in the magnetic field direction, the path Λ^* in k-space corresponding to Λ is real space is given by the relations:

$$\begin{aligned} \Lambda_u &= -\Lambda_v^* \left(\frac{\hbar}{eH}\right) \\ \Lambda_v &= \Lambda_u^* \left(\frac{\hbar}{eH}\right) \end{aligned} \qquad (A\text{-}21)$$

so that

$$\begin{aligned} J_u &= \frac{-e}{4\pi^3 H} \left\{ E_u \int \Lambda_v^* \, dS_u + E_v \int \Lambda_v^* \, dS_v \right\} \\ J_v &= \frac{e}{4\pi^3 H} \left\{ E_u \int \Lambda_u^* \, dS_u + E_v \int \Lambda_u^* \, dS_v \right\} \end{aligned} \qquad (A\text{-}22)$$

If the path of a carrier originates at a point M and ends at M', then averaging over all origins and terminal points yields:

$$\int \Lambda^* dS_u = [U' - U] S_u$$

and (A-23)

$$\int \Lambda^* dS_v = [V' - V] S_v$$

where U and V are the centroids of creation of a particle under an impulse E_u or E_v respectively, U' and V' are the corresponding centroids of termination, and S_u and S_v are the projected areas of the F.S. in the $\vec{u}$ and $\vec{v}$ directions, respectively.

Thus

$$\begin{aligned} \sigma_{uu} &= -e/4\pi^3 H \ (U'-U)_v \ S_u \\ \sigma_{uv} &= -e/4\pi^3 H \ (V'-V)_v \ S_v \\ \sigma_{vu} &= e/4\pi^3 H \ (U'-U)_u \ S_u \\ \sigma_{vv} &= e/4\pi^3 H \ (V'-V)_u \ S_v \end{aligned} \qquad (A\text{-}24)$$

The case of open orbits consisting of semi-circles, as shown in fig. 28, may be treated simply. In orbit "a", electrons are created by the field E_u, with H out of the figure, and move in the negative $\vec{u}$ direction, thus making σ_{uu} a positive term.

The centroid U is given by:

$$OU = \frac{\int_0^{\pi} R_0^2 \sin^2\theta \, d\theta}{\int_0^{\pi} R_0 \sin\theta \, d\theta} \qquad (A\text{-}25)$$

so that

$$OU = \pi R_0 / 4$$

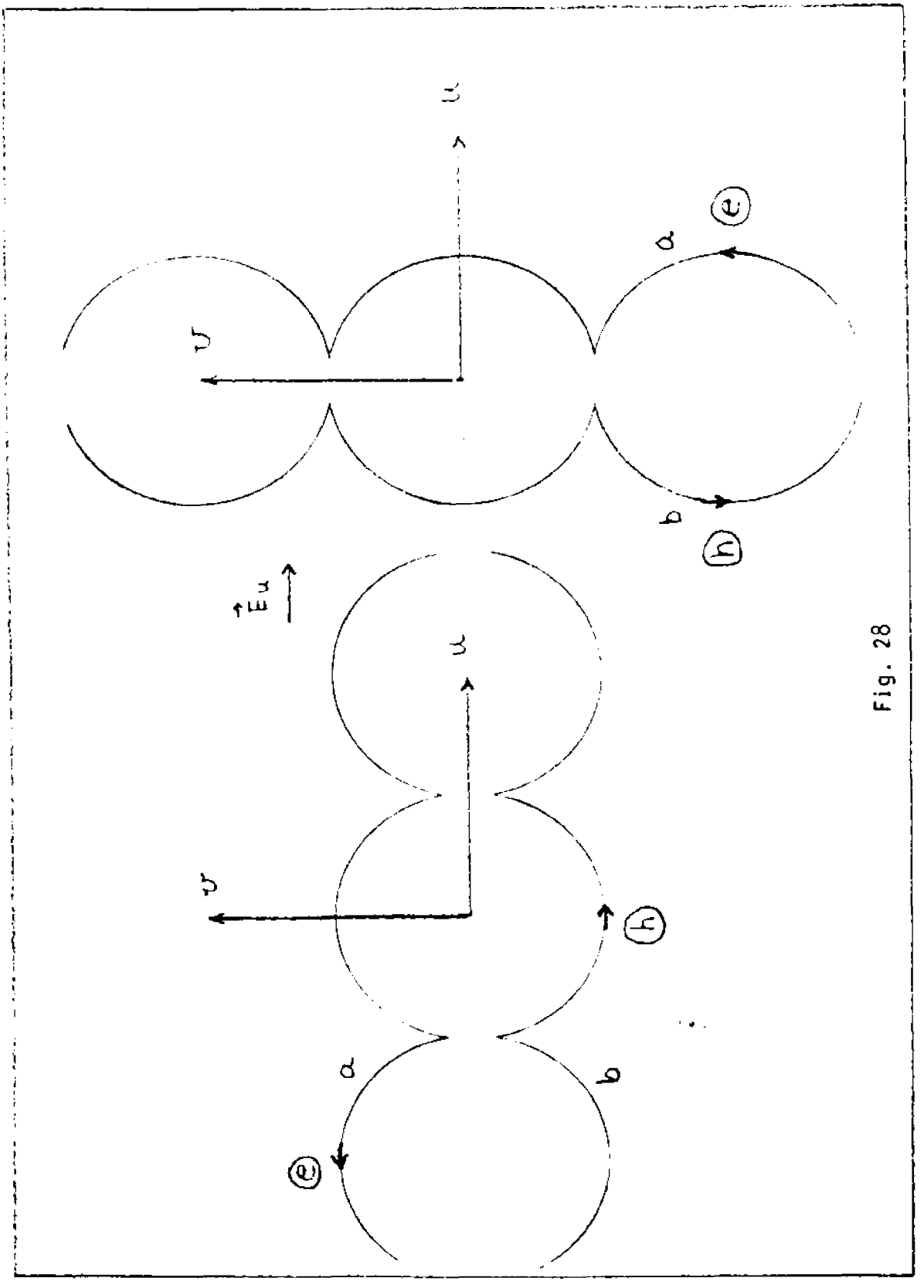

Fig. 28

and the area of the semi-circle is:

$$A = \int_{-k_o}^{k_o} k_u \, d k_v$$

where k_o is the radius of the circle.

The centroid U' is such that $[UU']_v$ corresponds to the classical mean free path τv_f. The motion in the H direction is neglected. In k-space the mean free path transforms into $-\frac{eH}{\hbar}\tau v_f$.

If the scattering is uniform along the semi-circle, then the asymptotic value of $[OU']_u$ is given by

$$[OU']_u = \frac{\int_o^{\pi} k_o^2 \sin\theta \, d\theta}{\int_o^{\pi} k_o \, d\theta}$$

so that

$$[OU']_u = \frac{2k_o}{\pi}$$

For a slice of open orbit "a" of thickness Δk_z, the conductivities are given by:

$$\sigma_{uu} = e/4\pi^3 H \left(\Delta k_z \, 2k_o\right)(eH/\hbar)\,\tau\, v_f = (e^2 n/m)(4\tau/\pi)$$

$$\sigma_{vu} = e/4\pi^3 H \left(\Delta k_z \, 2k_o\right) k_o \left(\frac{2}{\pi} - \frac{\pi}{4}\right) = -e/H\,(n - n_o) \qquad (A\text{-}26)$$

In these equations n is the number of holes in the semi-circular cylinder of thickness Δk_z; n is also the number of holes in the slice of thickness Δk_z, length $2k_o$ and width OU', and $n-n_o$ is the number of states in a similar slice of width [UU'].

Associated with the slice of orbit of type "a" at k_z, there exists a slice of type "b" at $-k_z$ whose contribution is identical to that of slice "a" for both σ_{uu} and σ_{vu}. If both slices are taken into account, then the equations are unchanged but n and n_o correspond to slices of thickness $2\,\Delta k_z$ rather than just Δk_z.

Under a positive impulse E_v, electrons are created in the upper quarter of the "a" and "b" orbits and holes created in the lower quarter. The centroids for the electrons are given by:

$$OV \begin{cases} k_o/2 \\ \pi k_o/4 \end{cases} \qquad OV' \begin{cases} 2k_o/\pi \\ 2k_o/\pi + \lambda \end{cases}$$

and for the holes:

$$OV \begin{cases} k_o/2 \\ -\pi k_o/4 \end{cases} \qquad OV' \begin{cases} 2k_o/\pi \\ -2k_o/\pi + \lambda \end{cases}$$

Thus $\sigma_{uv} = -\sigma_{vu}$ and $\sigma_{vv} = 0$. Should an higher approximation be performed one should find $\sigma_{vv} \sim H^{-2}$. Therefore the tensor σ' for semi-circular orbits is of the form

$$\sigma' = \begin{pmatrix} \frac{e^2 \tau n}{m} & -\frac{e(n-n_o)}{H} \\ \frac{e(n-n_o)}{H} & \sim O\,H^{-2} \end{pmatrix} \qquad (A \cdot 27)$$

One may expect that the general form of σ' is similar to the one found for semi-circular orbits. If this is so then the analysis performed to separate the open orbit contribution from the closed

orbit contribution is still applicable since to the order of H^{-2} terms, the conductivity may be written as:

$$\hat{\sigma}^{o} = \begin{pmatrix} \sigma' & 0 \\ 0 & 0 \end{pmatrix} + \begin{pmatrix} 0\, H^{-2} & \beta^{o} H^{-1} \\ -\beta H^{-1} & 0\, H^{-2} \end{pmatrix}$$

i.e. as $\sigma^{o} = \sigma^{o}{}' + \sigma_{c}^{o}$.

The important effect is in the contribution of the open orbits in the Hall effect and thus in the definition of an effective number of carriers.

APPENDIX C: EFFECTIVE NUMBER OF CARRIERS AND THE HALL EFFECT

In the case of thallium, the hexagonal direction is a singular direction[25] in the sense that a fraction of the carriers in the 4th electron zone do not behave as electrons, but have a hole behavior. see figure (29) Thus the metal, instead of being compensated, exhibits an excess of holes corresponding to

$$\Delta N_h + \Delta N_e = \frac{1}{4\pi^3} \Delta k_3 \{ A_h + A_e \} = \frac{1}{4\pi^3} V_3 \qquad (A\cdot 28)$$

The first term accounts for the number of acting holes and the second term accounts for the number of inactive electrons corresponding to the compensation condition. The volume V_3 corresponds to a slice of the zone limited by a thickness Δk_3, the smallest caliper of the F.S. fourth band net in the hexagonal direction.

The experimental determination of the Hall effect leads to an excess of holes of $\approx 2.16 \times 10^{22}$ per cm^3, which gives a value for $\Delta k_3 = 0.69$ Å^{-1}. This value should be compared to the caliper of the B' - B' orbit in Coon's[26] magnetoacoustic attenuation study. It is interesting to note that they obtained a caliper of 0.67 Å^{-1} for this direction and though it was attributed to another orbit it could, perhaps, correspond to the B' - B' orbit.

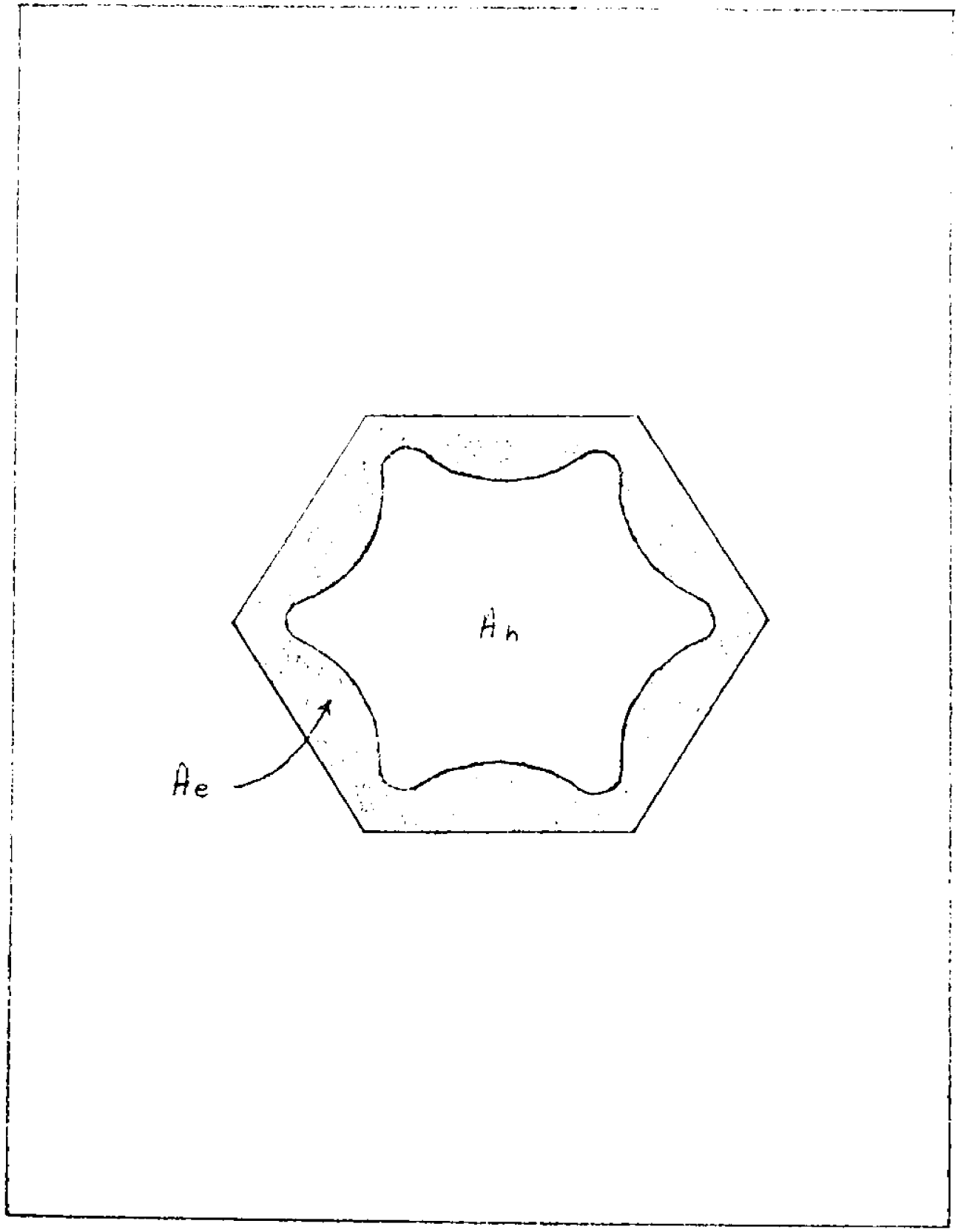

Fig. 29

A caliper of this value would indicate that the branches of the hexagonal net are rather cylindrical since Coon's data indicates that the belly of the branch is near 0.8 $\AA^{-1}$. This value of Δk_3 agrees qualitatively with the dimension obtained for the stereographic region of type B open orbits given by Milliken and Young[27] (see fig. 26).

When the magnetic field H is tilted by a small angle α with respect to the principle axis of a crystal, certain calculations relative to the effective number of carriers may be made. Figure 30 shows a schematic side view of a square net with cylindrical arms. The effective number of holes, n, which is measured by the Hall conductivity is given by

$$n = \frac{1}{4\pi^3}\left[V_1 + V_2 - V_2' + V_4 \right] \qquad (A\text{-}29)$$

where V_1 corresponds to the volume limited by the part of the F.S. on which the closed orbits are hole-like and by limiting planes P and P'. V_2 is the volume limited by the part of the F.S. on which open orbits exist, and by the two sets of planes P,Q and P',Q'. V_4 corresponds to the volume within the F.S., i.e., the volume of the occupied states classified as electrons. On fig. 30, the volumes V_1, V_2, V_4 correspond to a single zone and are respectively schematized by the curvilinear quadrangle 1A2A' the curvilinear triangles 1A'B' and the semi-circles, A1B'A.

It can be seen in this case that $V_1 + V_2 + V_4 = V_3$ where

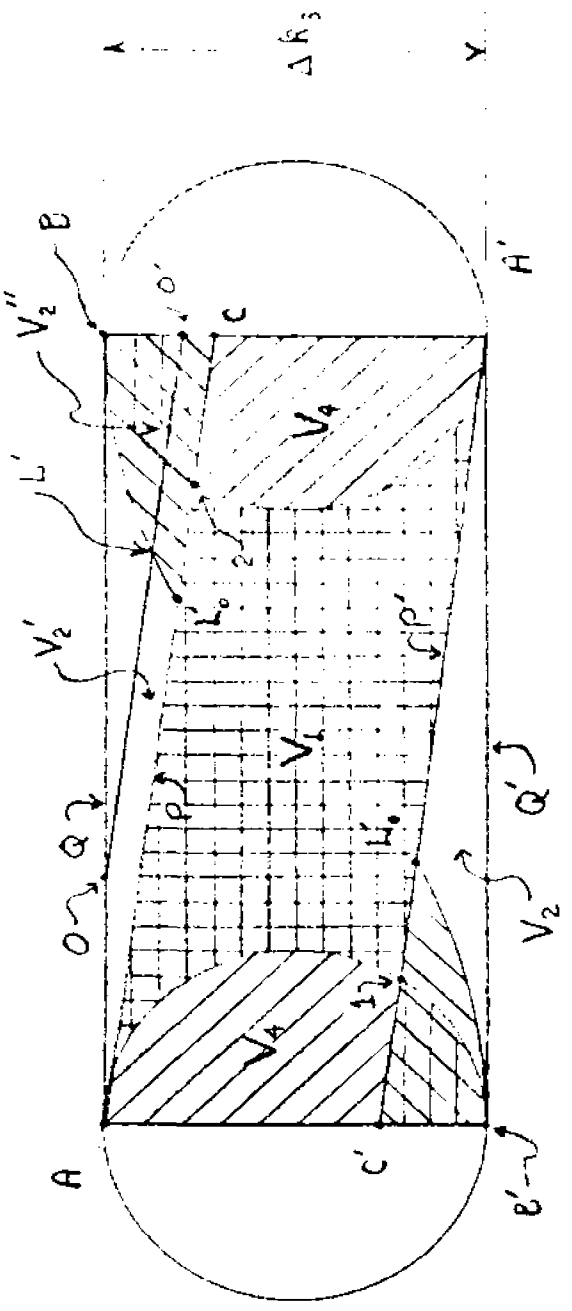

Fig. 30

V_3 corresponds to the volume for the case of H parallel to the four-fold axis.

The volume comes from the creation centroid of the open orbits when the position of the centroid of a particular cut 00' is measured from the intercepts 0.

The volume V_2', comes from the centroid of the terminal of the open orbit also measured from the point 0. The magnitude of this term depends on the scattering if the scattering changes along the open orbit. The volume V_2' may be assimilated with the volume of a prism of length $2k_o$ and a curvilinear section ABL_o', where BL_o' is the projection of the terminal point L' for the different section 00'.

If the positions of the centroids are measured from 0' instead of 0, then n takes the form $\frac{1}{4\pi^3}(V_1' + V_2'')$ where V_1' is the volume of the slice of the zone limited by the plane PP', and $\frac{1}{4\pi^3} V_2''$ is in a way the contribution of the open orbit electrons to the number of carriers. With the terminal centroids on the line BL_o', then V_2'' is the volume of the prism whose area is limited by the curvilinear triangle, $L_o'BL$, and whose height is limited by the length of the zone in the open orbit direction. i.e., $2k_o$.

Thus V_1' is determined only by the topology of the F.S. while V_2'' depends on the scattering as well as on the F.S. topology. If there are "hot zones" along the orbit where small angle scattering is particularly efficient, then the terminal

point will be displaced toward these zones. Therefore the number of carriers measured by the Hall effect and Righi-Leduc effect may reflect the existence of small angle scattering. If one assumes that the small angle scattering is more uniform in the Righi-Leduc effect than in the Hall effect, one could predict whether or not the scattering is more efficient in one part of the open orbit than in some others.

A first consequence of equation A29 for the case of the cylindrical net is that the effective number of carriers should decrease as a function of α, i.e., ρ_{21} and γ_{21} should increase with α. The fact that this does not occur in the thallium data may just indicate the departure of the arms of the net from a simple cylindrical shape.

The preceeding considerations do not explain another feature of the data, viz, the fall of γ_{21}LnT as a function of the temperature, while the corresponding values for ρ_{21} remain relatively invariant. This behavior might be due to phonon drag, a topic which is to be discussed in the next appendix.

APPENDIX D: PHONON DRAG

Phonon drag is known to cause large effects in the thermoelectric coefficient and usually negligible effects in the electrical and thermal conductivity coefficients. Those phonons which are dragged by the electrons appear to be less efficient scatters than if they were able to relax to the equilibrium state after being scattered. To account for this effect, σ_{11}, λ_{11}, and λ_{12} are multiplied by factors of the form $(1 - a)$, where $a \leq 1$ accounts for the degree of drag by the electrons. The coefficient σ_{12} appears to be unaffected. If one writes (in the asymptotic, classical situation of one electron band) the coefficient λ_{12} in the form given by Akhiezer et al.,[28] then one has:

$$\lambda_{12} = (L_n T \sigma_{12}) \left\{ 1 - 12(2\pi)^3 (T/\theta)^3 \int_0^\infty \left(\frac{A_1}{1 + \chi A_1} + \frac{A_2}{1 + \chi A_2} \right) \frac{\chi^4 G_1(\chi)}{e^\chi - 1} \, d\chi \right\}$$

The different quantities appearing in this formula are enumerated in the reference and are, at the moment, not of primary interest. What should be noted at this point is the temperature dependence of λ_{12}, viz.

$$\lambda_{12} \sim L_n T \sigma_{12} \left(1 - c T^3 \right)$$

where cT^3 is only a small term at low temperature. The coefficient c depends on the drag and is small when the drag is small. Thus, L_nTY_{21} could decrease as T gets smaller, as the data indicates, although the variation obtained experimentally departs from the law given above and as $T \rightarrow 0$, λ_{12} departs from $\sigma_{12}L_nT$ instead of tending toward it.

Another line of thought may be pursued at this point. In the analysis of the small angle scattering data, one assumes that the phonon scattering term of σ_{11} and λ_{11} of the open orbit measures the degree of efficiency of the scattering. As pointed out earlier, the effect of drag is to lessen this efficiency and, therefore, may affect the interpretation given to the slope ratio. Arguments of a qualitative nature may help, nevertheless, to justify this interpretation.

a) There are few open orbits. If the corresponding electrons exchange momentum and energy with the phonons, those in turn have the opportunity to relax into near equilibrium by scattering with the closed orbit carriers which are there in large amounts. This will minimize the dragging of phonons by the open orbit electrons.

b) Scattering is considered inefficient in the case of drag because of the required condition of the conservation of momentum in the system. When an electron is scattered by a phonon through $\Delta k = q$ it requires the same change in momentum, through re-creation of a phonon, i.e., $-\Delta k = -q$, to be restored to its original momentum. The situation of electrons scattered from open orbits

into closed orbits by $\Delta k \sim q$ is different from the preceeding case because the inverse scattering (after randomization) does not compensate for it. Therefore, the small angle scattering effect described here will be quite insensitive to drag, but may make the vertical process of scattering inefficient and bring the same efficiency of scattering to electrical and thermal effects.

APPENDIX E

This appendix will consist of a) experimentally determined coefficients, b) physical constants and c) approximated values, i.e., order of magnitude values of certain quantities appearing in this study. The values are obtained using various approximations and available experimental data. Since these values are given only as general information, no specific explanation or reference to their source will be given.

$\rho_{300^oK}/\rho_{4.2^oK} \sim 10{,}400$

$\rho_{4.2} \approx .3 \times 10^{-8}\ \Omega$ - cm

$B \approx 3.45 \times 10^{11}$ G/ Ω - cm = 3.1×10^{23} gaussian units

$n \approx 2.16 \times 10^{22}$ el/cm^3 = 1.19 el/atom (for H//[0001])

$N_h \approx 2.37 \times 10^{22}$ holes/cm^3 = 1.32 holes/atom

$N_e \approx .22 \times 10^{22}$ el/cm^3 = .15 el/atom

$n' \approx N_h + N_e \approx 2.6 \times 10^{22}$ el/cm^3 = 1.45 el/atom

m^* (3rd zone) $\approx .66\ m_o$

m^* (4th zone) ≈ 1.0 to $1.4\ m_o$

Λ (mean free path, 3rd zone) ≈ 1.3 mm at 1.2^oK (ultra-sound)

$\tau_\sigma \approx 1.7 \times 10^{-9}$ sec. " "

$H_{s\sigma} = m^* c/e\ \tau_\sigma \approx 30$ to 40 gauss " "

$\tau_\sigma = 5 \times 10^{-11}$ at 4.2^oK (resistance at zero field)

open orbit data	1.6°K	2.0°K	3.0°K	4.1°K
σ^o(Ω-cm) at 20 div, $\sin^2\theta$=1, B=const.	12.5×10^6	10.5×10^6	5.3×10^6	1.3×10^6
σ^o(Ω-cm) at 90 div, $\sin^2\theta$=1, B=const.	93×10^6	81×10^6	45×10^6	14.6×10^6
σ^o(Ω-cm) at 180 div, $\sin^2\theta$=1, B=const.	286×10^6	244×10^6	167×10^6	58×10^6
$\lambda^o/LnT(\Omega\text{-cm})^{-1}$ 20 div, $\sin^2\theta$=1, B=const.	4.6×10^6	3.2×10^6	1.5×10^6	1.9×10^6
$\lambda^o/LnT(\Omega\text{-cm})^{-1}$ 80 div, $\sin^2\theta$=1, B=const.	28.5×10^6	20×10^6	8.0×10^6	5.0×10^6
$\lambda^o/LnT(\Omega\text{-cm})^{-1}$ 180 div, $\sin^2\theta$=1, B=const.	76×10^6	53×10^6	22.6×10^6	11.2×10^6
$H_{s\sigma}$(G) (from ultrasonics)	45G			
$H_{s\sigma}$(G) (from zero resistance)				1000
$H_{s\sigma}$(G) (Guess)		100	300	
$H_{s\lambda}$(G) (Guess)	150	500	2000	5000
A (in $10^{13}G^2/\Omega$-cm)	1.8	4.1	12.5	41
A'LnT	6	20	82	205
$\sigma^o A/B^2$ (for 180 div)	4.5%	8%	17%	20%
$\lambda^o A'/B'^2$ "	4%	9%	15%	19%
λ_g (from L_o' approx., in W/cm-°K)	.013	.021	.047	.09
λ_g (from calculation in W/cm-°K)	.005	.007	.015	.023

$\lambda_g/LnT\ (\Omega\text{-cm})^{-1}$				
from L_o'	$.33\times10^6$	$.43\times10^6$	$.64\times10^6$	$.9\times10^6$
$\lambda_g/LnT\ (\Omega\text{-cm})^{-1}$				
from calculation	$.13\times10^6$	$.14\times10^6$	$.20\times10^6$	$.23\times10^6$
$\lambda_g(\lambda_o+\lambda_g)B'^{-2}$ in 10^{-12}				
at 180 div from L_o'	210			85
$\lambda_g(\lambda_o+\lambda_g)B'^{-2}H^2$ at H=20kG				
from L_o'	8%			3%
$\lambda_g(\lambda_o+\lambda_g)B'^{-2}H^2$ at H=20kG				
from calculation	3%			1%

LIST OF SYMBOLS

A. Coordinate systems

1) 1,2,3 : Coordinate system of the rectangular parallelepiped sample where 1, 2 and 3 correspond to the sample length, width and thickness, respectively.

2) 1',2',3' : Crystallographic coordinates, $[10\bar{1}0]$, $[\bar{1}2\bar{1}0]$, and [0001], respectively.

3) u,v,z : z is the magnetic field direction, v is the intersection of the basal plane, (1',2') with the plane perpendicular to z.

4) x,y,z : Transport effect coordinate system, where z is the magnetic field direction, x is the intersection of the u,v plane with the 1,3 plane and y is the direction perpendicular to z and x. It is also understood that x is the vertical direction and $\vec{yz}$ define the horizontal plane.

5) 1,2 : Indices used (particularly in Appendix A) to characterize the closed orbit contribution when the (1',2'), x,y), (u,v) and (1,2) planes are nearly the same.

B. Miscellaneous Symbols

θ : 1) The angle between the x-direction and the open orbit current direction. 2) Same as above but under high field asymptotic conditions for which v is the intersection of the x,y plane with the 1',2' (basal) plane, then θ is approximately the angle between v and 2,2' or y or the angle between u and 1,1' and x.

$(\alpha),\alpha'$: Tilt angle, i.e., the angle between the magnetic field direction z and the (3) or 3' direction. (This definition of α is of no interest).

α : Is also the angular rotation of the magnetic field relative to the horizontal projection of the 3' direction ($\alpha = \alpha'$ for 3' horizontal).

β : Angle between 3' direction and horizontal phase. To a first approximation $\alpha' = \sqrt{\alpha^2+\beta^2}$ and $\tan\theta = \alpha/\beta$.

$\vec{H}$: Magnetic field

$\vec{G}$: Negative of the gradient of temperature i.e., $\vec{G} = -\vec{\nabla}T$

$\vec{E}$: Electric field.

$\vec{J}$: Electric current density.

$\vec{W}$: Heat current density.

ρ or ρ^T : Electrical resistivity tensor.

γ : Thermal resistivity tensor.

Ln : The Lorentz number (2.45×10^{-8} V^2/deg^2).

σ or σ^T : Total electrical conductivity tensor.

σ^o or $\sigma^{o'}$: Open orbit contribution to the electrical conductivity. σ' is also used in place of σ^o.

σ^c or σ : Closed orbit contribution to the electrical conductivity.

λ : Total thermal conductivity tensor.

λ^o : Open orbit contribution to the electronic thermal conductivity. λ' is also used in place of λ^o.

λ^c : Closed orbit contribution to the electronic thermal conductivity.

λ_g : Lattice conductivity.

B : The coefficient defined by the equation $\sigma_{xy} \approx \sigma_{12} \rightarrow B/H$, where σ_{12} is the high field limit of the x,y component of the closed orbit* electrical conductivity. B = nec.

B' : The coefficient defined by the equation $\lambda_{xy} = \lambda_{12} \rightarrow B'/H$ where λ_{12} is the high field limit of the x,y component of the closed orbit* electron contribution to the thermal conductivity. B' = LnT B.

A : The coefficient defined by the equation $\sigma_{11} \rightarrow A/H^2$ where σ_{11} is the high field limit of the xx component of the closed orbit* electrical conductivity. $A \approx e^2 N \tau_\sigma/m$.

A' : The coefficient defined by the equation $\lambda_{11} \rightarrow A'/H^2$ where λ_{11} is the high field limit of the xx component of the closed* orbit contribution to the thermal conductivity. $A' \approx e^2 N \tau$ LnT/m. (* It is shown in Appendix B that the coefficients A, B, A' and B' receive a small contribution from the open orbit).

δC and δE : Coefficients appearing in σ_{13} and σ_{23}.

N_e : Number of carriers with electron-like characteristics.

N_h : Number of carriers with hole-like characteristics.

n : The excess of holes over electrons. $n = N_h - N_e$.

N : Total effective number of carriers. $N = N_h + N_e$.

m : Mass of the electron $m = 1.109 \times 10^{-28}$ g.

τ_σ : Closed orbit relaxation time for electronic conduction.

τ_λ : Closed orbit relaxation time for thermal conduction.

ω_c^{-1} : Open orbit relaxation time for thermal conduction and collision time.

ω_{eff}^{-1} : Open orbit relaxation time for electronic conduction.

S' : The slope of the curve ρ_{xx} vs H^2.

S'' : The slope of the curve $H\rho_{xx}/\rho_{yx}$ vs H^2.

L' : The slope of the curve LnT γ_{xx} vs H^2. ($L' = L'_o$ for $\alpha=0$).

L'' : The slope of the curve $H\gamma_{xx}/\gamma_{yx}$ vs H^2. ($L'' = L''_o$ for $\alpha=0$).

$\bar{r}, (\bar{r}_p)$: The inverse of the scattering efficiency, ω_c/ω_{eff}; ($\bar{r}_p$ applies for phonon scattering only).

$\bar{r}', \bar{r}'', \bar{r}'_c, \bar{r}''_c$ represent respectively the ratios S'/L', S''/L'', $S'/(L'-L'_o)$, $S''/(L''-L''_o)$.

Λ, Λ^* : Average path of an open orbit in real and k-space, respectively.

U, V : Centroids of creation of a particle under an impulse E_u, E_v, respectively.

U', V' : Centroids of termination of the particle path.

V_i, V_j : Volumes in k-space.

V_x, V_y, V_z, V_d : represent also velocities of electrons in real space.

REFERENCES

1. A. B. Pippard, Proc. Roy. Soc. (London) A305, 291 (1968).
2. P. G. Klemens and J. L. Jackson, Physica 30, 2031 (1964) and Physica 31, 1421 (1965).
3. P. Cotti, E. M. Fryer, and J. L. Olsen, Helv. Phys. Acta 37, 585 (1964).
4. O. P. Katyal, A. N. Gerritsen, J. Ruvalds, R. A. Young, and L. M. Falicov, Phys. Rev. Letters 21, 694 (1968).
5. R. L. Powell, Proc. of the Ninth Int. Conf. on Low Temp. Physics, edited by J. G. Daunt, D. O. Edwards, F. J. Milford, and M. Yaqub (Plenum Press, New York, 1965), Part B, p. 732.
6. Pippard, op. cit., A305, 291.
7. E. Fawcett, Advances in Physics 13, 139 (1964).
8. N. E. Alekseevskii and Yu. P. Gaidukov, Zh. Eksperim. i. Teor. Fiz. 43, 2094 (1962) [English translation: Soviet Physics - JETP 16, 1481 (1963)].
9. A. R. Mackintosh, L. E. Spanel, and R. C. Young, Phys. Rev. Letters 10, 434 (1963).
10. J. C. Millican and R. C. Young, Phys. Rev. 148, 558 (1966).
11. R. C. Young, Phys. Rev. 163, 676 (1967).
12. J. B. Coon, C. G. Grenier, and J. M. Reynolds, J. Phys. Chem. Solids 28, 301 (1967).

13. J. A. Rayne, Phys. Rev. 131, 653 (1963).

14. Y. Eckstein, J. B. Ketterson, and M. G. Priestley, Phys. Rev. 148, 586 (1966).

15. M. G. Priestley, Phys. Rev. 148, 580 (1966).

16. P. Soven, Phys. Rev. 137, A1706 (1965) and A1717 (1965).

17. Cominco Products, Inc., Spokane, Washington.

18. J. R. Long, Ph.D. Dissertation, Louisiana State University 1965 (unpublished).

19. Alekeevskii and Gaidukov, op. cit., 16 1481

20. P. G. Klemens, Solid State Physics, F. Seitz and D. Turnbull, editors (Academic Press, New York, 1958), Vol. 7, p. 1

21. N. V. Zavaritskii, JETP 12, 1093 (1961).

22. M. Garfinkel and P. Lindenfeld, Phys. Rev. 110, 883 (1958).

23. R. A. Young, to be published.

24. A. B. Pippard, Proc. Roy. Soc. A282, 464 (1964) and Proc. Roy. Soc. A287, 165 (1965).

25. E. Fawcett, op. cit., 13 301.

26. Coon, op. cit., 28 301.

27. Millican and Young, op. cit., 148 558

28. A. I. Akhiezer, V. G. Bar'yakhtar and S. V. Peletminskii, Soviet Physics JETP 21, 136 (1965).

VITA

Robert Eugene Hamburg was born December 21, 1937 in Bayou D'Inde, Louisiana. He completed his elementary and secondary education at Westlake High School in 1956. In 1961 he graduated from McNeese State College with a B.S. degree in physics. He remained at McNeese State College as an assistant in physics during the spring semester, 1961 and in May 1961 married the former Dora Ann Stolhand.

In January 1964, he received an M.S. degree in physics from L.S.U. and is now a candidate for the degree of doctor of philosophy in the department of physics and astronomy at Louisiana State University.

EXAMINATION AND THESIS REPORT

Candidate: Robert Eugene Hamburg

Major Field: Physics

Title of Thesis: Transport Properties of Thallium and the Effects of Small Angle Scattering in Metals

Approved:

Major Professor and Chairman

Dean of the Graduate School

EXAMINING COMMITTEE:

Date of Examination:

January 12, 1970